DUPLO Deliverable D4.1.2

Performance of Full-Duplex Systems

Project Number:	**316369**
Project Title	**Full-Duplex Radios for Local Access – DUPLO**
Deliverable Type:	**PU**

Contractual Date of Delivery:	**April 30, 2015**
Actual Date of Delivery:	**May 22, 2015**
Editor(s):	**Ari Pouttu, Hirley Alves(UOULU)**
Author(s):	**Ali Cirik , Hirley Alves , Carlos Lima , Kari Rikkinen (UOULU); Jawad Seddar (TCS); Mir Ghoraishi , Mohammed Al-Imari (UNIS),**
Workpackage:	**WP4**
Estimated person months:	**25**
Security:	**PU**
Nature:	**Report**
Version:	**1.0**

Abstract: This deliverable provides final full-duplex system performance results. A short review to relevant literature is given and main small cell full-duplex operation modes are illustrated. System performance is evaluated through mathematical optimization frameworks and simulations, resulting in achievable rate region analyses, spectral efficiency and beamformer optimizations and small indoor and outdoor cell throughput simulations. All these provide comparison against half-duplex counterparts and show clear potential for full-duplex systems.

Keyword list: rate region, spectral efficiency, beam former design, power allocation, sub-carrier allocation, system simulations, error vector magnitude, small cells

Executive Summary

This deliverable outlines key findings and numerical results of the DUPLO WP4 work. The focus is on studying point-to-point full-duplex links, standalone single/multi-user small cells with single/multiple full- and/or half-duplex links, full-duplex relaying and their performance. As a clear distinction to D4.1.1 this deliverable also addresses multi-cell networks in more details and provides results on IEEE802.11 Full-Duplex *Mobile Ad-hoc NETworks* (MANET) developed in the project.

Chapter 2 provides an analysis on full-duplex link rate region as well as power allocation policies for single full-duplex links. Therein, numerical results for uniform and adaptive non-uniform power allocation are discussed. Small cells with short link distances and low transmission powers are the preferred scenario for full-duplex links. By loosening rate region requirement full-duplex links become feasible also in energy efficiency point of view. Additionally, results show that under given power allocation policies the downlink data rate improves significantly, which results in an increase of overall system performance in the presence of asymmetric traffic for full-duplex networks.

Chapter 3 provides a comprehensive set of performance results for single full-duplex small cell deployment. Therein, power allocation and scheduling polices for multi-user half-duplex and full-duplex small cell are introduced. Additionally, a performance assessment at the network level is provided assuming that all nodes operate in full-duplex fashion. Multiple-antenna and device-to-device scenarios are also investigated. All in all the results introduced herein show that a full-duplex system is capable to achieve a higher performance than half-duplex systems. These performance gains become more significant if at least 70dB self-interference cancellation is achieved.

Chapter 4 assesses the performance of multiple full-duplex small cells. Herein, the focus is on investigating the impact of inter-cell interference due to full-duplex transmission. As a result, we provide the SINR and outage probability, throughput and sum-rate comparisons under indoor and outdoor environments with variable density of full-duplex small cell set-ups.

Chapter 5 addresses full-duplex relaying, where performance analysis of full-duplex relaying protocols is provided, and a new selection algorithm is introduced. Results show that full-duplex relaying overcomes the spectral inefficiency of half-duplex cooperative schemes, and also that much higher data rates can be achieved self-interference cancellation is of at least 70dB.

Chapter 6 analyses a MAC protocol for IEEE802.11 MANET. Throughput and traffic routing are provided under the scope of IEEE802.11 MANET. Moreover, substantial throughput gains can be achieved even with non-symmetrical traffic, for instance when using TCP as a transport protocol.

Chapters 7 and 8 discuss the main results and conclusions of the deliverable and finally Chapter 9 enlists the referred biography.

Authors

Partner	Name	Email
UOULU	Hirley Alves	hirley.alves@ee.oulu.fi
	Kari Rikkinen	kari.rikkinen@ee.oulu.fi
	Ali Cagatay Cirik	acirik@ee.oulu.fi
	Carlos Lima	carlos.lima@ee.oulu.fi
UniS	Mir Ghoraishi	m.ghoraishi@surrey.ac.uk
	Mohammed Al-Imari	m.al-imari@surrey.ac.uk
TCS	Hicham Khalife	hicham.khalife@thalesgroup.com
	Jawad Seddar	jawad.seddar@thalesgroup.com

Abbreviations

BS	base station
CCI	co-channel interference
CDF	cumulative distribution function
CP	cyclic prefix
CSI	channel state information
CQI	channel quality indicator
dB	decibel
DL	downlink
DUPLO	full-DUPlex radios for LOcal access
D2D	device-to-device
EVM	error vector magnitude
FD	full duplex
FDD	frequency division duplexing
FDMA	frequency division multiple access
HD	half duplex
IEEE	Institute of Electrical and Electronics Engineers
ITU	International Telecommunication Union
IWF	iterative water filling
LNA	low noise amplifier
LOS	line-of-sight
LTE	long term evolution
MAC	medium access
MANET	mobile ad-hoc network
MCS	modulation and coding set
MIMO	multiple input multiple output
MSE	mean square error
NLOS	non line of sight
OFDM	orthogonal frequency division multiplexing
PPP	Poisson point process
QAM	quadrature amplitude modulation
QoS	quality of service
RF	radio frequency
RR	Round Robin
SE	spectral efficiency
SI	self-interference
SIC	self-interference cancellation
SINR	signal-to-interference and noise ratio
SIR	signal-to-interference ratio
SNR	signal-to-noise ratio
TCP	transmission control protocol
TDD	time division duplexing
TDMA	time division multiple access
UE	user equipment
UDP	user datagram protocol
UL	uplink

WLAN	wireless local area network
WP	work package
3GPP	3rd Generation Partnership Project

CONTENTS

1. INTRODUCTION

Full-duplex (FD) transmission is a potential air interface technology to improve spectral efficiency in wireless communication systems. Full-duplex offers the opportunity to increase the two-way traffic rate in wireless communications by enabling simultaneous transmission and reception on the same carrier frequency, but it also sets many challenges for implementing wireless transceivers. One of the main challenges is the self-interference (SI) caused by the full-duplex transceiver communicating on both the uplink and downlink directions simultaneously. Provided that this SI can be significantly suppressed, full-duplex transceivers can nearly double their two-way traffic rate in ideal cases [1].

In order to mitigate the strong self-interference, many recent full-duplex transceiver designs consider hybrid approaches, where the self-interference suppression is performed in multiple stages including 1) antenna isolation, 2) RF cancellation, and 3) digital baseband cancellation. Motivated by many promising results that have been obtained using these approaches, e.g., [1]-[3], the full-duplex technology is further investigated as a potential candidate for the 5G communication systems in DUPLO project.

This deliverable summarizes our system performance studies in WP4 of the DUPLO project. In the rest of this chapter, we first give a brief overview of the DUPLO project, then revisit the use cases assessed in WP4, as well as outline the document structure. The algorithms and protocols related to the assessed study cases in this deliverable are described in detail in another DUPLO WP4 report, D4.2 [5].

1.1. DUPLO project overview

Different from previous contributions in full-duplex technology development, the DUPLO project focuses not only on the design of full-duplex radios but also on their operation in practical system deployments by considering realistic conditions and constraints. And yet different solutions to obtain an operational validation platform are considered here as well.

In the DUPLO project, there are 5 technical WPs covering different aspects of the full-duplex technology. As the first step of the project, WP1 investigated the application of full duplex in future-oriented mobile wireless communication networks and identified the main design requirements and constraints. Following the recent evolution trend of wireless communication networks, DUPLO identifies small cell and mesh networks as the main areas of interest for the project, which are then further studied within the WP4.

WP2 and WP3 focus on developing the solutions to suppress the self-interference in full-duplex transceivers. In particular, antenna isolation and analog RF cancellation are investigated in WP2, while

the digital baseband processing is assessed in WP3. By combining the WP2 and WP3 outputs, a robust implementation for full-duplex transceivers will become viable. In addition, the non-ideality problem of such transceivers will be investigated in WP2, while baseband solutions to compensate for this non-ideality will be developed in WP3.

WP4 focuses on evaluating how full-duplex systems perform with respect to distinct radio resource management solutions. Specifically, we assess the benefits and attainable gains of using full-duplex transceivers at different network nodes, develop interference and radio resource management strategies and protocols for full-duplex transmissions, as well as design networks deployments where half- and full-duplex nodes coexist and share available resources

WP5 concentrates mainly on developing the proof-of-concept demonstrator. The demonstrator integrates set of antenna, RF and baseband solutions developed in WP2 and WP3 together into a complete full-duplex transceiver. Furthermore, two full-duplex transceivers can be connected together enabling to study full-duplex operation in practice in short transmission link distances.

1.2. Scope of this deliverable

Full-duplex communications have gained considerable attention from academia and industry. Intuitively FD communication should be easily attainable given that the signals are known and all needed is extra circuitry to subtract it from the receiving end. However, in practice this assumption does not hold since the transceivers considerably distort the transmitted signal due to the (non) linearity of the radio circuitry and noise [2]. Note that a comprehensive review of the state of the art is provided in Deliverable D4.2[5]. Current systems suffer from a power leakage between transmit and receive antennas, which is known as self-interference. Recent works have tackled such an issue and have shown that FD communication is feasible even though suffering from self-interference, see for instance a summary in [1]. Even though the reported results showed great promise by demonstrating the feasibility and benefits of using full-duplex technology, these papers did not answer important basic questions, such as: what are the optimal full-duplex configurations to achieve the best link performance? And how does the adaptive power control affect the full-duplex gain? Equally importantly, there are questions regarding the system level implementation of such full-duplex networks, which include but are not limited to the following:

1. How can the full-duplex technology support different multi-user access schemes in the context of the upcoming small cell deployment scenarios?
2. How do full-duplex networks cope with the aggregate interference generated by co-channel links?
3. How do full- and half-duplex nodes coexist and share resources in wireless networks?

4. How link- and system-level aspects are affected by non-ideal implementation of practical transceivers in the full-duplex investigation scenarios?

Despite being relevant, the current state-of-the-art literature fails to properly address these problems and provide clear answers to those open questions. In fact, this deliverable aims to shed light on these problems and by doing so enable practical full-duplex deployments.

1.2.1. Assessed Use cases

This deliverable summarizes full-duplex system performance investigations conducted in DUPLO WP4. The reference scenarios, which were previously defined in the deliverable D1.1 [6] , are revisited here. It is worth noticing that the algorithms and protocols related to the assessed study cases are described in detail in another DUPLO WP4 deliverable, D4.2 [5]. A point-to-point link is an essential unit and basic building block of many wireless networks. For example, in a wireless local area network (WLAN), every transmission between user devices and their access point (AP) can be regarded as a point-to-point link during the transmission period. Yet another example would be wireless backhauling in small cell deployments on mobile platforms such as trains, cars or airplanes. We start to introduce our full-duplex system studies from the point-to-point link as shown in Figure 1.

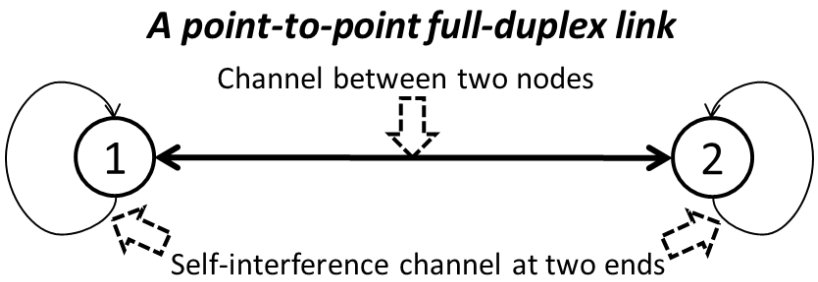

Figure 1 A point-to-point link constitutes the minimum full-duplex system in this deliverable

By assuming that both ends of the point-to-point link have full-duplex technology and use bi-directional power control, we investigate what is the achievable rate region and transmit power efficiency of the resulting full-duplex connections. The OFDMA radio access technology is also considered in these studies. In addition, both non-uniform and uniform power allocations over sub-carriers are considered and the corresponding system performance is investigated under flat and frequency selective radio channels. Power allocation strategies and achievable two-way link throughput in asymmetric traffic cases are also investigated.

Currently, all wireless networks have been designed to support multi-user communications. Different multi-user access techniques have been devised so as to multiplex the data streams from or

to multiple users on certain radio resources. Traditionally, multi-user access schemes, such as TDMA, FDMA and OFDMA among others, have been used together with half-duplex technology, and it is still unknown how the full-duplex configuration affects their performances. In this deliverable, we are going to assess the impact of using full-duplex transceivers at different nodes of small cell deployments. Particularly, we studied three small cell scenarios, which were defined in the deliverable D1.1 [6].

In the first scenario, we consider a standalone small cell with a full-duplex base station serving multiple half-duplex UEs, as shown in Figure 2.

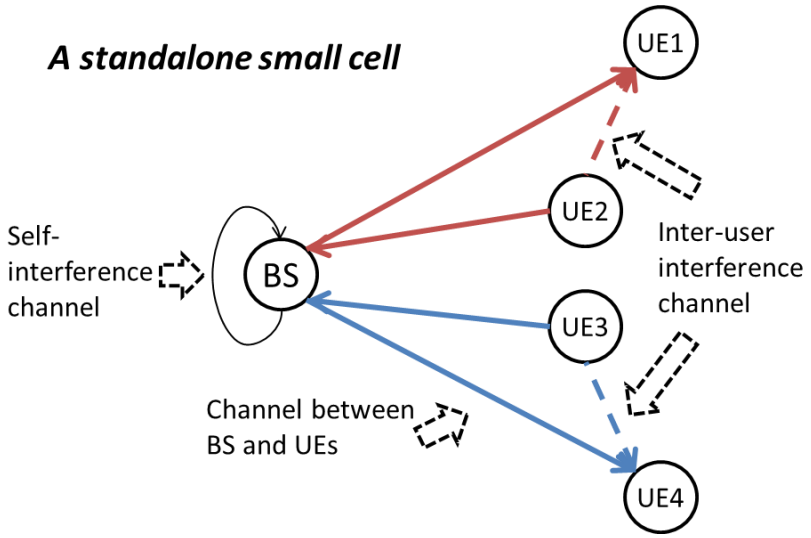

Figure 2 Example of a small cell with a full-duplex BS and half-duplex UEs.

Since the BS has a full-duplex transceiver, up to four simultaneous transmissions are supported over two orthogonal radio resources. Assuming either FDMA or TDMA multi-user access scheme, we show two usage examples in Figure 3 a) and b), respectively.

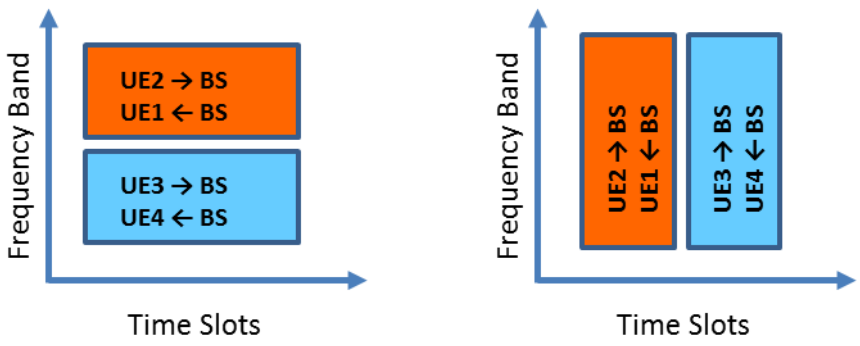

a) FDMA multi-user access scheme b) TDMA multi-user access scheme

Figure 3 User scheduling and resource allocation for a full-duplex BS with four half-duplex UEs.

In this scenario, two interference components dominate the performance: (i) the BS suffers from the **self-interference** of its own transmission, while (ii) UE1 and UE4 suffer from **inter-user interference** caused by UE2 and UE3 transmissions, respectively. One of the main challenges in this scenario is how to optimally allocate radio resources for different BS-UE connections.

In the second scenario, we still consider a standalone small cell but now both the base station and the UEs operate in full-duplex mode as shown in Figure 4

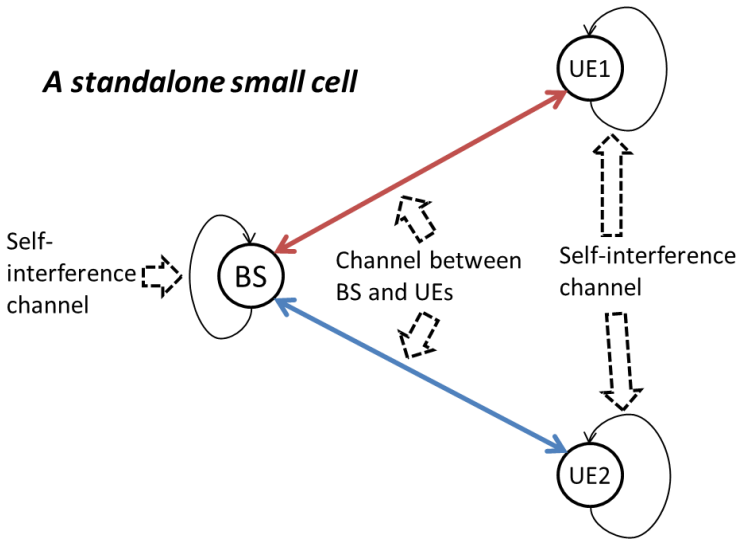

Figure 4 Example of a small cell scenario with full-duplex BS and UEs.

In a straightforward application of this scenario, the serving BS always establishes full-duplex links to the scheduled UEs. By doing so, a given UE simultaneously transmit to and receive from its serving BS on the same set of radio resources, while different UEs use distinct resources. Two examples are shown in Figure 5 a) and b).

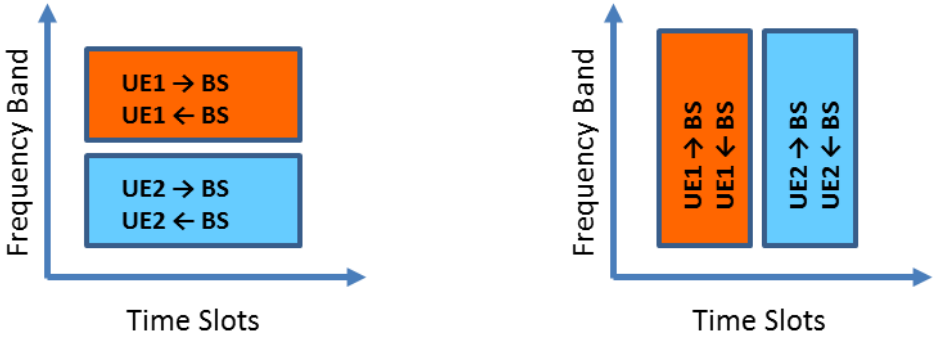

a) FDMA multi-user access scheme b) TDMA multi-user access scheme

Figure 5 User scheduling and resource allocation for both BS and UEs in full-duplex mode.

Generally, there is no co-channel interference in this scenario.[1] Therefore, the resulting self-interference at both BS and UEs dominate the corresponding performance and constitutes the primary challenge on each direction. There is also another challenge from the traffic load because the maximum throughput in this scenario can only be achieved when UEs have balanced downlink and uplink traffics. When the two-way traffic is asymmetric, a hybrid mode that combines Figures 3 and 5 is necessary to optimize the system throughput. More detailed analysis of this scenario can be found in the following chapters.

The next scenario considers a multi-cell deployment in which both base stations and UEs operate in full-duplex mode as shown in Figure 6.

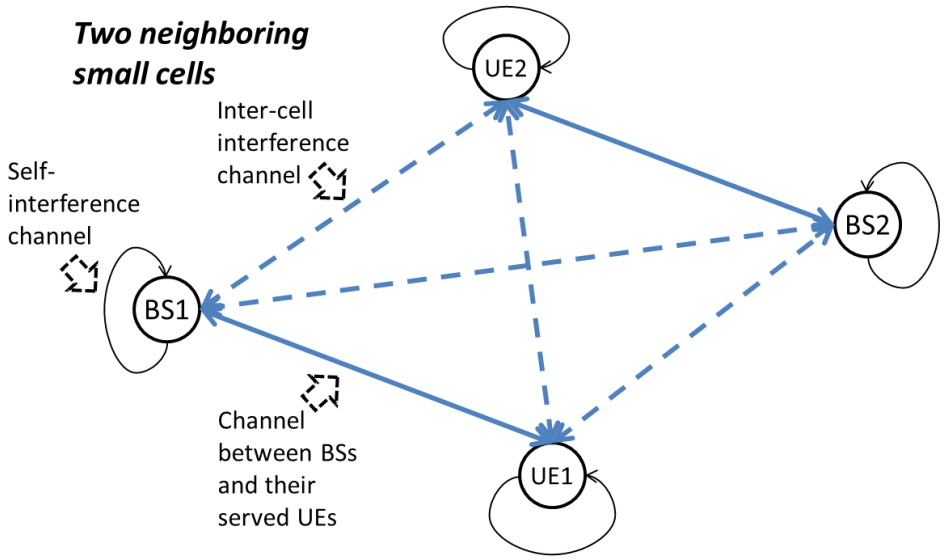

Figure 6 Example of two neighboring small cells with full-duplex BS and UEs.

The multi-cell deployment is an interference-limited scenario wherein both ends of a full-duplex link will generate inter-cell interference. Therefore, the self-interference and the inter-cell interference dominate the performance in this scenario. This document investigates how the full-duplex technology affects the inter-cell interference and the achievable system performance in multi-cell network.

The next scenario considers relaying schemes, where a FD BS helps the communication between two UEs, as depicted in Figure 7. In this scenario, the FD BS implements cooperative protocols in order to help the communication between two UEs.

Finally, scenarios IEEE 802.11 FD *Mobile Ad-hoc NETworks* (MANET) are investigated and the scenarios are described in details in Chapter 6 of the DUPLO deliverable D4.2 [5].

[1] However, adjacent channel interference could be a problem, e.g., in such FDMA case where UE1 and UE2 are close to each other and high Tx power of one UE could block wideband Rx LNA of the other UE (if both sub-bands are close enough to belong to filter passband).

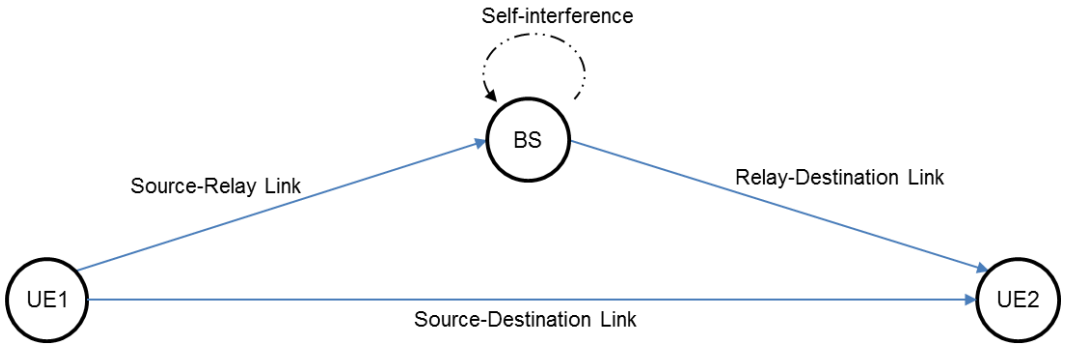

Figure 7 Example of two EUs communicating with help of a FD BS acting as a relay node.

1.3. The document structure

When organizing our studies in this deliverable, we start from the simplest full-duplex system and move forward to more complicated ones. Following this logic, the remainder of this deliverable is organized as follows.

In Chapter 2, the performance of the minimum full-duplex system, a point-to-point full-duplex link, is analyzed under both frequency flat and frequency selective environments. Its achievable rate region, energy efficiency and power allocation policies are studied as well.

In Chapter 3, we analyze the system-level performance of single small cell deployment with full-duplex transceivers at different/multiple network nodes. The provided results are based on the three aforementioned small cell scenarios.

In Chapter 4, we provide a performance assessment of multi cell deployment. This chapter tackles the issue of impact of inter-cell interference due to full-duplex transmission.

In Chapter 5, we analyze the performance of full-duplex relaying schemes in single and multi-cell scenarios as well as a relay selection algorithm.

In Chapter 6 we focus on the full-duplex networking aspects of wireless MANET. Routing solutions and design control plane are investigated for MANETs having full-duplex nodes.

Finally, Chapter 7 summarizes the key findings and sheds light on the remaining work. Chapter 8 draws the main conclusions attained in this project. Then, references are listed in Chapter 9.

2. SINGLE FULL-DUPLEX LINK

2.1. Rate Regions

In this section, we give the performance results of a full-duplex bi-directional link by taking the transceiver non-ideality into account. In practical systems, the non-ideality is usually captured by a measure named as the error vector magnitude (EVM) level. In [3]**,** it was shown that the impact of transceiver non-ideality is similar to the noise added at the transmitter. To simplify the link performance analysis in our study, we take the conclusion of [3] and approximate the non-ideality as a transmitter noise added at the transmitter in a way similar to [4]. The noise has average power proportional to that of the original signal, which is called as the EVM noise in [3] and [4].

EVM level limits the achievable signal-to-noise ratio (SNR) of a practical link. Many standards have specified the minimum requirements for EVM. 3GPP has given a requirement that BS should keep the EVM level below 8% for 64-QAM modulation [7]. This corresponds to a SNR about 22 dB. In our numerical analysis, we have used lower EVM levels (i.e., 30 or 40 dB below the original signal level), which assumes the use of more advanced transceivers. It is also assumed in our analysis that self-interference cancellation is performed in three stages: 1) ***antenna isolation***, 2) ***RF cancellation***, and 3) ***digital baseband cancellation***. In the former two stages the original signal and EVM noise can be suppressed equally but in the third stage the SI due to EVM noise cannot be cancelled any further.

We assume in our analysis that cyclic prefix (CP) assisted OFDM technique has been used by the two-way transmission. Two power allocation strategies over sub-carriers are considered. The first one considers a low complexity design where uniform power allocation over sub-carriers is used. The second one considers an optimized design where adaptive power allocation over sub-carriers is used. The algorithms used for the rate region calculation with different transmission strategies are explained in detail in [3] and [4], and section 2.1 of DUPLO deliverable D4.2 [5]. Main findings and key results of these papers are summarized in the next section.

2.1.1. Analysis parameters, assumptions and numerical results

Rate regions of the half- and full-duplex links are compared in this section with uniform and non-uniform sub-carrier power allocation strategies. Both flat and frequency selective fading channels are considered. Table 1 lists the key parameters used to generate numerical rate region results.

Table 1. Common parameters shared in numerical evaluations.

Parameters	Values	Unit
Transmission power	20	dBm
Signal bandwidth	10	MHz
Carrier frequency	2	GHz
Antenna gain	0	dB
Thermal noise power density at the receiver	-174	dBm/Hz
Receiver noise figure	10	dB
EVM level	-30	dBc
Number of sub-carriers	64	
Baseband interference cancellation	-40	dB
Distance between two transceivers	30	m

In the frequency flat scenario all sub-carriers have uniform gain. The assumed path loss between the two nodes obeys outdoor line-of-sight (LOS) model [8], i.e., $PL = 103.8 + 20.9 \log_{10} \frac{d}{1000}$ (dB), where d is the distance between the two nodes in meters. The influence of the self-interference cancellation is taken into consideration by attenuating the SI power by 60 dB on each sub-carrier, i.e., assuming that total antenna plus RF SI cancellation capability is 60 dB. Additional baseband SI cancellation of 40 dB is applied to transmit signal component, but not to EVM noise, thus implying 100 dB SIC level. Figure 8 reveals that both power allocation strategies end up in the similar achievable rate regions due to the flatness of the channel model. However, FD is seen to have about 18% maximum gain in bi-directional throughput over HD scheme.

In the frequency selective fading scenario two time domain multipath channel models are used. The channel between the two nodes follows ITU outdoor model A having 6 taps with relative delays [0, 300, 700, 1100, 1700, 2500] ns and average powers [0, -1, -9, -10, -15, -20] dB, respectively. The effective SI is now generated by a 4-tap model with exponentially decaying channel gain on each tap. Similarly to the previous case the average analog SI power reduction is 60 dB. Figure 9 illustrates that non-uniform power allocation provides up to 36% throughput gain for FD over HD whereas the corresponding gain with uniform power allocation is half of that.

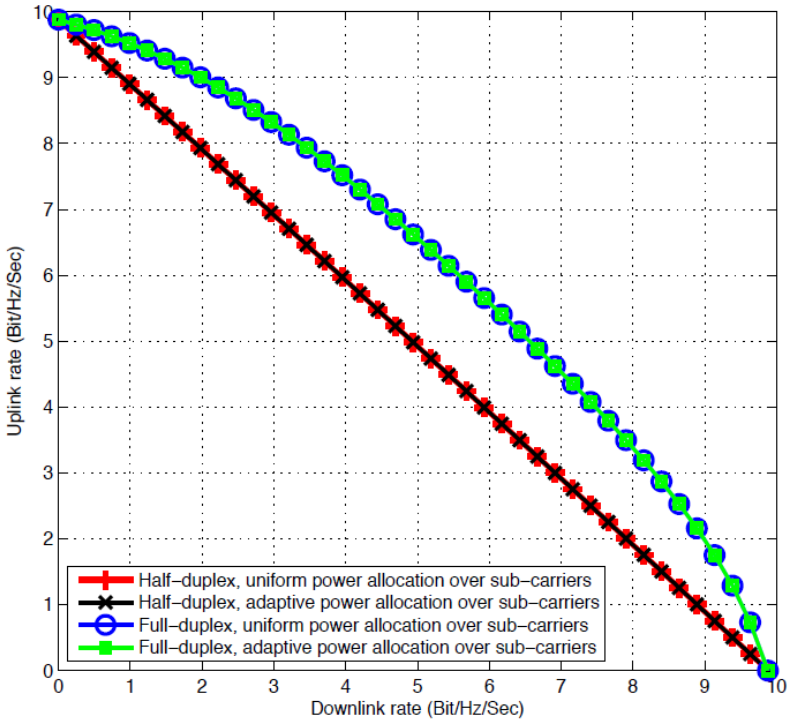

Figure 8 Half- and full-duplex rate regions with uniform and non-uniform power allocation frequency flat environment.

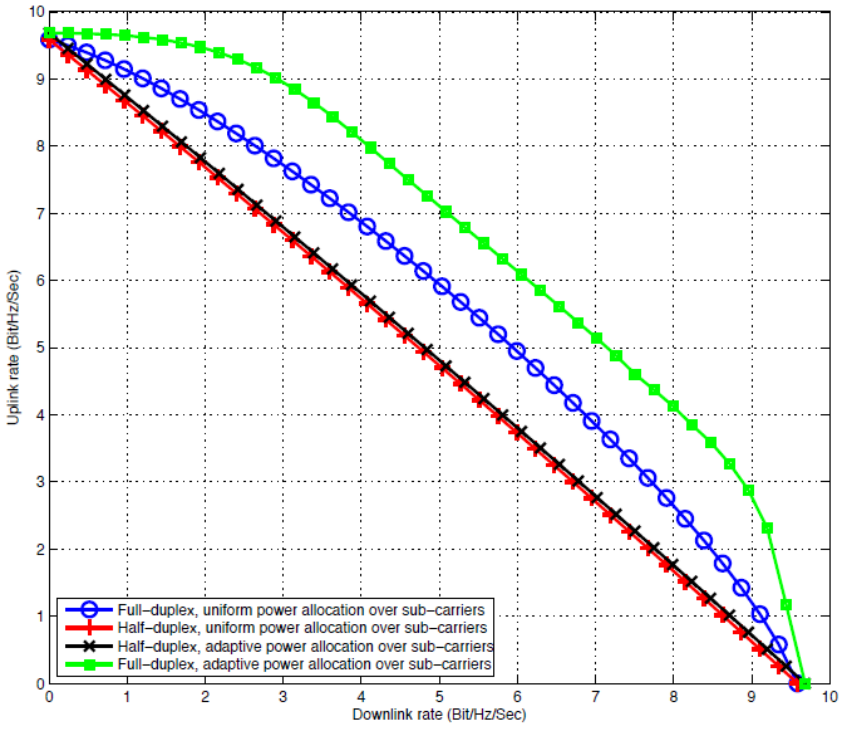

Figure 9 Half- and full-duplex rate regions with frequency selective environment with channel reciprocity and equal transmission power per node.

When the maximum uplink transmission power is decreased from 20 dBm to 0 dBm, the rate region becomes asymmetric as visualized in Figure 10. The main benefit of FD non-linear power

allocation is realized in high downlink rate regime in this case, which of course is very typical use case in small cell deployments.

The next example uses separate antennas for transmission and reception, and thus the channel reciprocity may not hold. In the simulation this is arranged by randomizing each link tap gain and phase. Figure 11 depicts the rate regions and shows that FD with non-uniform power allocation has much larger rate region than with uniform power allocation or HD with any power allocation.

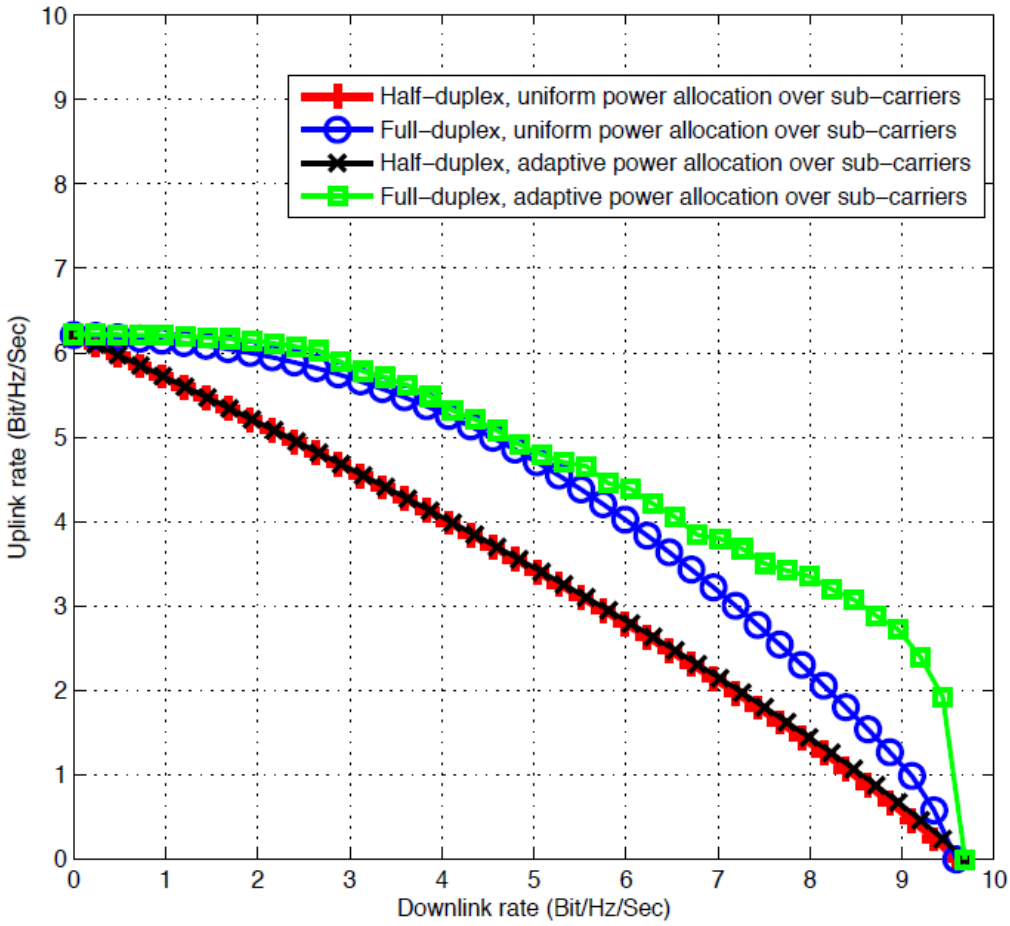

Figure 10 Half- and full-duplex rate regions in frequency selective environment with uniform and non-uniform power allocation, and channel reciprocity plus unequal transmission power per node.

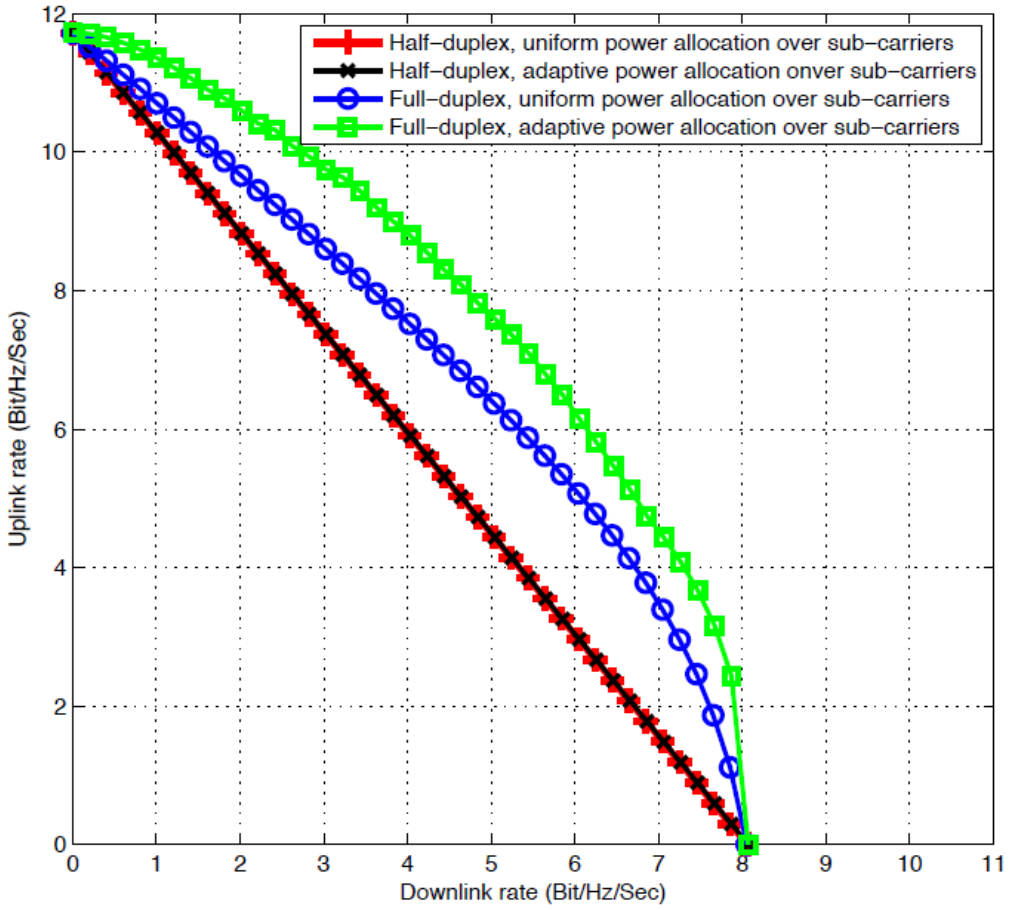

Figure 11 Half- and full-duplex rate regions in frequency selective environment with uniform and non-uniform power allocation and no channel reciprocity.

In the following numerical studies the impact of variable EVM noise level, various self-interference cancellation capabilities, different maximum transmission power and variable communication range are investigated. Figure 12 illustrates that 120 dB SI cancellation is required to fully realize FD potential in the absence of EVM noise. When SI cancellation capability is reduced to 90 dB the rate regions of FD and HD become almost the same. However, when EVM noise level is set to -30 or -40 dBc (decibels relative to the carrier), only 85 or 87 dB SI cancellation is needed to have approximately the same performance as with HD scheme, respectively. In this example the distance between two transceiver nodes is 20 m and both of their maximum transmission powers are 20 dBm. Separate transmit and receive antennas are assumed with the path loss between antennas being 20 dB. SI cancellation parameters $\beta_{1,i}$ and $\beta_{2,i}$ denote the RF and baseband cancellation capabilities, respectively.

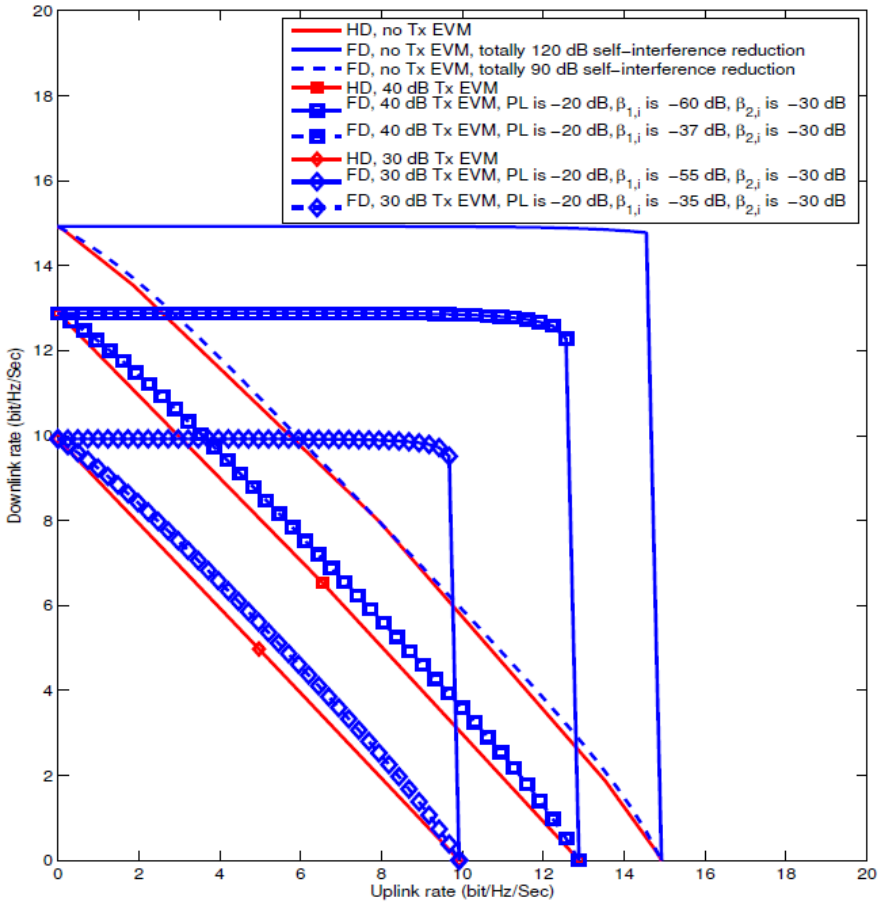

Figure 12 Full-duplex and half-duplex rate regions with different EVM noise levels.

Figure 13 demonstrates how the FD vs. HD relations are altered when maximum transmit power is scaled from -10 dBm up to 20 dBm. In addition, the distance between nodes is 20 m, the EVM noise level is -40 dBc and the total SI cancellation budget is 90 dB, including the impacts of antenna separation, RF and baseband SI cancellation. According to the results, the maximum sum rate of FD is almost double of that HD when the lowest transmission power of -10 dBm is used. By increasing the transmission power, the rate regions also increase but the relative gain of FD over HD decreases at the same rate. With the maximum transmit power of 20 dBm, the maximum FD rate gain over HD is only about 20%.

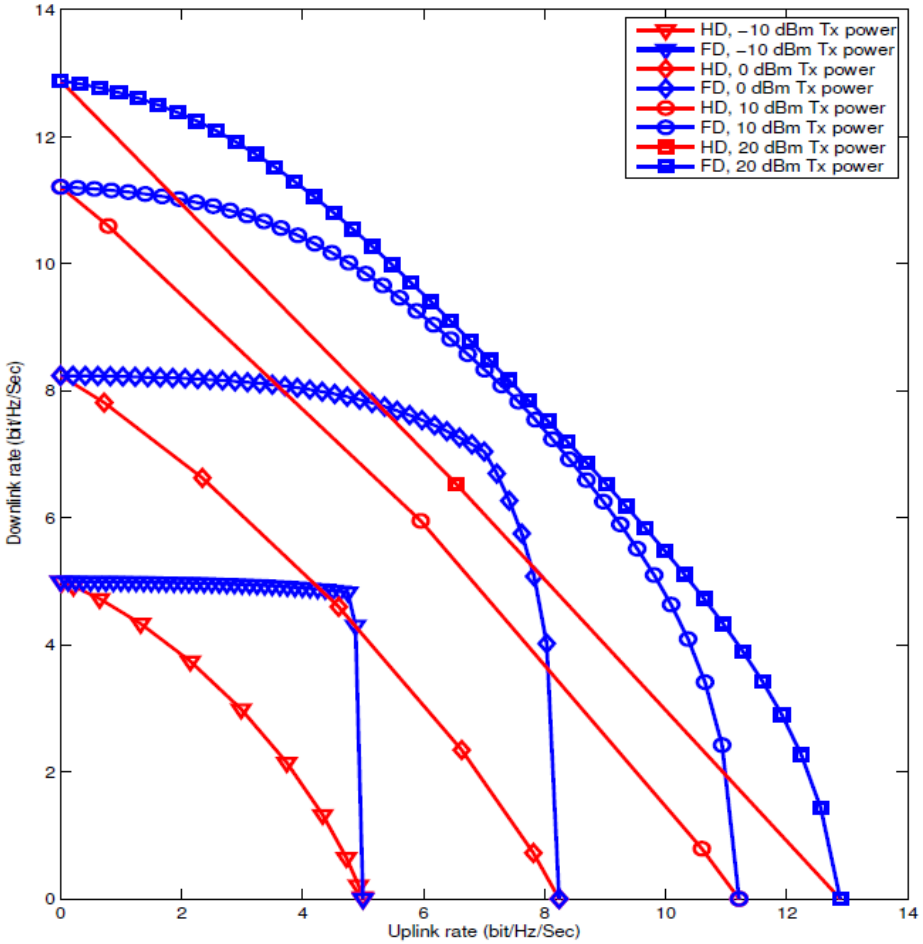

Figure 13 Full-duplex and half-duplex rate regions with different maximum transmission powers.

The strict distance limitation of FD links is clearly shown in Figure 14 where the distance between communication nodes is varied from 5 to 50 meters. While the shortest distance provides significant gains for FD, the longest distance reverses the situation. It is worth noting that the FD rate region remains convex while larger than that of the HD mode. Figure 15 details the general full-duplex rate region at 50 m link distance. The dashed line represents the boundary of the general FD rate region that is larger than the directly achievable FD one (blue line with circular markers) and only slightly lesser than that of the HD mode.

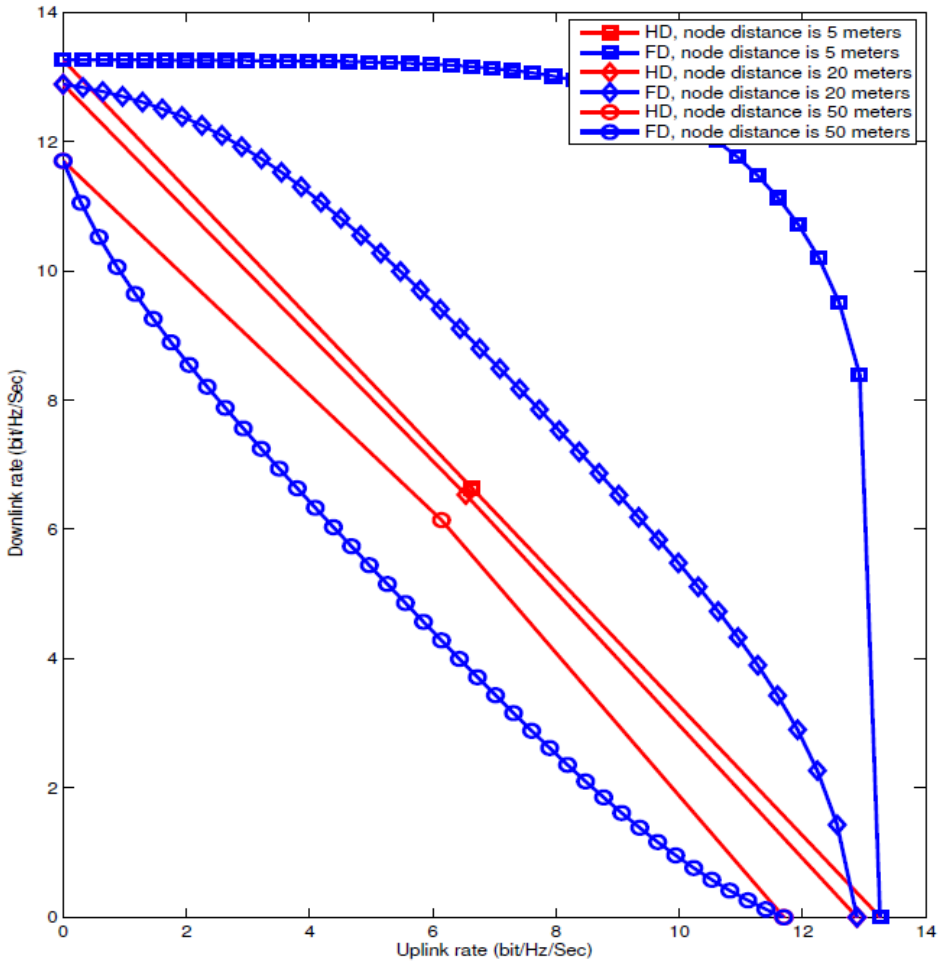

Figure 14 Full-duplex and half-duplex rate regions with different communication ranges

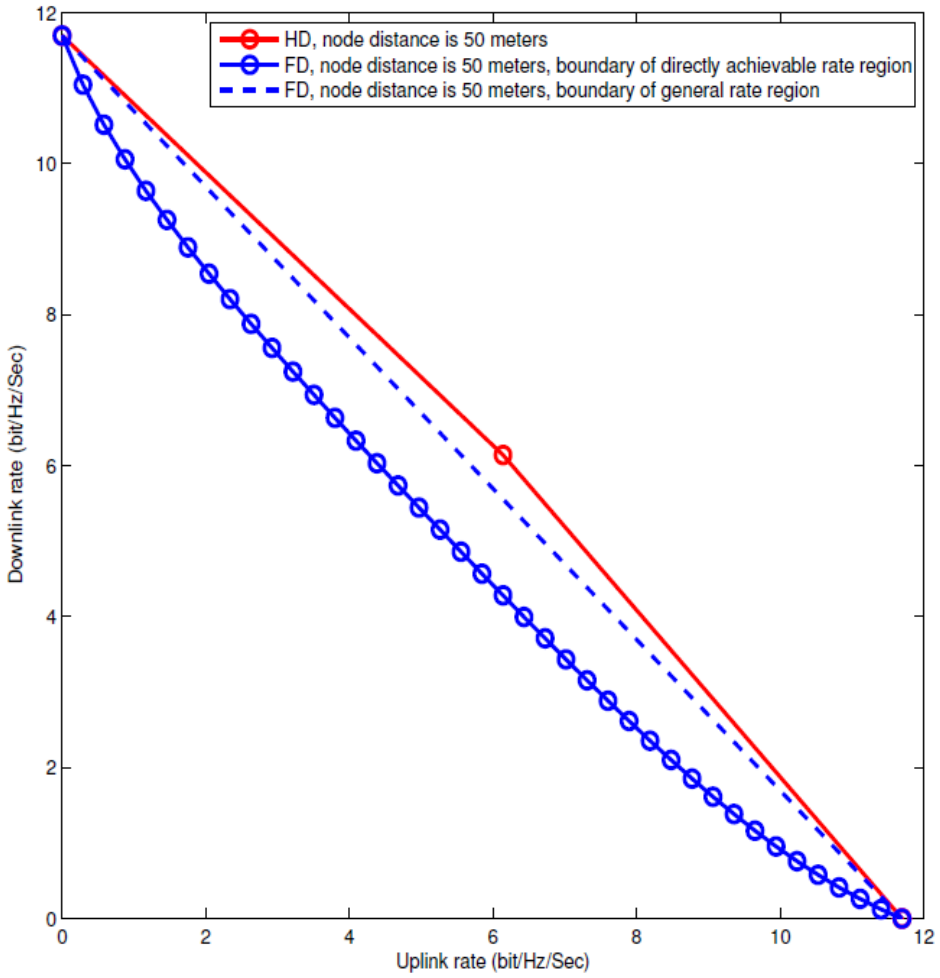

Figure 15 Full-duplex and half-duplex rate regions with general boundaries using time sharing method.

Energy efficiency is also important to be assessed in the comparative framework of FD and HD communications. For that, the consumed transmission power to achieve a certain rate region is evaluated next. Figure 16 plots the achievable rate region contours with different power consumption values. It can be concluded that FD link can achieve over 75% of its rate region with 1 dB less power consumption than that of the HD link. Furthermore, in the area around downlink-uplink rate pair {4.5, 4.5} bit/Hz/s the power efficiency advantage is larger than 6 dB.

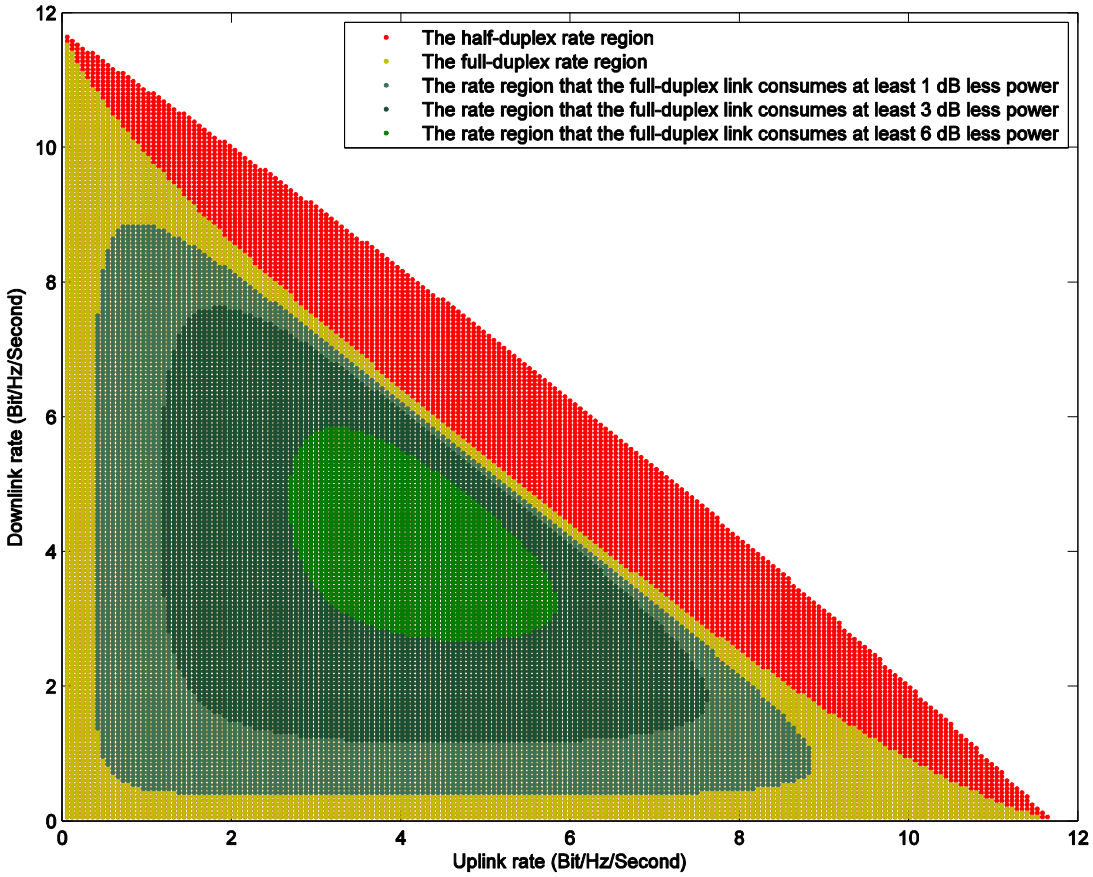

Figure 16 Sum transmission powers of using full- and half-duplex technologies.

As a conclusion of the rate region study we can state that in the comparison of uniform and non-uniform power allocation the latter allows for higher full-duplex throughput gain over half-duplex in frequency selective fading environment. In the presence of -30 or -40 dBc EVM noise and having respective total SI cancellation 85 or 87 dB ensures comparable FD and HD rate regions. At low transmission powers the maximum FD rate can be twice the HD rate but by increasing Tx power the gap between them decreases. FD link distances should be short enough. Finally, FD has also good energy saving properties when achieving the maximum link rate is not the primary target.

2.2. Power Allocation polices

In this section, we will present the performance analysis of full-duplex transmission link and power allocation scheme to accommodate the asymmetric traffic distribution between downlink and uplink. The objective in the conducted joint rate and power allocation scheme study is to enhance the overall performance of BS-UE connection in asymmetric traffic case, by maximizing the downlink data rate while keeping the uplink at required quality of service (QoS) level [34], section 2.2 of DUPLO D4.2 [5].

2.2.1. Introduction

The link level model with full-duplex node at both ends is presented in Figure 17. The simulation parameters are listed in Table 2. An OFDM signal over the 20 MHz bandwidth is assumed. The desired signal passed through an additive white Gaussian noise (AWGN) channel which attenuates the signal at 70 dB. Assuming a single path propagation channel and free-space path-loss, this would be equivalent to a distance of 38 m at 2.0 GHz, or a distance of 15 m at 5.0 GHz. It is assumed that the SI channel is AWGN, and the full-duplex transceiver is capable to provide SI cancellation at both ends. To evaluate the overall performance of the system, achieved BER at the receiver and throughputs are calculated.

Table 2 Simulation parameters

Parameters	Value
Bandwidth	20 MHz
Transmit power BS	[0, 20] dBm
Transmit power UE	[0, 10] dBm
Channel path loss	70 dB
Cancellation at BS	90 dB
Cancellation at UE	70 dB

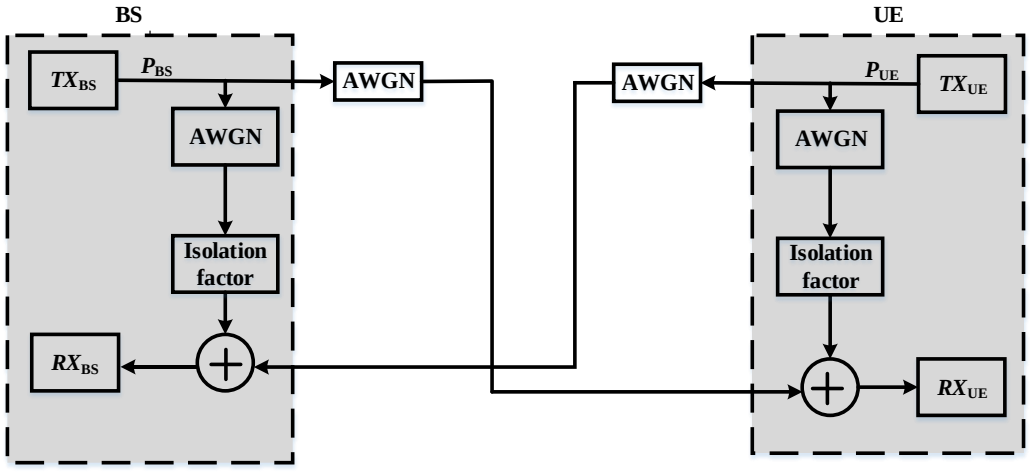

Figure 17 Simulation Model

2.2.2. Numerical Results

To characterize the full-duplex transmission and validate the performance of the designed scheme, performance measure based on BER and throughput is considered with different modulation schemes like BPSK, QPSK, 16-QAM and 64-QAM. Furthermore, a comparison between full-duplex without power control and full-duplex with proposed power control is presented to highlight the potential gain in downlink data rate in case of asymmetric traffic. In the full-duplex without power control (FD-T) scenario, power allocation is fixed for both downlink (FD-D) and uplink (FD-U) users. On the other hand, in the proposed scheme, power allocation is optimized according to the required uplink SINR and traffic conditions to improve the downlink rate.

In Figure 18 the BER performance of the full-duplex transmission with different modulation schemes for downlink and uplink is shown. It can be noted that initially uplink SINR 'Υ_{UL}' is 20 dB to illustrate the effect of increase in downlink SINR 'Υ_{DL}'. The detrimental effect in Υ_{UL} is due to the increase in interference caused by the collocated transmitter. The increase in collocated transmitter power will effect until a certain threshold after which BER of the collocated receiver get worse and no more transmission is observed. The results exhibit that with the increase in the downlink power level, DL becomes better but at the same time Υ_{UL} degrades with the same factor. Thus, uplink with a low power can coexist, as an underlay transmission, with the downlink on the same frequency band. The coexistence depends on the transmission power at both nodes.

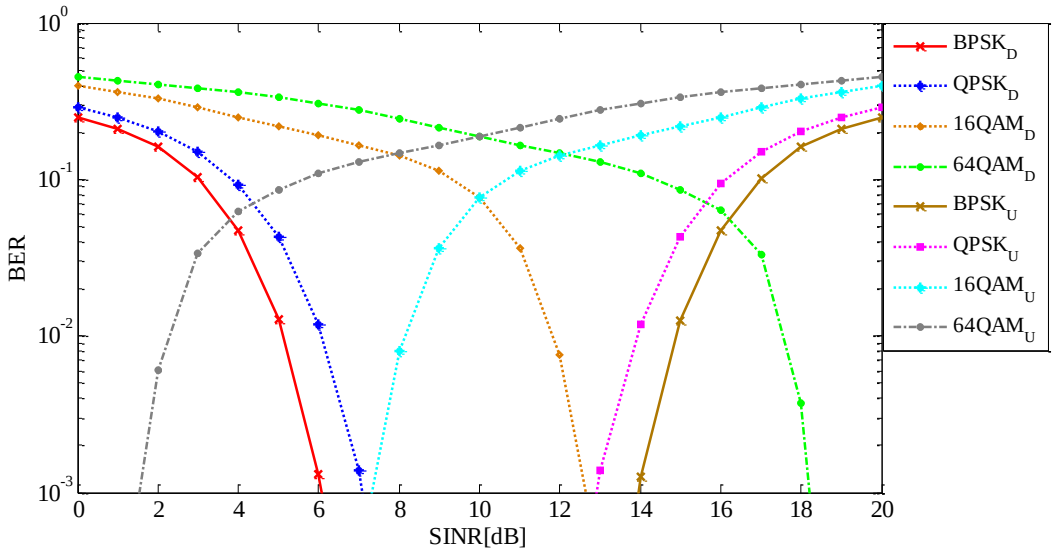

Figure 18 BER performance of full-duplex transmission

Figure 19 shows the overall system throughput comparison between half-duplex, full-duplex and full-duplex with the proposed scheme. It can be seen that with the proposed scheme, the downlink rate can be increased with the degradation in uplink while satisfying the SINR and QoS constraints. When we consider both the physical layer and the MAC layer, the low SINR region suffers from the low packet transmission rate and the high SINR region suffers from the increased interference. At the optimal SINR the physical layer and the MAC layer are balanced to achieve the maximum throughput.

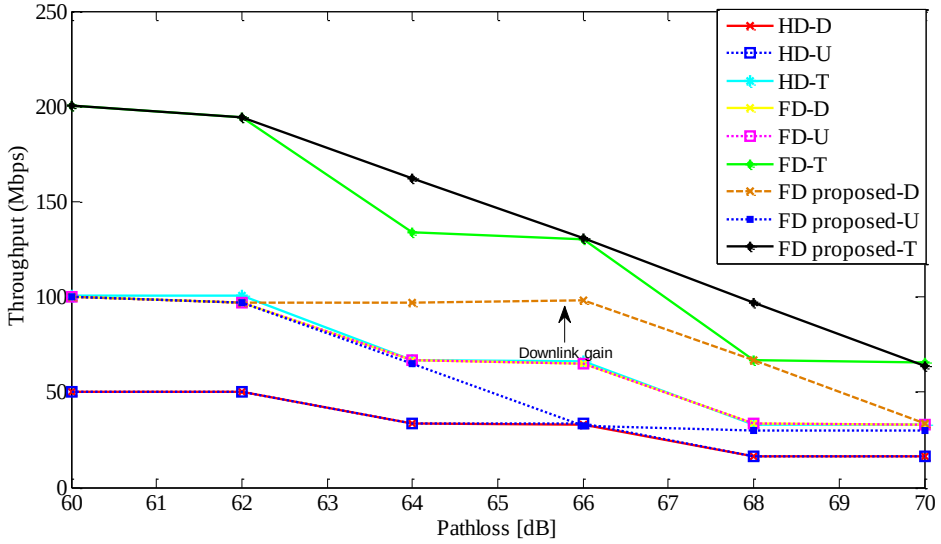

Figure 19 Throughput performance comparison

The improvement rate of the proposed scheme over the general full-duplex in the presence of asymmetric traffic between downlink and uplink is shown in Figure 20. Asymmetric traffic is modelled in a way that during general full-duplex transmission, the resource block allocation depends on the uplink traffic buffers where as in the proposed scheme the resource block remains constant but the modulation scheme is chosen according to the power allocated to both downlink and uplink. It can be seen that after 50% of uplink traffic, with the proposed scheme the overall throughput of the system improves greatly but the uplink degrades. This is because of the trade-off that the downlink performance improves while the uplink performance degrades. Furthermore, after achieving a saturation point of downlink, there is degradation to overall system throughput. Thus, the proposed model with power and rate control is effective for asymmetric traffic accommodation in full-duplex networks as well as improve overall system throughput greatly.

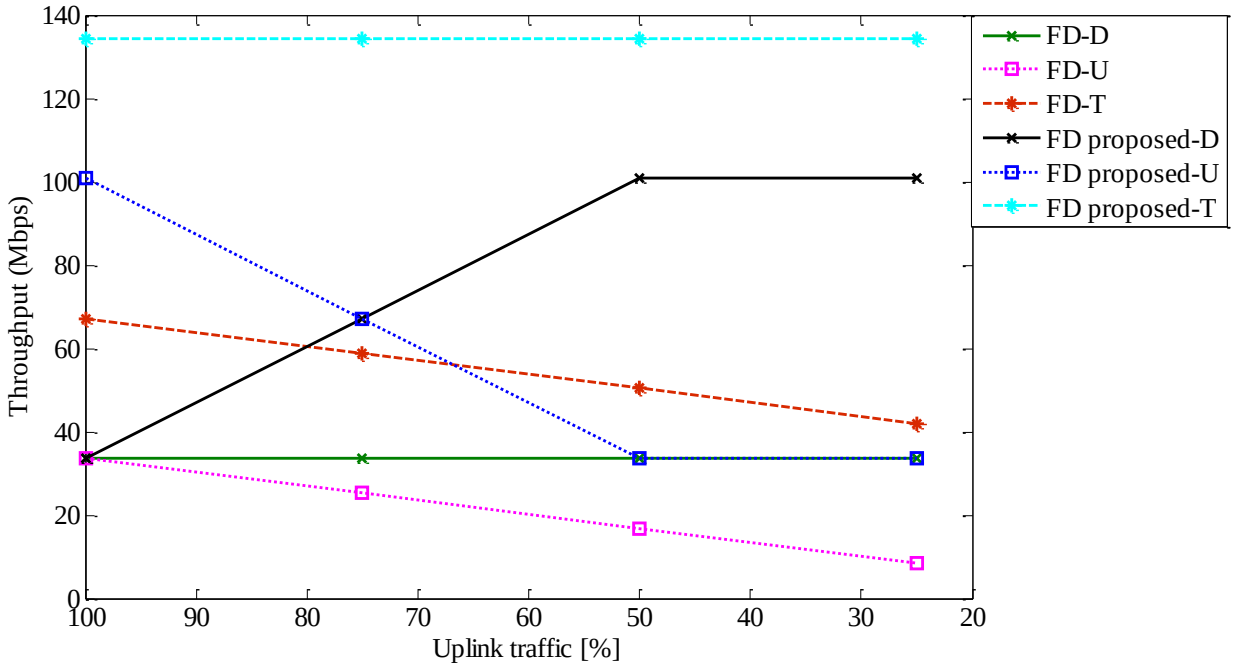

Figure 20 Throughput comparison in asymmetric traffic

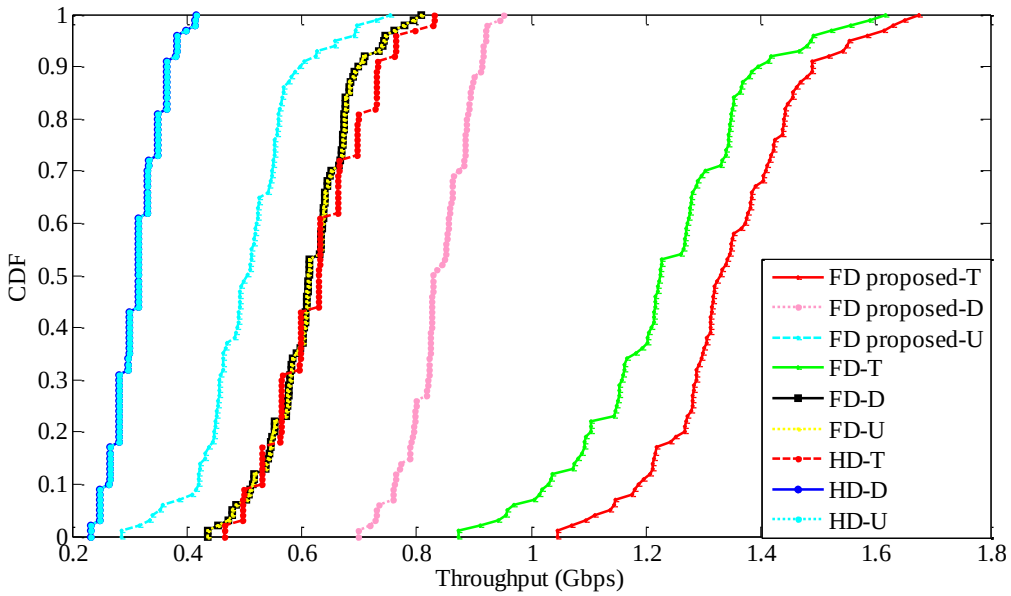

Figure 21 Throughput performance in multiuser scenario

To reflect the results achieved with proposed scheme in multiuser scenarios, a cell with randomly distributed users is simulated. The medium access is based on time-slot with each user having downlink and uplink at the same time. Figure 21 shows CDF graph of throughput performance of half-duplex, full-duplex and full-duplex with proposed scheme. It can be seen that the same improvement in throughput with the proposed scheme is observed when employed on a network with multiple nodes.

The average throughput of the downlink improves thus resulting in increase of overall system performance. Although the uplink performance degrades compared with the general full-duplex transmission, its throughput is still higher than half-duplex one. Therefore, it can be concluded that the proposed scheme helps to accommodate the asymmetric traffic and results in better system performance.

This section provided a model to accommodate the asymmetric traffic in full-duplex network when the communicating nodes employ SI cancellation. The cross-layer scheme consisting of power and rate allocation has been proposed to enhance the overall system performance particularly in downlink data rate while keeping uplink at required QoS. The BER and throughput performance have been evaluated by simulations to analyse the full-duplex transmission and to demonstrate the effectiveness of the proposed scheme. The simulation results illustrate that the downlink data rate improves significantly resulting in increase of overall system performance in the presence of asymmetric traffic for full-duplex networks.

3. SINGLE FULL-DUPLEX SMALL CELL

Using the target scenarios identified in DUPLO deliverable D1.1 [6] and Section 1.2.1 of this deliverable, the system performance of different types of full-duplex small cells is discussed here.

3.1. Multiple HD UEs per FD BS in single cell deployment scenario

3.1.1. Power allocation strategies

In this section, the system-level performance of the proposed radio resource allocation in Section 3.4 of DUPLO Deliverable D4.2 [5] is evaluated through Monte Carlo simulation. A single-cell with 200 m radius is considered, where the users' locations are randomly generated and uniformly distributed within the cell. The full-duplex base-station has 30 dBm maximum transmit power, and the half-duplex users each has 23 dBm maximum transmit power. The total number of users is 20, with 10 downlink users and 10 uplink users. In the simulation, the iterative algorithm stops if the gain in spectral efficiency between two successive iterations is less than 10^{-5} bit/s/Hz. The system bandwidth is 10 MHz consisting of 50 resource blocks, and the noise power spectral density is −173 dBm/Hz. Noise figures of 5 dB and 9 dB are considered for the base-station and user equipment, respectively. The ITU pedestrian B fast fading model and the line-of-sight (LoS) pathloss model for pico-cell environment are used [6]-[8]. With 2 GHz frequency, the pathloss will be

$$PL_{\text{LoS}} = 41.1 + 20.9\log_{10}(d), \quad \text{(dB)}, \tag{1}$$

where d is the distance in meters between the users and the base-station. COST231 Hata propagation model [9] is used to obtain the large scale fading between two users, which is given by

$$PL_{\text{UE2UE}} = 35.68 + 38\log_{10}(d), \quad \text{(dB)}. \tag{2}$$

3.1.1.1. Simulations parameters and numerical results

First, we examine the convergence behavior of the algorithm. Figure 22 shows the average rate of convergence of the algorithm in terms of percentage of the equilibrium, where the results are averaged over 100 channel realizations. The results show that, on average the algorithm reaches about 99% of the convergence point with 6 iterations only, which is significantly faster than algorithms seeking the optimal solution of nonconvex problem. Based on this observation, for further simulations we have used 20 as the maximum number of iterations for the algorithm to keep the complexity low.

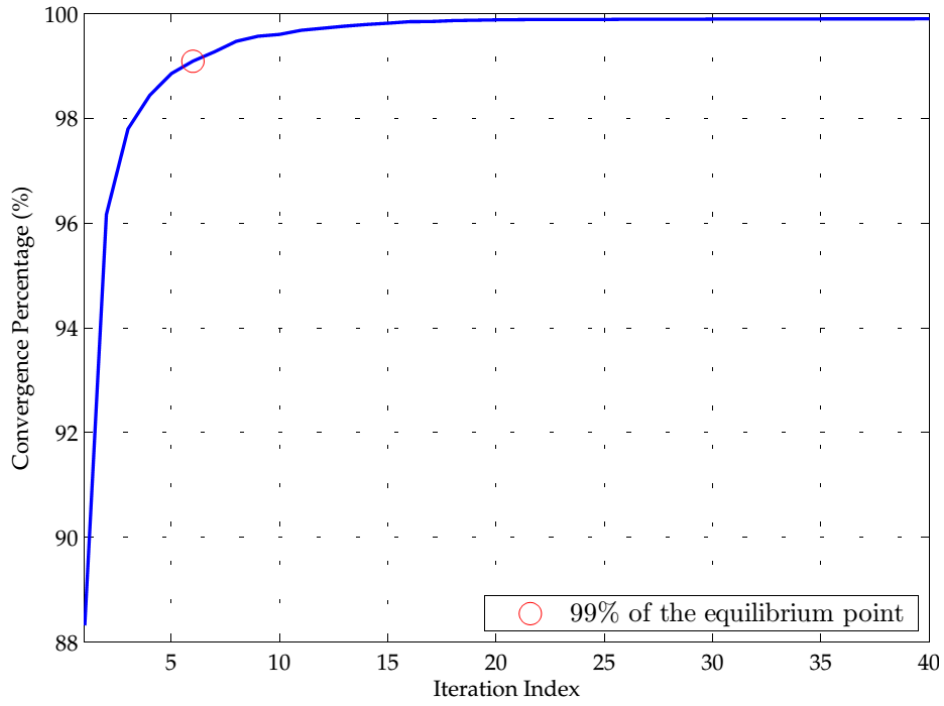

Figure 22 Average convergence of the proposed iterative algorithm.

Figure 23 shows the cumulative distribution function (CDF) of the sum-rate for full-duplex system, with different self-interference cancellation values. As benchmarks for comparison, we used full-duplex with equal power allocation and time-division duplex (TDD), i.e. half-duplex system, with optimal subcarrier and power allocation. For the TDD downlink, the resource allocation from [10] is used, while for uplink we use the iterative water-filling [11]. It is worth mentioning that these two algorithms give an upper bound on the TDD system sum-rate. The equal power allocation is simulated with −100 dB self-interference cancellation. The figure shows that the proposed resource allocation algorithm can significantly improve the full-duplex performance comparing to equal power allocation. For the same cancellation factors, the proposed algorithm achieves about 70% gain in average sum-rate comparing to equal power allocation. Also, the figure shows that for self-interference cancellation more than −85 dB, the full-duplex significantly improves the system spectral efficiency comparing to the half-duplex system. Figure 24 shows the percentage of full-duplex gain in average sum-rate over half-duplex system. Up to 40% gain can be achieved with the currently reported self-interference cancellation capabilities [12].

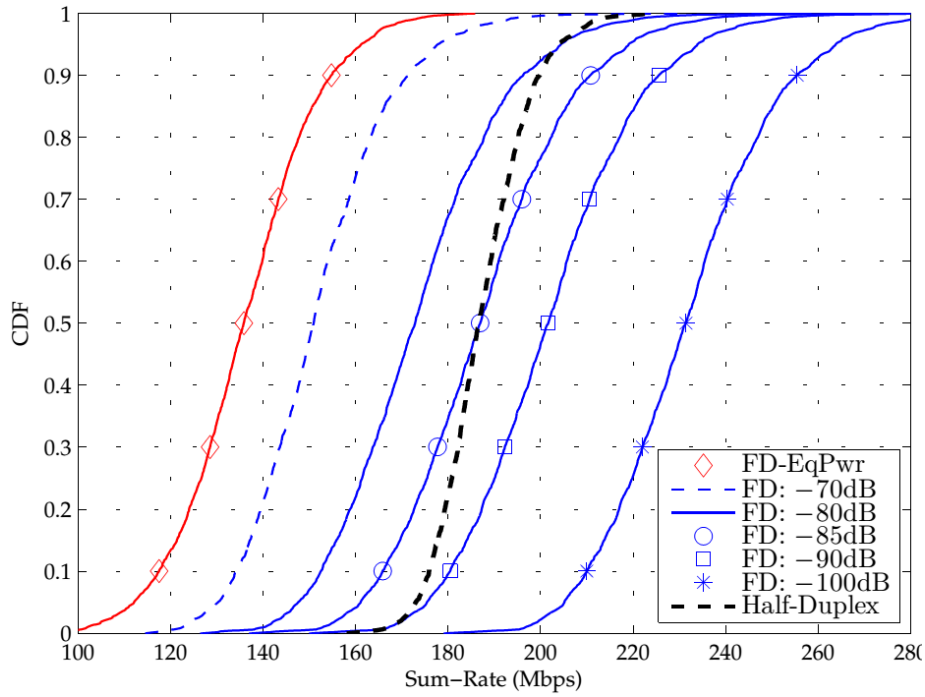

Figure 23 Sum-rate comparison for full-duplex and half-duplex systems.

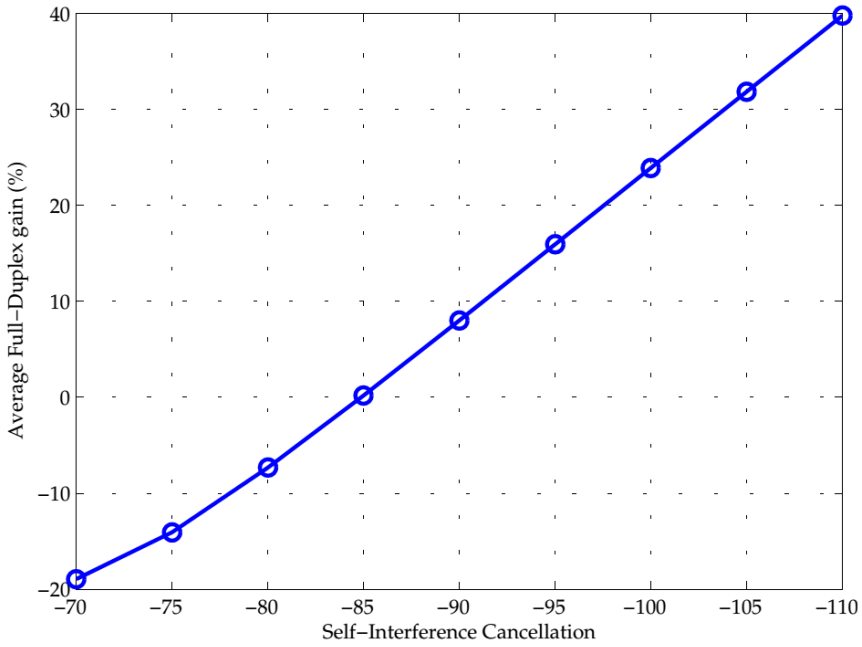

Figure 24 Sum-rate gain of full-duplex comparing to half-duplex.

Overall, it can be concluded that the proposed algorithm has fast convergence rate, and greatly outperforms the equal power allocation approach. Also, with proper radio resources allocation, considerable gain in sum-rate can be achieved by using the full-duplex technique with the currently

feasible self-interference cancellation capabilities. We believe these results give insights into the potential gains and provide practical guidance for implementing the full-duplex technique.

3.1.2. Scheduling methods for FD single cells

Next generation wireless communication systems dynamically schedule users, and allocate subcarriers and power among them in order to meet the quality of service (QoS) requirements of each user, and to utilize the limited resources efficiently. The scheduling issue of the full-duplex cellular networks, where a full-duplex mode base station communicates with half-duplex mode users, was considered in [21]-[23]. In particular, a sub-optimal scheduling algorithm to maximize the system throughput is proposed in [23], and a hybrid scheduler that can switch between full-duplex and half-duplex modes to maximize the system throughput as well as to ensure fairness is proposed in [21], but these works have not considered the power allocation.

In this section, we evaluate the performance of three resource allocation algorithms discussed in [24]-[26] which consider both the subcarrier and power allocation for an OFDMA system having a full-duplex base-station with randomly distributed half-duplex uplink and downlink users. A simple three-step algorithm is proposed in [24] to maximize the sum-rate of the full-duplex system subject to predefined target rate constraints at the uplink and downlink users, and transmit power constraints at the base-station and uplink users. Depending on the locations of the mobile users, propagation channels, the self-interference cancellation capability of the base-station, transmission power of the mobile users and base-station, etc, it might be better to switch to half-duplex mode. Therefore, a dynamic hybrid scheduler that can switch between half-duplex uplink, half-duplex downlink and full-duplex mode opportunistically to maximize the sum-rate has been designed in [25]. The algorithms in [24]-[25] assume perfect channel state information (CSI) at the transmitting nodes which may be unrealistic because of user mobility, feedback/processing delay and small channel coherence time. Therefore, a subcarrier and rate allocation for full-duplex OFDMA systems under imperfect CSI has been studied in [26]. The scheduling algorithms are described in section 3.2 of DUPLO deliverable D4.2 [5].

The simulation results in [24]-[26] show that under 3GPP LTE, the proposed scheduling algorithms outperform half-duplex scheduling at self-interference cancellation levels that have been achieved recently.

3.1.2.1. Simulations parameters, assumptions and numerical results

In this section, we compare the proposed full-duplex scheduling algorithms in [24]-[26] with the traditional half-duplex scheduling algorithms under the 3GPP LTE specifications for small cell

deployments [27]. A single hexagonal cell having a base-station in the center with randomly distributed 10 uplink and 10 downlink users is studied. The channel between base-station and users are assumed to experience the path loss model for line-of-sight (LOS) and non-line-of-sight (NLOS) communications depending on the probability

$$P_{\text{LOS}} = 0.5 - \min(0.5, 5\exp(-0.156/d)) + \min(0.5, 5\exp(-d/0.03)), \quad (3)$$

where *d* is the distance between base-station and users in km. Without loss of generality, power constraints of uplink users are assumed to be equal. Detailed simulation parameters adopted from [27] are shown in the Table 3. The channel gains between nodes include both small scale fading following a complex Gaussian distribution with zero mean and unit variance and large scale fading consisting of path loss and shadowing calculated from a specific path loss model given in Table 3.

Table 3: Simulation Parameters

Parameter	Settings
Cell Radius	40m
Number of subcarriers	$N = 1024$
$\left[\left\|\mathcal{I}^{UL}\right\|, \left\|\mathcal{K}^{DL}\right\|\right]$	[10, 10]
Bandwidth	10MHz
Maximum BS Power	$P_{\mathcal{T}} = 24$dBm
Maximum user Power	$P_i = 23$dBm
Thermal Noise Density	-174dBm/Hz
Noise Figure	BS: 13dB, User: 9dB
Path Loss (dB) between BS and users (d in km)	LOS: $103.8 + 20.9\log_{10} d$ NLOS: $145.4 + 37.5\log_{10} d$
Path Loss (dB) between users (d in km)	LOS: $98.45 + 20\log_{10} d$, $d \leq 50$m NLOS: $175.78 + 40\log_{10} d$, $d > 50$m
Shadowing Standard Deviation	LOS: 3dB, NLOS: 4dB
Rate Target	$R_t^{DL} = 4$Mbps, $R_t^{UL} = 2$Mbps

We will first start with evaluation of the algorithm proposed in [24]. In Figure 25, the distribution of average full-duplex (FD), half-duplex uplink (HD-UL), and half-duplex downlink (HD-DL) rates over 500 drops are shown under various self-interference cancellation levels. It is seen that the self-interference needs to cancel at least 80dB so that full-duplex system achieves higher sum-rate than half-duplex system.

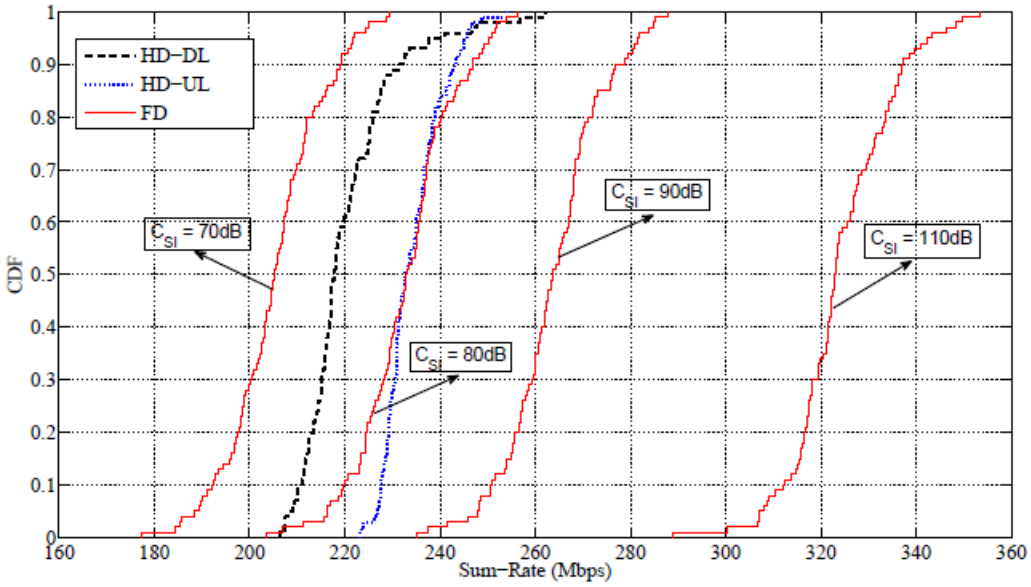

Figure 25: Average sum-rate comparison of FD and HD systems under iterative water-filling.

Since self-interference cancellation level, i.e. C_{SI} only affects the uplink rate, in Table 4 we show the average gain of full-duplex uplink channel over half-duplex uplink channel. Note that we also observe 23% average gain in the downlink channel.

Table 4: Average Rate Gain of Full-duplex Uplink System over Half-duplex system

C_{SI}	85dB	90dB	100dB	110dB	120dB	130dB
	0.86%	11%	39%	61%	75%	78%

In Figure 26, we show the distribution of the average full-duplex uplink rate under equal power allocation and iterative-water-filling (IWF) algorithms. It is seen that at high self-interference cancellation values, they give similar performance. There are two reasons: First, it is well known that at high signal-to-interference-to-noise-ratio (SINR), the performance gain of water-filling algorithm vanishes. Secondly, a user is assigned only to subcarriers with good channel conditions. And since variations among the channel gains of subcarriers assigned to each user are small, water-filling algorithm results in near-flat power allocation.

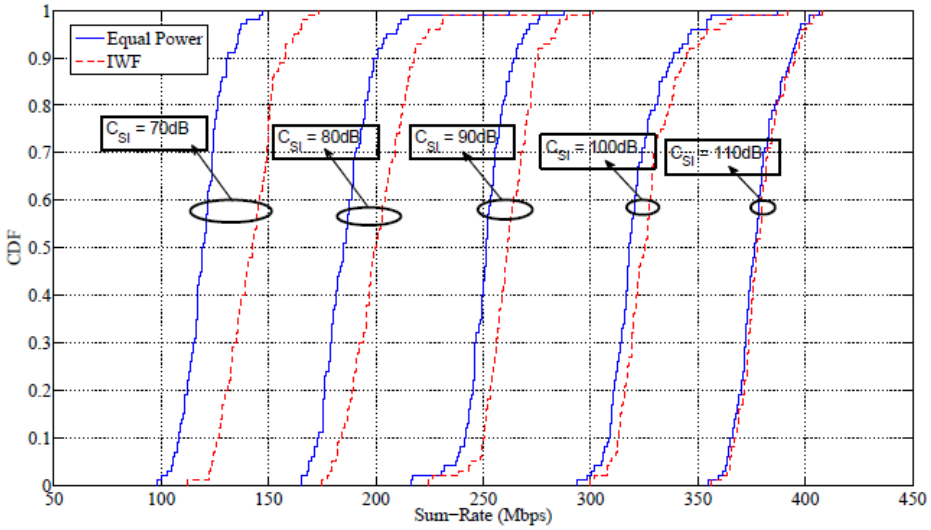

Figure 26: Uplink sum-rate comparison of FD systems under equal power allocation and iterative water-filling.

In Figure 27, the full-duplex (FD) system is compared to full-duplex Round-Robin (FD-RR) scheduling to demonstrate the importance of intelligent scheduling. It is seen that even at 130dB self-interference cancellation, FD-RR system can still not achieve the performance of the half-duplex systems. The reason is that FD-RR does not require the knowledge of CSI, and allocates the subcarriers sequentially to all uplink (downlink) users so that each uplink (downlink) user has an approximately equal number of subcarriers allocated. Therefore, it does not exploit multiuser diversity.

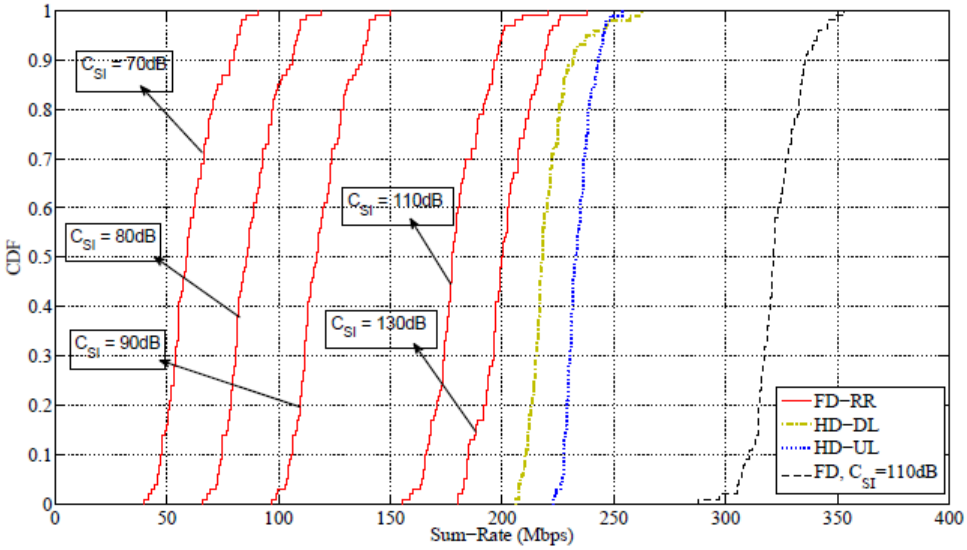

Figure 27: Average sum-rate comparison of FD and FD-RR systems under equal power allocation.

Next, we evaluate the performance of the algorithm proposed in [25]. For this algorithm, we used the same parameters as in Table 3. In Figure 28, we show the distribution of the average sum-rate for the hybrid scheduling under equal power allocation (EQ) and IWF algorithms over 500 time-slots. It is seen that at high self-interference cancellation values, the performance of two algorithms are almost the same and the reason is given in the discussion of Figure 26.

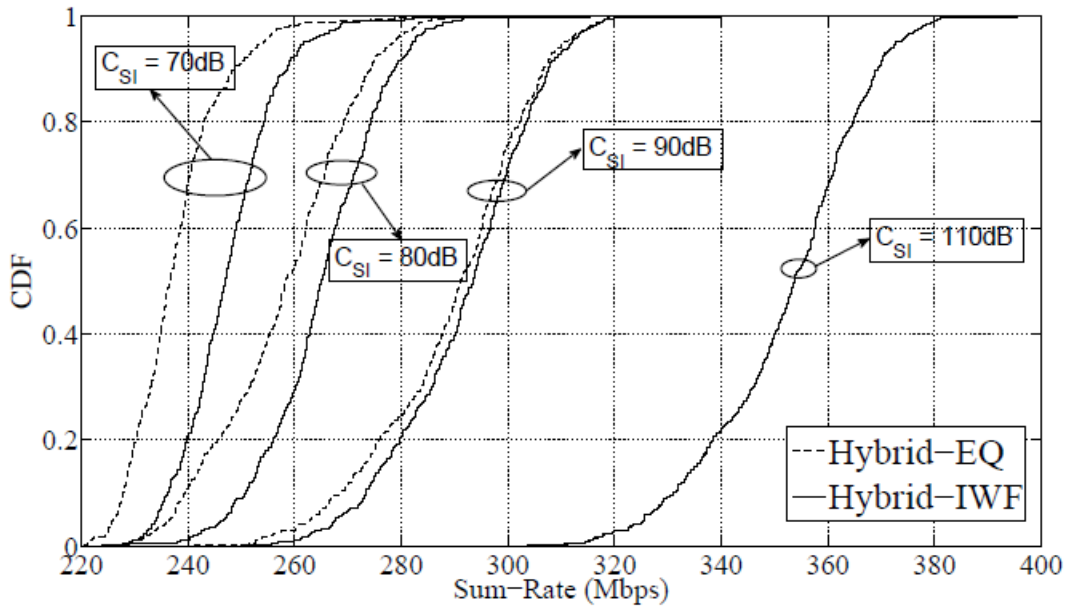

Figure 28: Average sum-rate comparison of hybrid scheduling under equal power allocation (EQ) and iterative water-filling (IWF).

In our next example, we compare the average sum-rate distribution of hybrid, half-duplex time division duplex (HD-TDD) and full-duplex (FD) scheduling. In Figure 29, it is seen that at high self-interference cancellation values, FD scheduling outperforms HD-TDD scheduling, and hybrid scheduling switches to the FD scheduling, so it is beneficial to allocate each time slot to simultaneous uplink and downlink transmission. On the other hand, at low self-interference cancellation values, HD-TDD scheduling outperforms FD scheduling, and hybrid scheduling starts switching to HD-TDD scheduling, so it is beneficial to allocate time slots either uplink or downlink transmission.

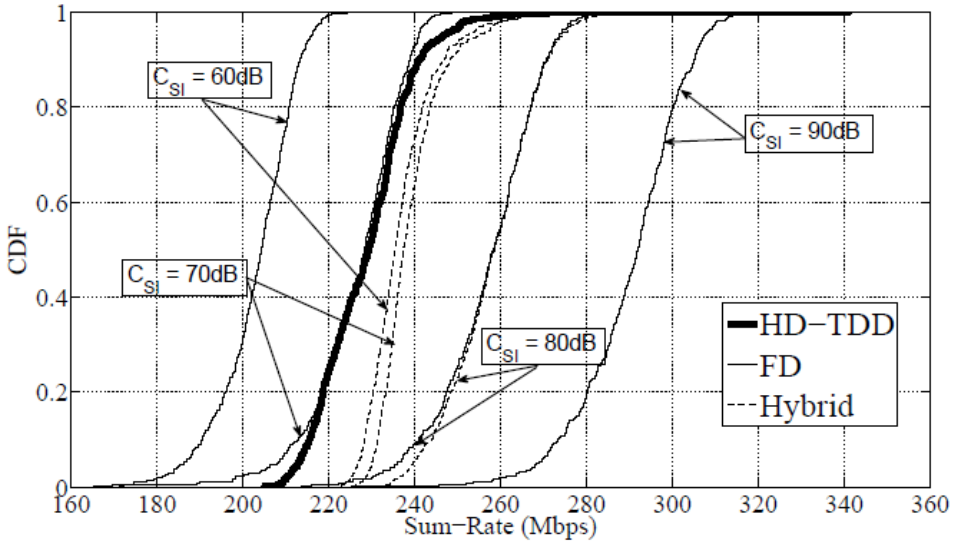

Figure 29: Average sum-rate comparison of hybrid, FD and HD-TDD systems under different self-interference cancellation values.

For the final performance analysis, unlike the previous two algorithms, we will evaluate the resource allocation for full-duplex systems under imperfect CSI. For this algorithm, we used the same parameters as in Table 3. We assume the same channel estimation error s_e^2 for all users. In Figure 30, the average goodput performance of the full-duplex system (uplink plus downlink) under different channel estimation errors and how much the performance degrades as the estimation error increases is shown.

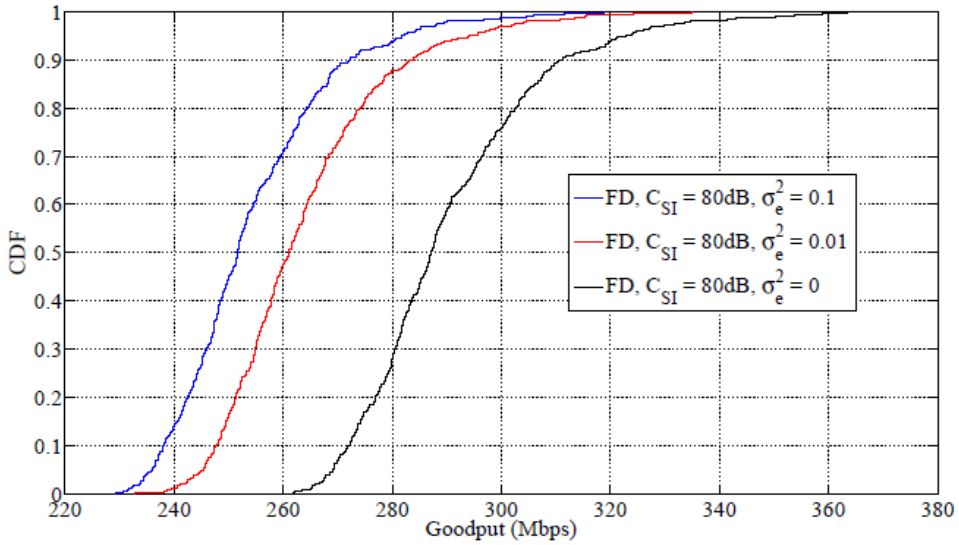

Figure 30: The CDF of full-duplex system under different channel estimation errors.

In Figure 31, we compare the uplink performance of full-duplex (FD-UL) and half-duplex (HD-UL) systems under different self-interference cancellation values, C_{SI} since uplink performance depends on C_{SI}. As it is seen, FD-UL achieves similar goodput as HD-UL around 85dB cancellation, and FD-UL outperforms HD-UL significantly at 110dB self-interference cancellation, which has been achieved recently.

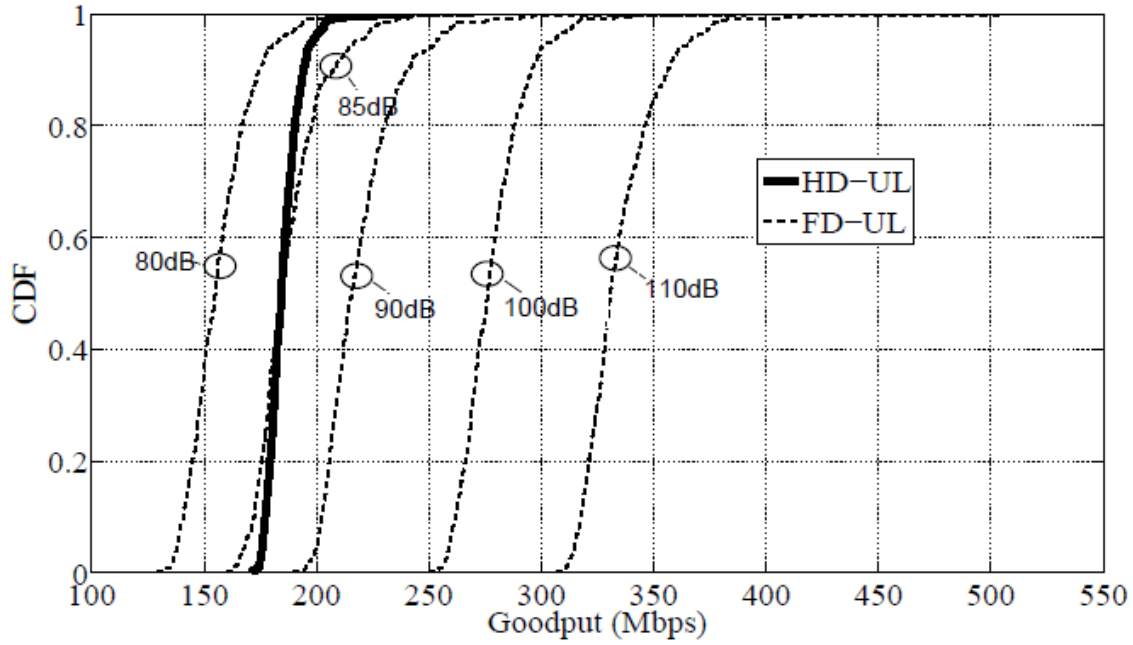

Figure 31: The goodput comparison of FD and HD uplink systems under different self-interference cancellation values.

3.1.3. Correlated co-channel interference from UL to DL

The scenario under investigation consists of users uniformly scattered over the network deployment area, operating in HD mode and sharing the whole spectrum. In every transmission interval each serving BS simultaneously schedules user terminals on both the UL and DL which share the available spectrum. The set of associated user terminals are also uniformly distributed within the transmission range of their serving cells. The serving BS transmits at a maximum power of 24 dBm and UEs use 21 dBm. UEs are distributed according to a homogeneous Poisson Point Process (PPP) so that the number of users in an arbitrary region R of area A m^2 is a Poisson RV with parameter λA. Resorting to the general framework described in [16]-[17], we can define the performance metrics presented next. Further details are found in Section 3.3 of DUPLO deliverable D4.2 [5].

3.1.3.1. Simulation parameters, assumptions and numerical results

We focus on the outage probability to assess the performance of this scenario, which is interference limited and hence the thermal noise is negligible in comparison to the resulting CCI. The evaluation scenarios are defined with regard to the correlation levels between the desired and interfering signals, transmission power and channel parameters, which are summarized in Table 5.

Table 5: Configuration Parameters

BSs Transmit Power	24 dBm
UEs Transmit Power	21 dBm
Path loss exponent	3.5
Inner radius R_m	50 m
Outer radius R_M	250 m
Standard deviation	10 dB
Nakagami-m fading figure	16

Results are given in terms of the outage which corresponds to the probability that the achieved SIR is below a predefined detection threshold. An observation region O is defined by an inner and outer radius of R_m= 50m and R_M=250m, respectively. We also consider a path loss exponent of α=3.5, a shadowing standard deviation of 10 dB, as well as a parameter m = 16 (which corresponds to a Rice channel with factor K = 14.8 dB for the Nakagami-m fading). In the default scenario, the serving BS transmits at 24 dBm, while the interfering co-site user transmits at 21 dBm.

Considering the configuration parameters given above in Table 5, Figure 32 compares the outage probability for two distinct cross-correlation values ρ = 0 and ρ = 0.8, solid and dashed lines, respectively. Results are shown for increasing separation distance between the serving BS and user of interest. The user of interest sustains a throughput of 2 bps/Hz with outage of nearly 2%, if the distance to serving BS is kept shorter than 75 m and cross-correlation is ρ = 0.8. In fact, when the separation distance is shorter, the user of interest achieves better performance in high cross-correlation scenario. However, if the separation distance to the serving BS is about 100 m, the user of interest benefits from channel diversity.

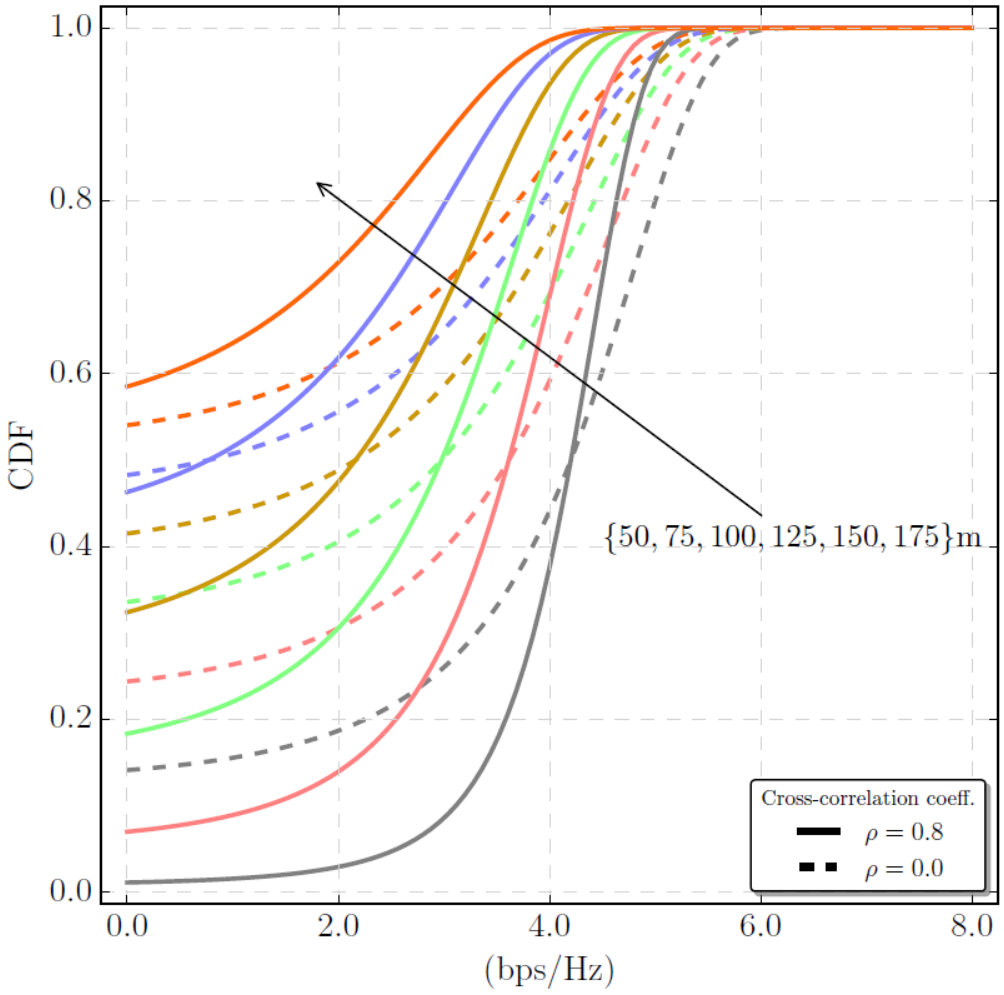

Figure 32 a) Outage probability (CDF) of the HD user of interest in the DL as function of increasing distance to the serving BS.

Figure 33 shows the performance for increasing transmission power of the interfering UL user. The serving BS transmits at 250 mW and separation distance is 75 m. Thus, the scenarios with cross-correlation of ρ = 0.8 present better performance. When compared to the previous scenario, the achievable performance is much more susceptible to the path loss attenuation than the interferer transmission power.

All in all, when the cross-correlation between the desired signal and interference component is high the SIR is sustained and the capacity is high as well. On the other hand, if the cross-correlation is low, the desired signal may fall, while the inference increases which degrades the overall system performance.

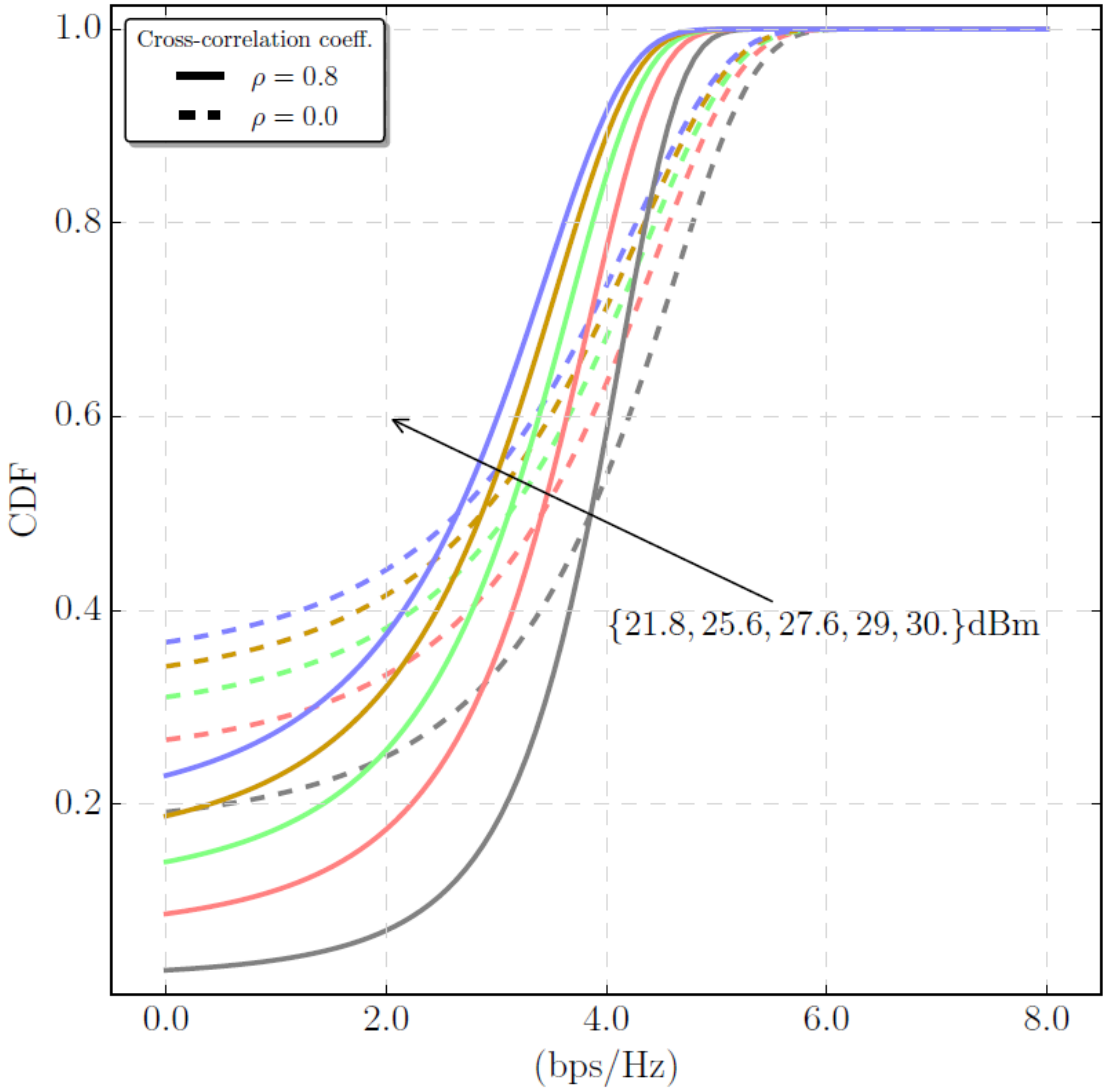

Figure 33 Outage probability of the HD user of interest in the DL as function of increasing transmission power of the interfering UL user.

3.2. Multiple FD UEs per FD BS in single cell deployment scenario

3.2.1. Numerical results

Here, we consider the same simulation parameters as in Section 3.1.1. of this deliverable. Further details are found in Section 3.4.3 of DUPLO deliverable D4.2 [5]. Figure 34 shows the cumulative distribution function (CDF) of the sum-rate for full-duplex system, with different self-interference cancellation values (assuming the same self-interference cancellation values for the user equipment and the base-station). As benchmarks for comparison, we used full-duplex with equal power allocation and time-division duplex (TDD), i.e. half-duplex system, with optimal subcarrier and power allocation. The figure shows that the proposed resource allocation algorithm can significantly improve the full-duplex performance comparing to equal power allocation. At 95 dB self-interference cancellation value, full-duplex starts to outperform half-duplex system. Figure 35 shows the percentage of full-duplex gain in average sum-rate over half-duplex system. Around 50% gain can be achieved with full-duplex using the proposed algorithm and the currently reported self-interference cancellation capabilities [12]

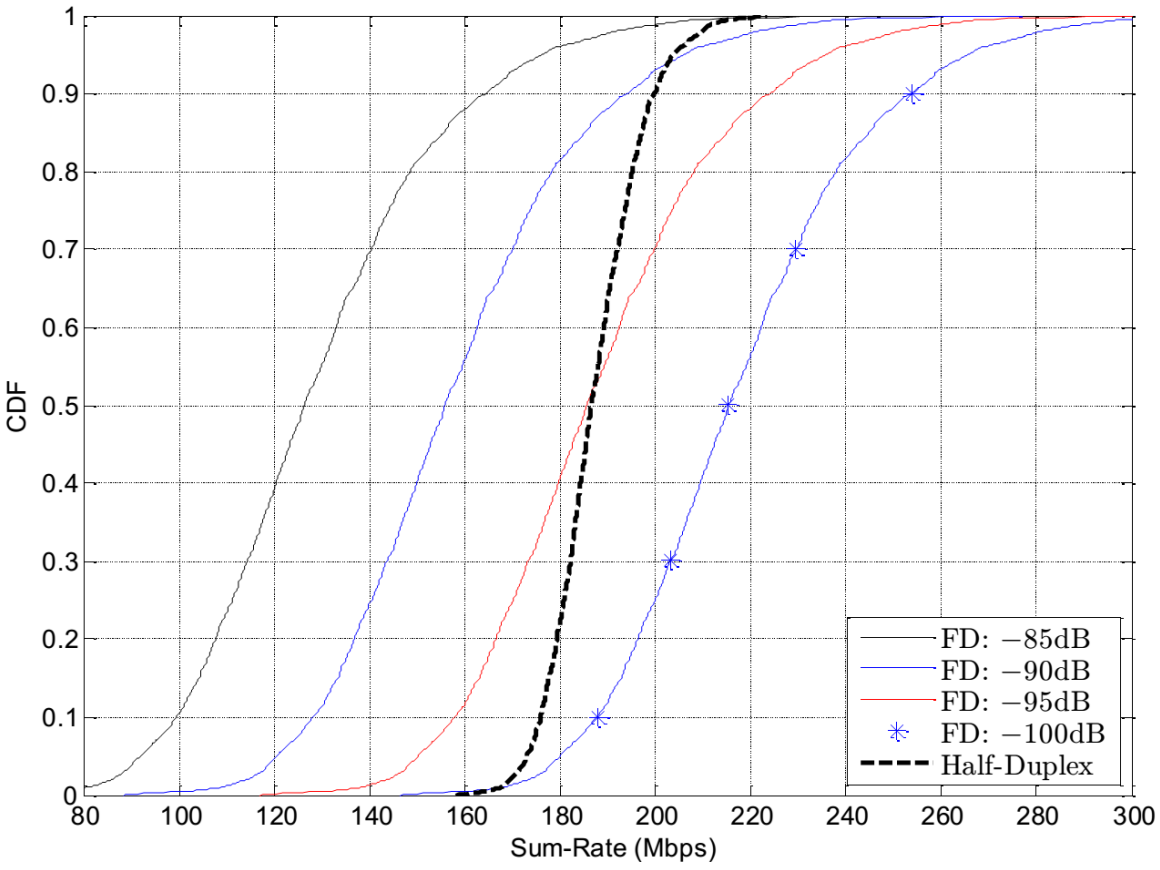

Figure 34 Sum-rate comparison for full-duplex and half-duplex systems.

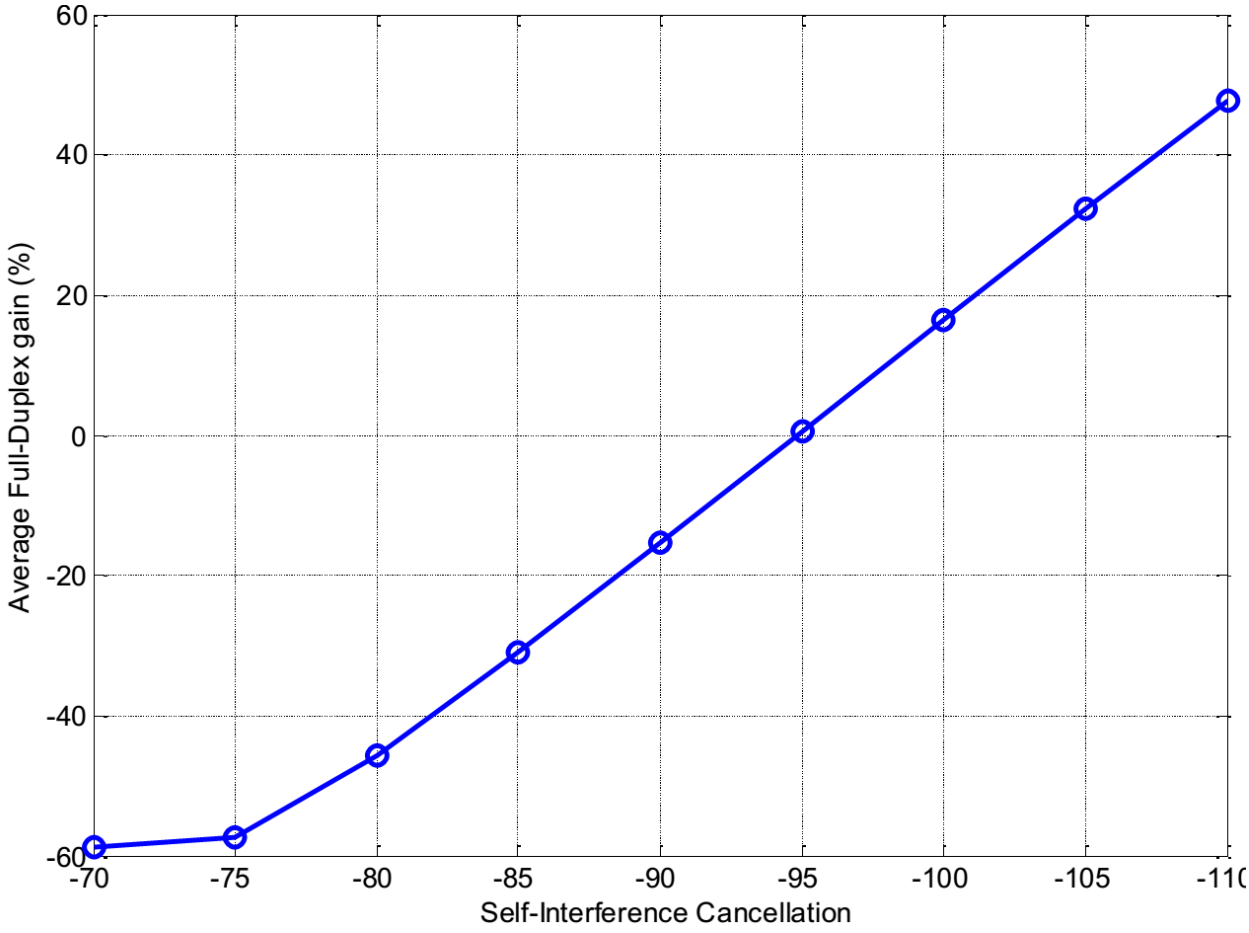

Figure 35 Sum-rate gain of full-duplex comparing to half-duplex.

3.3. Spectral efficiency and beamformer design

In this chapter we present the numerical results obtained from a study case, where a full-duplex capable base station having multiple TX/RX antennas is serving half-duplex users operating on the same frequency resources. The main objective here is to propose a joint beamformer design approach, which accounts for the downlink and uplink simultaneously. The related algorithms and protocols are defined in [31], [32], as well as in section 3.1 of DUPLO deliverable D4.2 [5].

3.3.1. Numerical Performance Results

The first set of numerical examples compares the complexity and convergence rate of the studied algorithms, i.e., determinant maximization (MAXDET) and semidefinite program (SDP) based algorithms, referred here 'Algorithm 3' and 'Algorithm 4', respectively [5]. Averaged over the number of random channel realizations we can observe from Figure 36 that convergence of the MAXDET-based Algorithm 3 is generally faster than that of the SDP-based Algorithm 4.

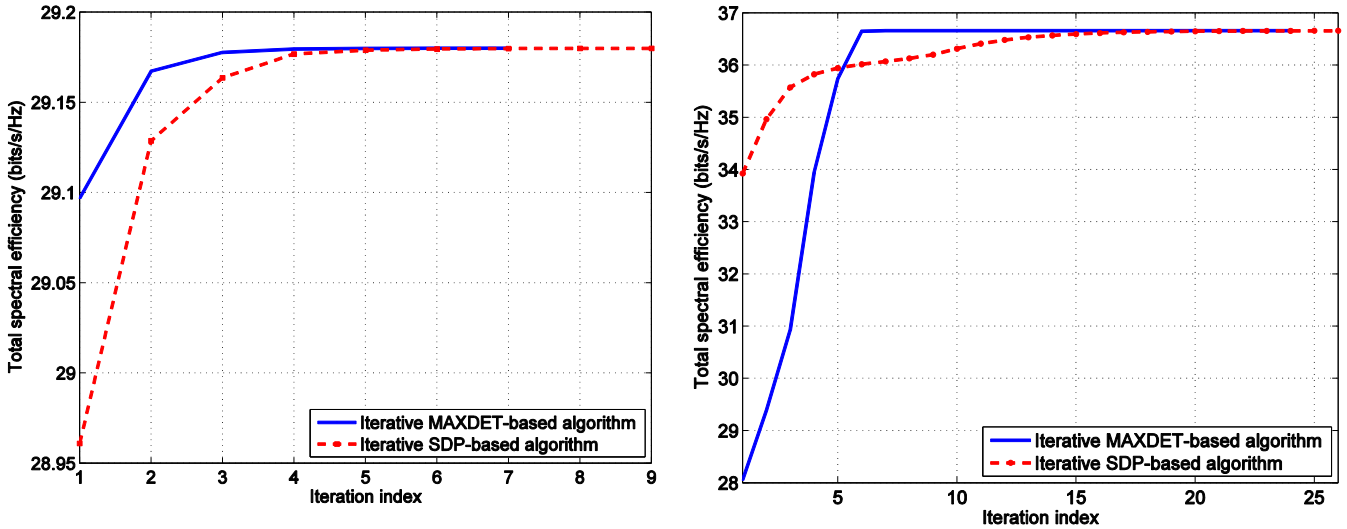

Figure 36. Convergence rate a) with i.i.d. channel realizations with $K_D = K_U = 4$ and $N_T = N_R = 4$, b) with more realistic channel with $K_D = 6$, $K_U = 4$ and $N_T = 4$, $N_R = 2$.

Figure 37-a) depicts the average spectral efficiency gain of FD over HD in the downlink direction as a function of residual SI. The system scenario assumes two fixed location downlink users and two fixed location uplink users around the base station (link distances ≤ 100 m). Maximum transmission powers both at the UE and BS are varied as shown in the legend. FD gives substantial SE gain in the

whole range of SI variance. The joint optimization schemes gradually reduce downlink transmission power as a function of SI variance to maintain spectral efficiency of the uplink channel. At higher levels of SI the uplink transmission power is significantly decreased (and thereby CCI) and thus the downlink spectral efficiency gain grows. The average uplink spectral efficiency gain decreases monotonically with increasing SI variance as illustrated in Figure 37-b). In the uplink FD performs better than HD only in the regime of low residual self-interference.

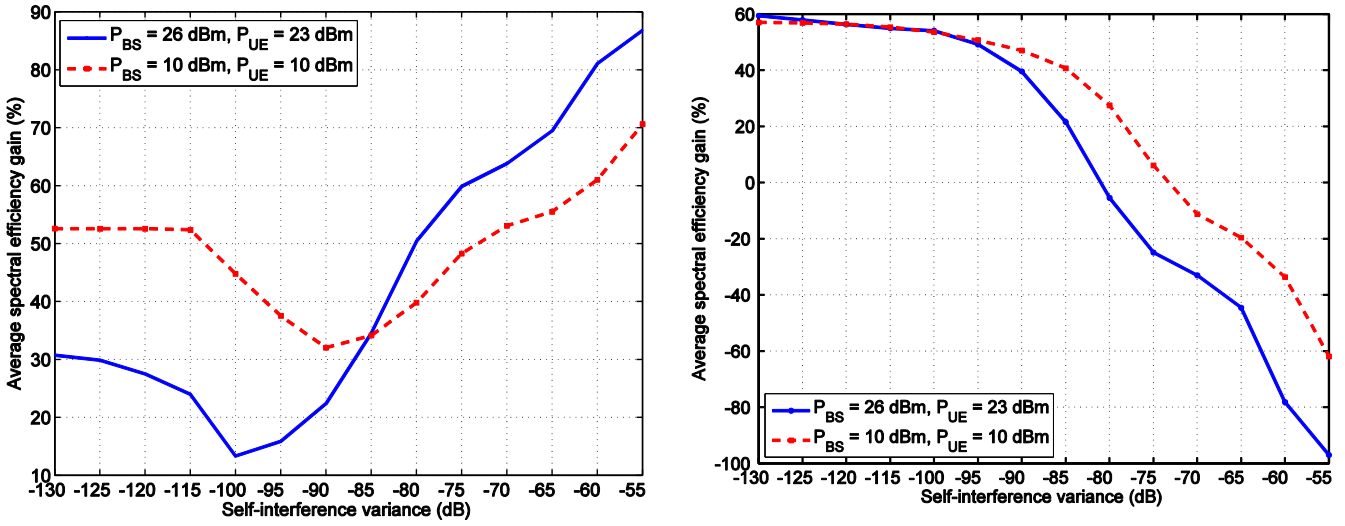

Figure 37. Average spectral efficiency gain of: a) downlink channel, b) uplink channel.

Figure 38-a) combines the performance of both link directions to obtain the total system gain. This gain decreases gradually as a function of SI variance σ_{SI}^2 up to the point around -60 to -55 dB where the HD starts to outperform the FD configuration in terms of the spectral efficiency. A slightly different view to the total spectral efficiency gain is plotted Figure 38 b) where the cumulative distribution function (CDF) of the total spectral efficiency gain is shown at two fixed levels of SI variance, namely σ_{SI}^2 = -90 and -80 dB. From these curves we can confirm (as already seen in earlier results) that lower transmit power provides better results. It can also be noted that with these levels of SI the negative SE gains are almost negligible at the tails of the CDFs.

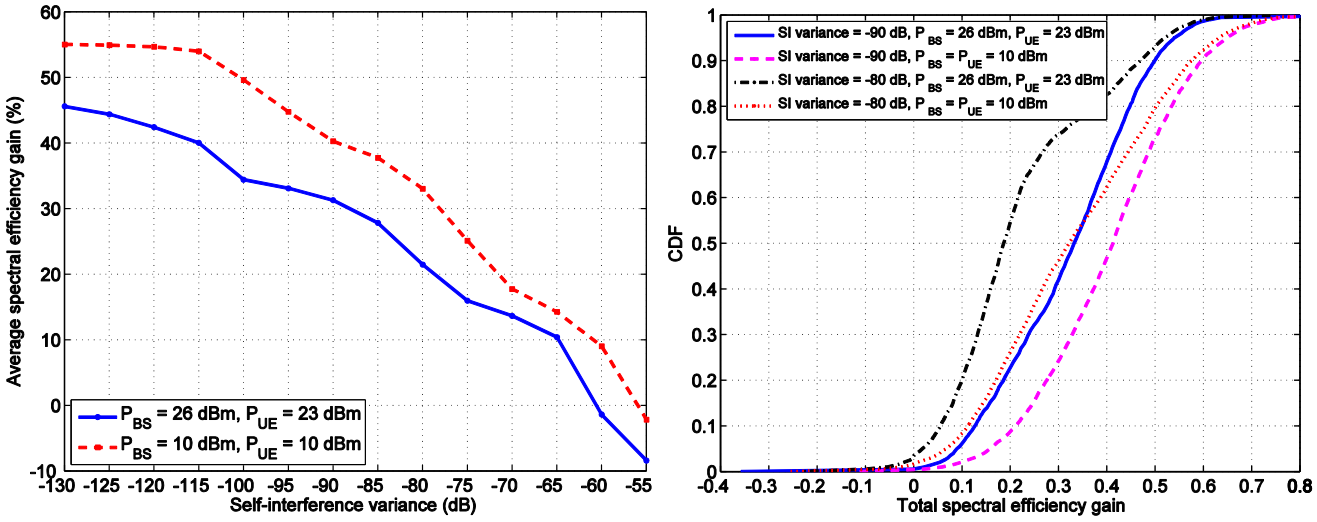

a) b)

Figure 38. a) Average spectral efficiency gain of the entire system, b) cumulative distribution function of the total spectral efficiency gain.

In another system setting, there are 1000 random network topologies created where all UEs are uniformly distributed over a circular area with radius of 100 m centered at the BS. For each topology, the SE gain is averaged over 500 random Rayleigh fading channel realizations. Downlink CDFs of the average SE gain are visualized in Figure 39 a), whereas the corresponding uplink results are seen in Figure 39 b). Again, the differences between downlink and uplink gains are significant. For example, even though the dash-dotted black curves have the same parameter setting on both plots, the downlink provides the largest gains of all four configurations; whereas the situation is right the opposite on the uplink direction.

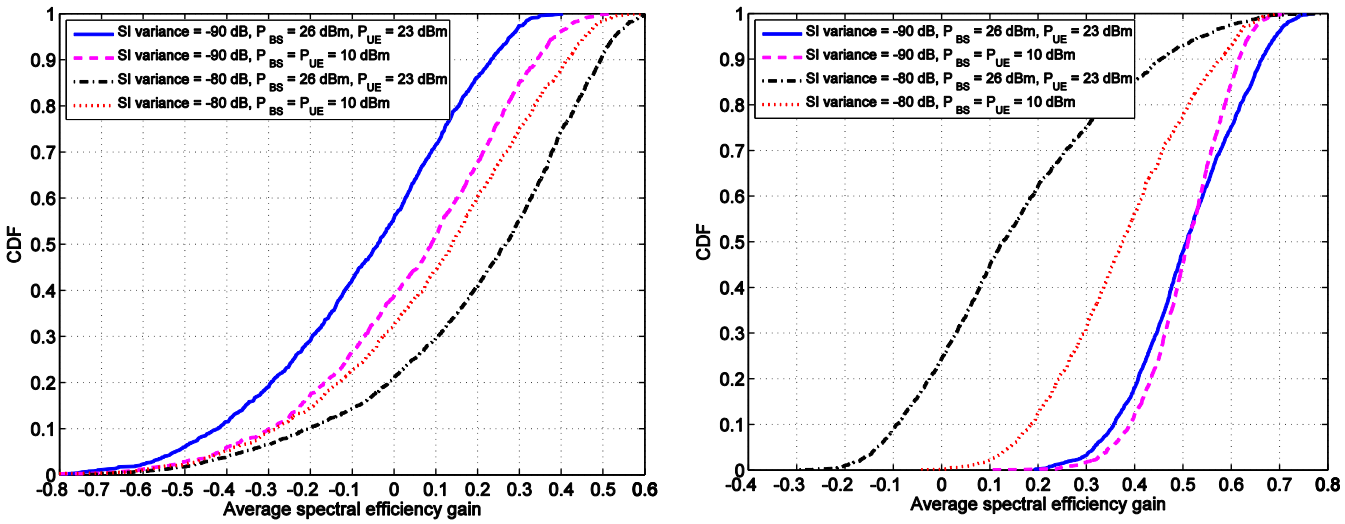

a) b)

Figure 39. CDF of average spectral efficiency of a) downlink channel, b) uplink channel.

By combining the conflicting results of Figure 39, we obtain the entire system gain metric that shows that the poor uplink performance pushes the black curve to be the worst, see Figure 40 a). The more efficient SI cancellation with lower transmission powers (pink dashed curve) is the best case from the overall system point of view.

In the next scenario the impact of co-channel interference (CCI) is elaborated. Now the SI variance level is fixed to -100 dB and uplink UE position is moved along the circle around BS so that the distance between uplink UE and downlink UE, denoted as d_{CCI}, varies between 15 m and 185 m. Figure 40 b) compares FD and HD downlink average spectral efficiencies as a function d_{CCI}. The main observation is that FD outperforms HD only when $d_{CCI} \geq 60$ m, i.e., when CCI is low enough. A similar comparison for the uplink in Figure 41 a) proves that uplink FD spectral efficiency is not sensitive to topology changes and FD provides large gain over HD in the whole d_{CCI} range. Again, looking at both links together the entire system SE is depicted in Figure 41 b). There, the FD turns out to be beneficial in practically all cases. However, if d_{CCI} = 15 m both duplexing schemes provide approximately the same average system spectral efficiency.

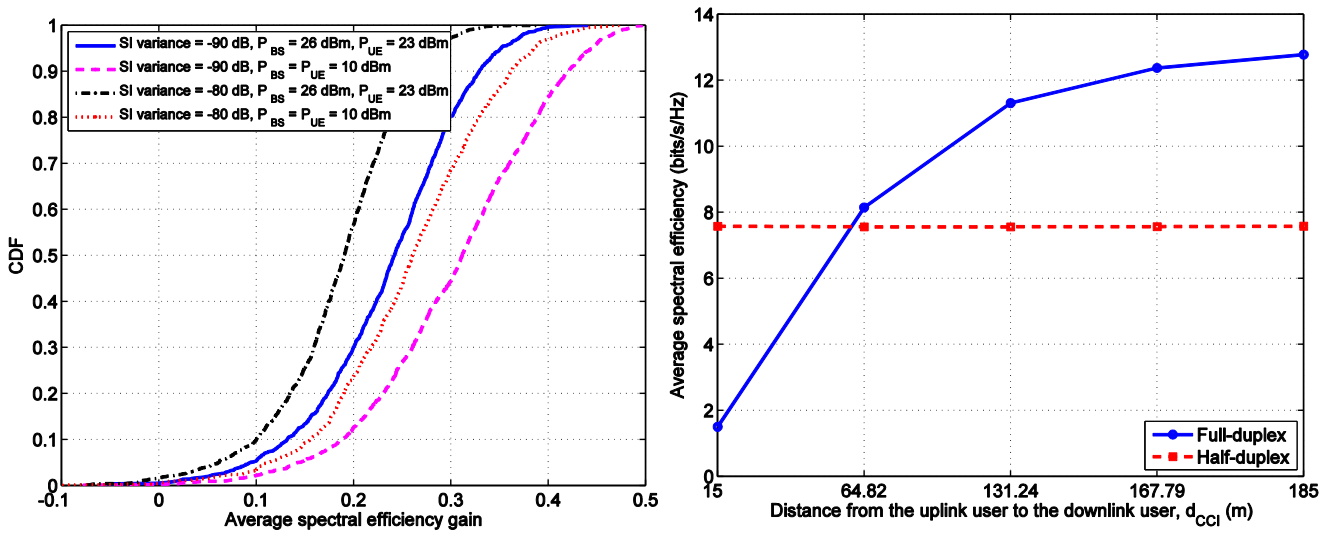

a) b)

Figure 40. a) CDF of the average spectral efficiency of the entire system, b) average spectral efficiency on the downlink direction.

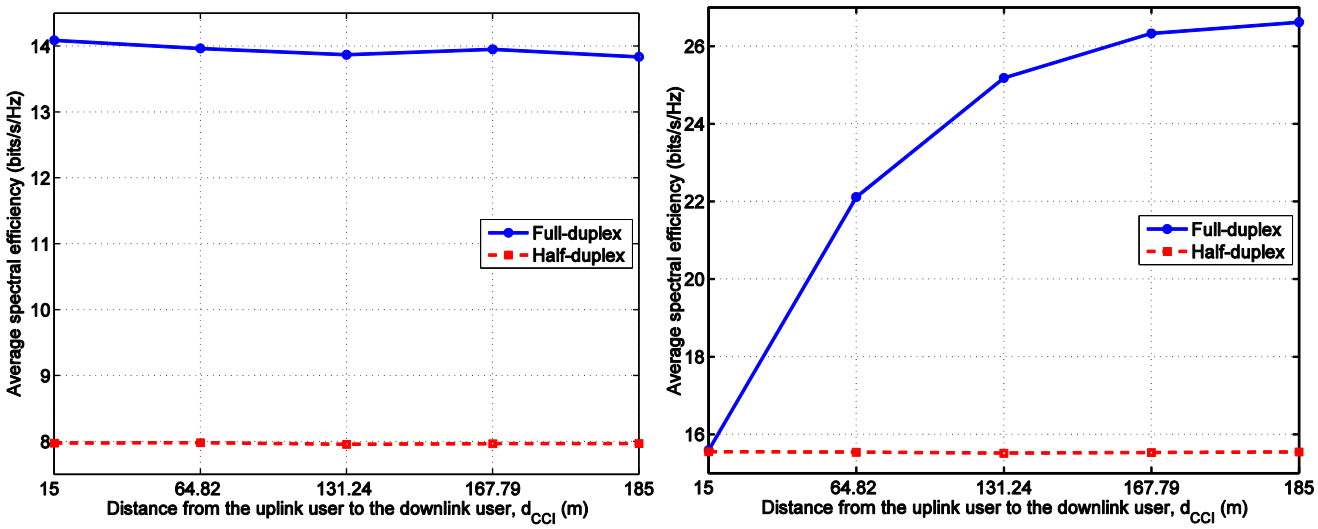

Figure 41. Average spectral efficiency a) on the uplink channel, b) over the entire system.

Finally, Figure 42 compares how much the average total SE is affected by either taking CCI into consideration or not. The new design is clearly seen to be more spectral efficient. Total SE is also increased when the number of downlink users is raised from 2 to 3 and in this case the gain of the new design is even higher.

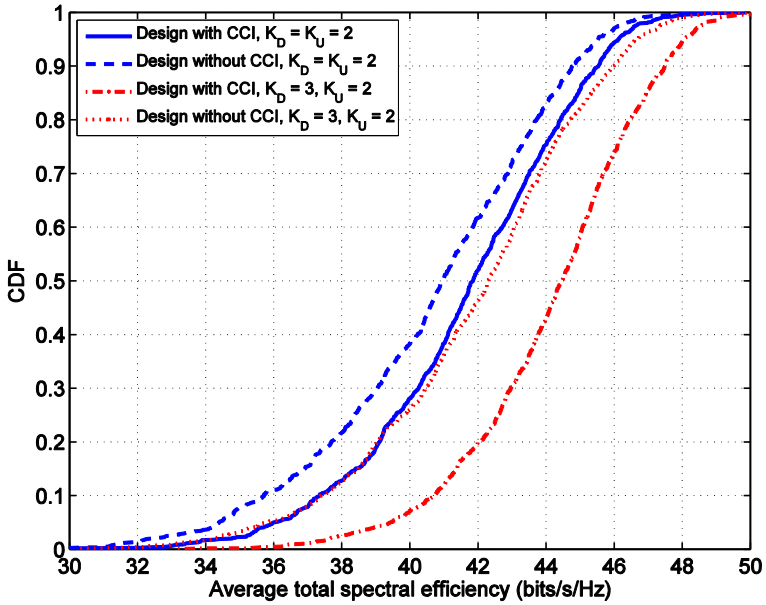

Figure 42. CDF of average total spectral efficiency of the proposed design and the earlier design with no consideration of CCI.

3.4. Multiple MIMO HD UEs per MIMO FD BS in single cell deployment scenario

3.4.1. Introduction

In this section, we numerically investigate the performance of the single-cell MIMO system, in which a full-duplex base-station serves multiple uplink and downlink users operating in half-duplex mode. Detailed derivation and system model description is provided in Section 3.5 of DUPLO deliverable D4.2 [5]. In addition to self-interference channel at the BS, the co-channel interference (CCI) caused by the UL users to downlink users is also taken into account, which increases the difficulty of the optimization problem further. We have studied different utility functions for this communication scenario, like sum-rate maximization, sum-MSE minimization, proportional fairness, etc. in [28]-[30]. Full-duplex multi-user systems have been investigated in [31]-[32]. However the CCI is not taken into account in [32], and single-antenna users are assumed in [31]. Moreover, [31]-[32] ignores several fundamental impediments of FD systems, i.e. transmitter and receiver distortion caused by non-ideal amplifiers, oscillators, ADCs/DACs, etc., i.e., several system parameters were ideally assumed. These practical considerations are carefully examined in our work [28]-[30]. The simulation results show that the proposed full-duplex system can achieve a significant improvement of throughput over half-duplex system.

3.4.2. Assumptions and numerical results

We compare the proposed algorithms with the half-duplex algorithm under the 3GPP LTE specifications for small cell deployments [27]. A single hexagonal cell having a base-station in the center with 2 transmit and 2 receive antennas with randomly distributed 3 uplink and 3 downlink users equipped with 2 antennas is simulated. The channel between base-station and users are assumed to experience the path loss model for LOS, and the channel between uplink and downlink users are assumed to experience the path loss model for NLOS communications. Detailed simulation parameters are shown in Table 3. For the self-interference channel, we adopt the model in [28], in which the self-interference channel is distributed as

$$\mathbf{H}_0 \sim \mathcal{CN}\left(\sqrt{\frac{\sigma_{SI}^2 K_R}{1+K_R}}\tilde{\mathbf{H}}_0, \frac{\sigma_{SI}^2}{1+K_R}\mathbf{I}_{N_0} \otimes \mathbf{I}_{M_0}\right) \quad (4)$$

where K_R is the Rician factor, $\mathbf{H_0}$ is a deterministic matrix, and s_{SI}^2 is introduced to parameterize the capability of a certain self-interference cancellation design.

The average sum-rate achieved in full-duplex system for uplink (FD-UL), downlink (FD-DL), and the entire system (FD-Sum) is shown in Figure 43. It is seen that while the sum-rate achieved in FD-UL system always decreases as s_{SI}^2 increases, the sum-rate achieved in FD-DL system decreases until a certain value of s_{SI}^2 = −80dB and increases after that. The decrease in the sum-rate performance of the FD-UL system is intuitive, since as the self-interference suppression capability decreases, a greater amount of self-interference power is added to the background thermal noise. The changing sum-rate performance of the FD-DL system is explained as follows. Since the proposed algorithm optimizes the uplink and downlink channels jointly, at low s_{SI}^2 values, the joint optimization scheme slightly reduces the transmit power of the downlink channel to maintain a good performance of uplink system. But, as s_{SI}^2 increases, the self-interference power starts overwhelming the desired signals coming from the uplink users, which reduces the achievable sum-rate in the uplink channel. Thus, the performance of the entire system is determined mostly by the downlink transmission. Therefore, reducing the transmit power in the uplink channel and concentrating on downlink channel is more beneficial. And also, as the transmission power of the uplink users is reduced, CCI is also reduced, resulting in improved performance in the downlink channel. A similar observation has been reported in [31].

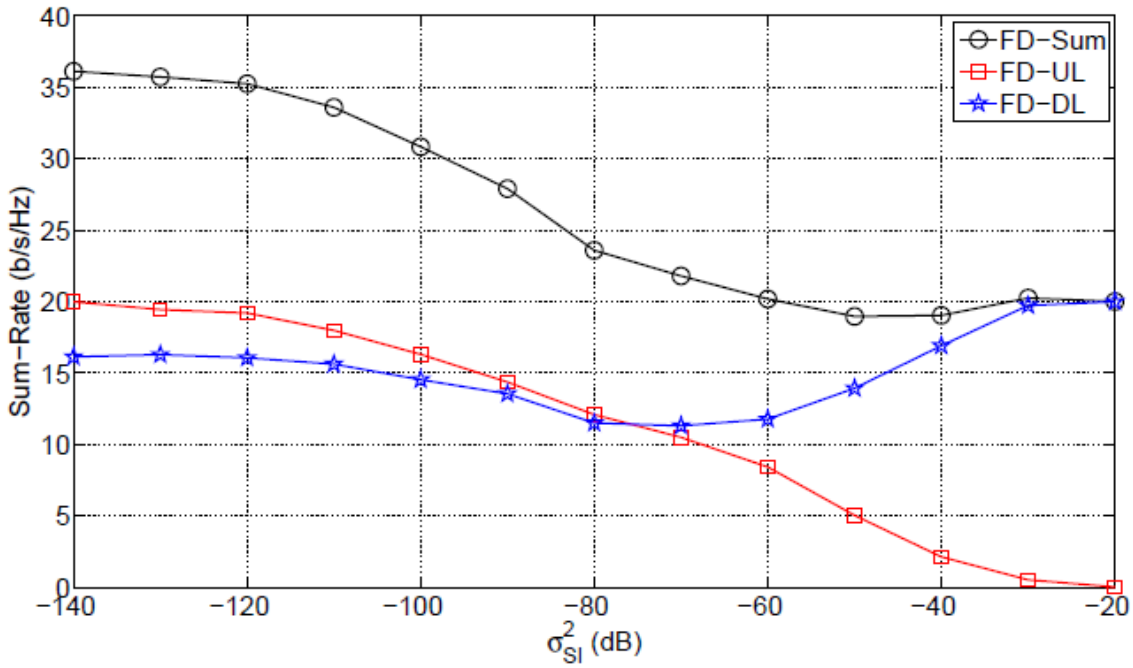

Figure 43: Sum-rate achieved in full-duplex cellular system versus s_{SI}^2.

The sum-rate comparison of full-duplex and half-duplex systems in uplink and downlink channels is depicted in Figure 44. As it is seen, the sum-rate achieved in FD-DL system is always

higher than that of HD-DL system, while FD-UL outperforms HD-UL in terms of sum-rate only when the self-interference is substantially suppressed. The sum-rate gains of the full-duplex system over half-duplex system as a function of s_{SI}^2 is shown in Table 6. It is demonstrated that for full-duplex system to achieve a higher sum-rate than half-duplex system, at least 70dB self-interference cancellation is required.

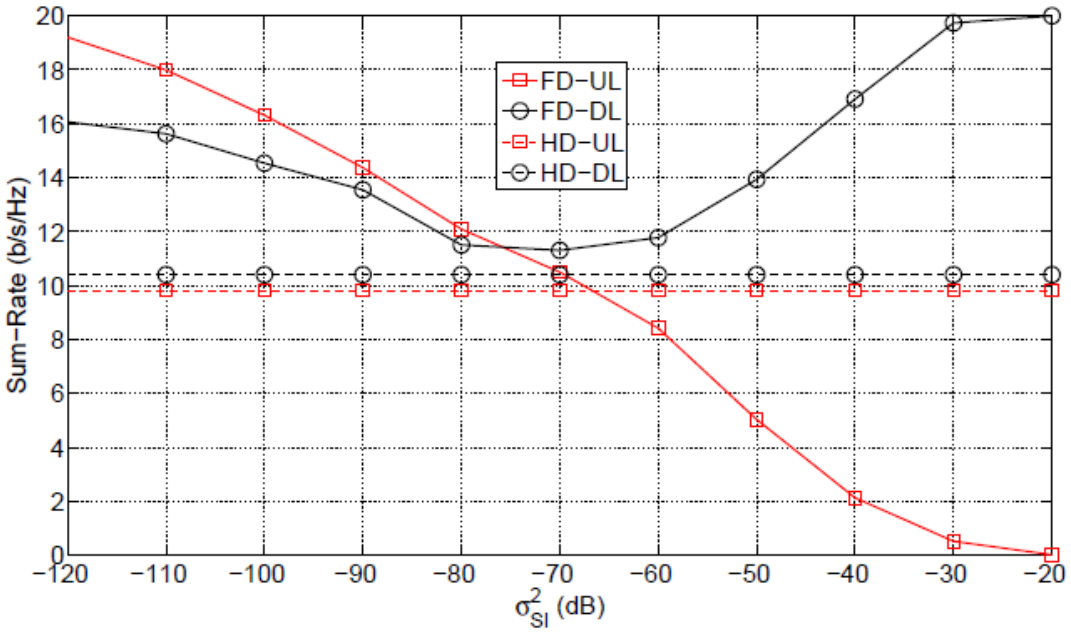

Figure 44: Sum-rate comparison of FD and HD systems in the UL and DL channel.

Table 6: Average rate gain of full-duplex uplink (downlink) system over half-duplex uplink (downlink) system

σ^2_{SI}	−110dB	−100dB	−90dB	−80dB	−70dB	−60dB	−50dB	−40dB	−30dB	−20dB
Uplink	83%	65%	45%	23%	3%	-16%	-51%	-78%	-94%	-99%
Downlink	50%	40%	25%	12%	5%	14%	36%	65%	91%	93%

3.5. Optimum User Selection for Hybrid-Duplex Device-to-Device in Cellular Networks

In this study case, we consider a cellular user selection scheme in a hybrid cellular and D2D network with one BS, one D2D pair and multiple cellular users. The aim is with proper cellular user selection enhance the throughput of the D2D connection without causing any harmful interference to BS. Therefore we assume that the BS supports a maximum interference, which is denoted by parameter I_{th}. The D2D connection can switch between HD and FD operation modes, and we also consider K user available. We assume the BS and each user are equipped with a half duplex antenna and D2D pair is equipped with a hybrid duplex antenna. The following links $S_i \rightarrow$ BS, $D_1 \rightarrow$ BS, $D_2 \rightarrow$ BS, $S_i \rightarrow$ D1, $S_i \rightarrow D_2$, $D_1 \rightarrow D_1$ and $D_2 \rightarrow D_2$, have the following SNR gains γ_{sib}, γ_{d1b}, γ_{d2b}, γ_{sid1} , γ_{sid2} , γ_{d1d1} and γ_{d2d2}. The procedure is described in detail in Section 3.6 of DUPLO D4.2 [5], while the observed performance results are given in this section.

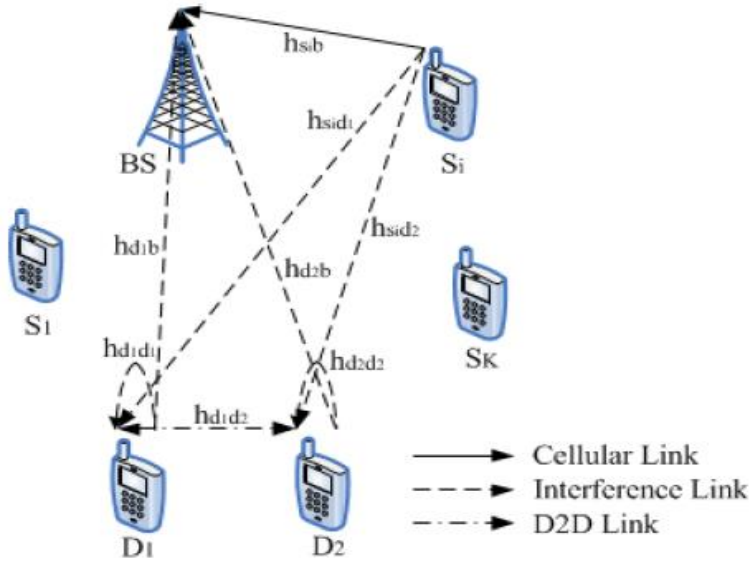

Figure 45 System model: hybrid cellular and D2D network with one BS, one D2D pair and K cellular users

3.5.1. Analysis parameters, assumptions and numerical results

In this section, simulation results are presented to verify the analysis given in D4.2, section 3.6 [5]. In the simulations below, the noise variances $\sigma_{d_1}^2$ and $\sigma_{d_2}^2$ and each cellular user transmission power are all normalized to unity. Additionally, assume that K users are available for selection, and consider that maximum interference threshold is I_{th}. All simulation results are also obtained by averaging over 1,000,000 independent runs via Monte Carlo simulation.

Figure 46 compares the theoretical analysis with the simulation results, where I_{th} = 2, and SNR gain between the device user and BS of $\gamma_{d_1 b}$ = 15 dB, and is SNR gain between the user and the second device γ_{sd_2} = 30 dB and target transmission rate of R_T = 1 bits/s/Hz. The analytical results based on the approximation of throughput (see section 3.6 in D4.2 [5] for more details) are shown. The results are compared under different settings of the mean channel gain $\gamma_{d_1 d_2}$ and number of available cellular users (K). It is obvious that under good channel conditions when the channel gains are high, the theoretical approximate and simulated throughput are very well matched. It is also shown in Figure 46 that the throughput is significantly improved by using our proposed cellular user selection scheme. For example, when $\gamma_{d_1 d_2}$ = 30 dB, the throughput with non-selection is around 0.13 bps/Hz, however, the throughput of our proposed scheme are 0.5, 0.63 and 0.7 bps/Hz for K = 10, 20 and 30 users, respectively.

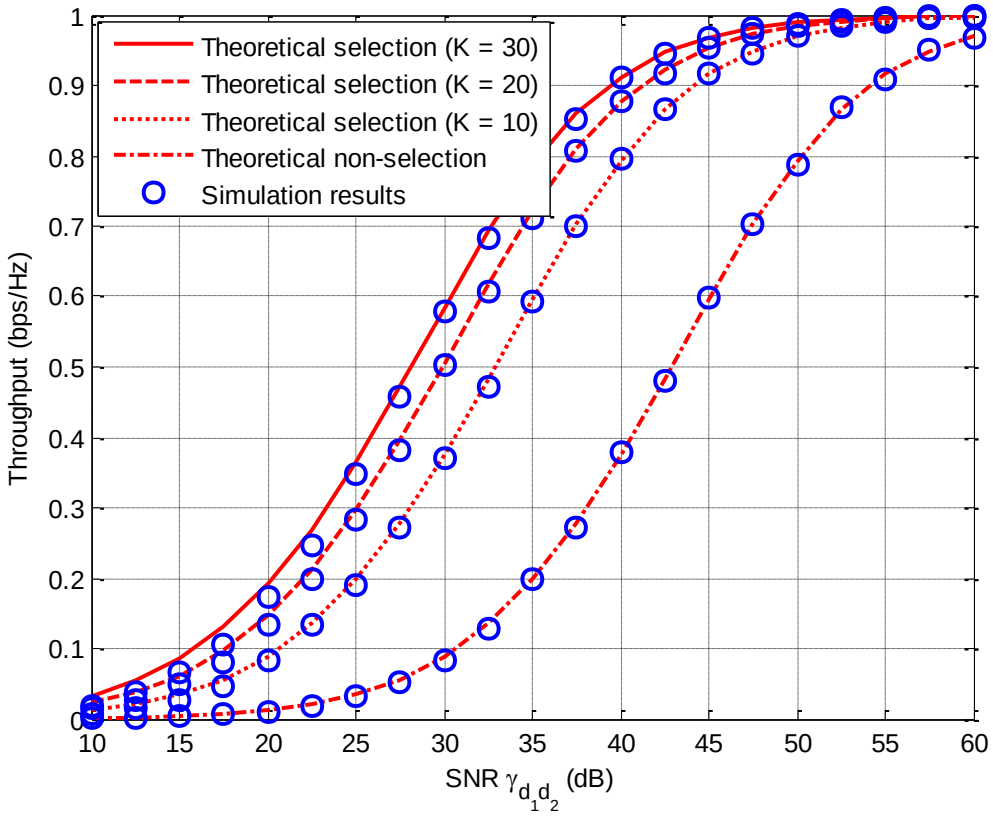

Figure 46 Theoretical vs numerical throughput of HD-D2D with different number of available users (K), where I_{th} = 2, $\gamma_{d_1 b}$ = 15 dB, γ_{sd_2} = 30 dB and R_T = 1 bps/Hz.

Figure 47 compares the theoretical analysis with the simulation results, where interference threshold is I_{th} = 1, while the average SNR between nodes is set as follows $\gamma_{d_1 b}$ = 15 dB, γ_{sd_2} = 30 dB, $\gamma_{d_1 d_1}$ = $\gamma_{d_2 d_2}$= 5 dB, and transmission rate of R_T = 1 bps/Hz. The results are compared under different

settings of the mean channel gain $\gamma_{d_1 d_2}$ and number of available users. It is obvious that under the good channel conditions, the theoretical approximate and simulated throughput match very closely. It is also shown in Figure 47 that the throughput is significantly improved by using our proposed user selection scheme, i.e., the throughput of non-selection is around 0.2 bps/Hz, however, the throughput of our proposed scheme are 0.72, 1 and 1.15 bps/Hz for K = 10, 20 and 30 users, respectively, when $\gamma_{d_1 d_2}$= 30 dB.

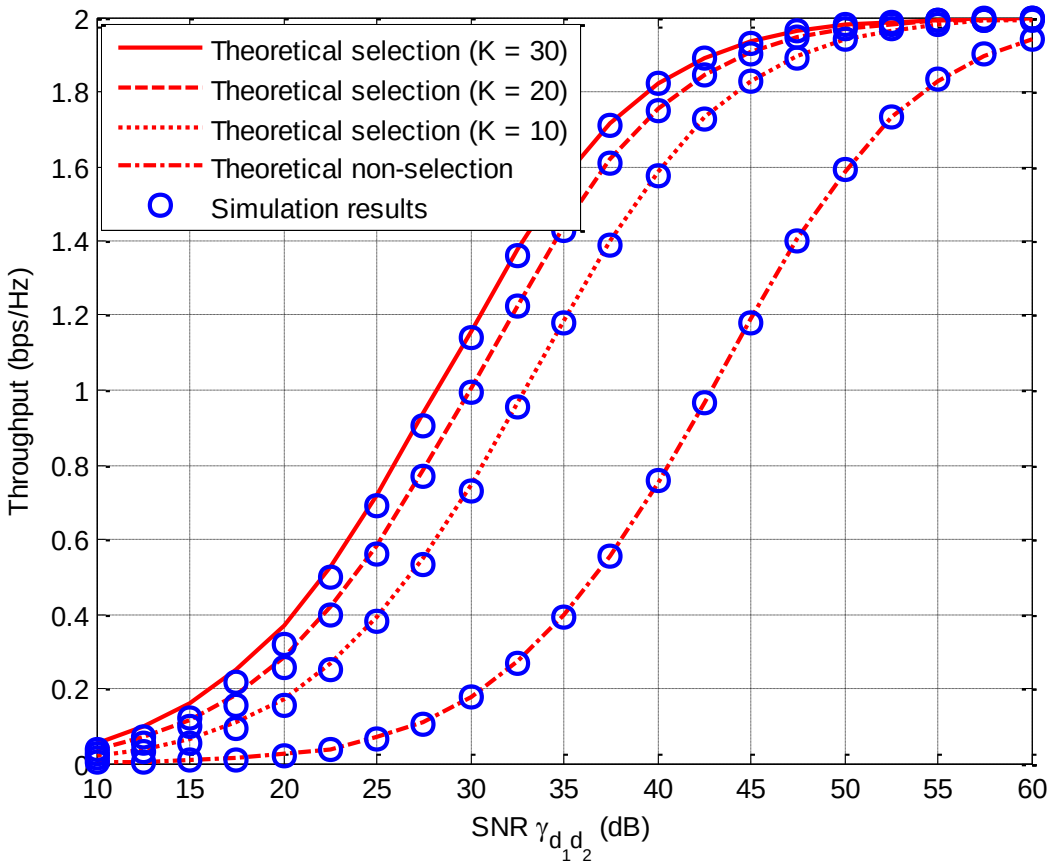

Figure 47 Theoretical vs numerical throughput of FD-D2D with different number of available users, where I_{th} = 1, $\gamma_{d_1 b}$ = 15 dB, γ_{sd_2} = 30 dB, $\gamma_{d_1 d_1}$ = $\gamma_{d_2 d_2}$= 5 dB and R_T = 1 bps/Hz.

Figure 48 shows throughput vs residual self-interference γ_{dd} = $\gamma_{d_1 d_1}$ = $\gamma_{d_2 d_2}$for half and full duplex D2D protocols, where R_T = 1 bps/Hz, $\gamma_{d_1 b}$ = $\gamma_{d_2 b}$ = 10 dB and γ_{sd_1} = γ_{sd_2} = 10 dB. Radio transmissions always encounter a bandwidth constraint that limits maximum SI cancellation; therefore, it is useful to consider the different residual SI SNR which can affect the performance of full duplex D2D scheme. In order to compare half and full duplex D2D scenarios fairly, in Figure 48, we set I_{th} = 2 and 1 for half and full duplex D2D, respectively. It is clearly shown that, when residual SI increases, the throughput of FD-D2D is adversely affected, but the throughput of HD-D2D keeps a constant. Furthermore, the throughput of HD-D2D with the proposed selection scheme (K = 10 available users)

or non-selection are always less than that of FD-D2D, when γ_{dd} is less than 20 or 19 dB, respectively. Therefore, hybrid-duplex D2D can be selected between half and full duplex according to different residual SI to enhance the throughput of D2D link.

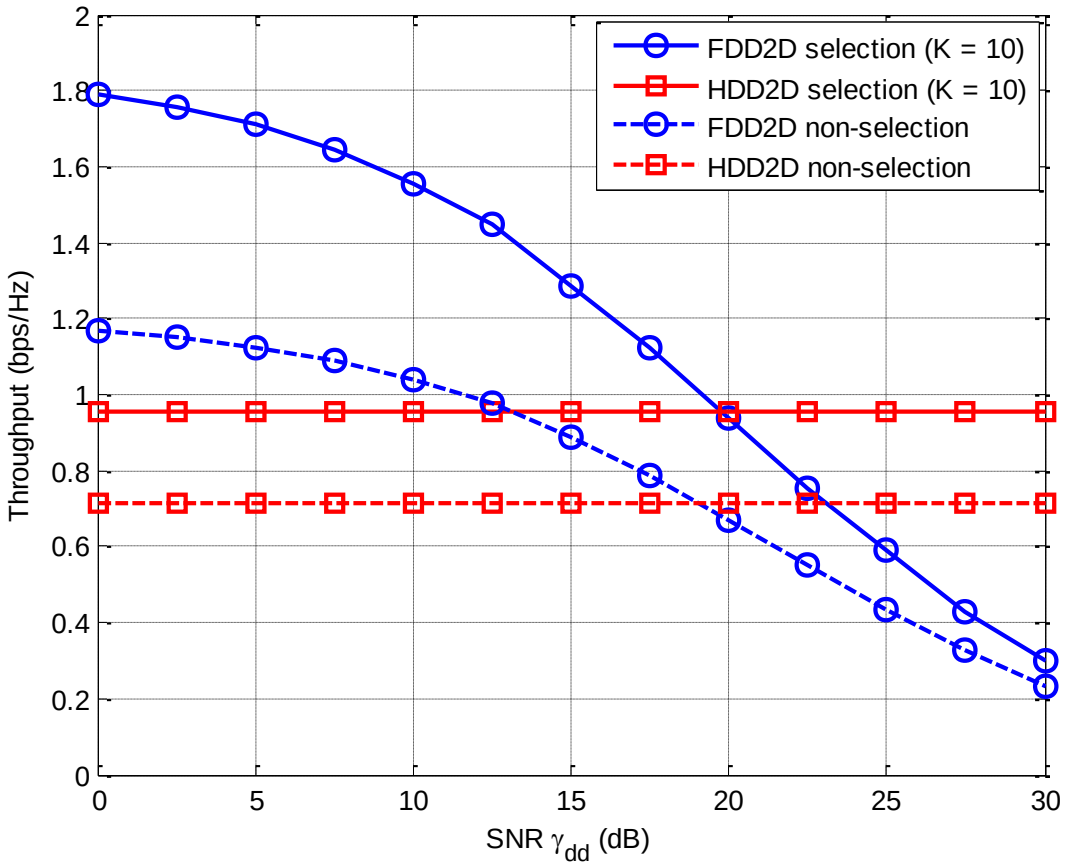

Figure 48 Throughput vs residual self-interference γ_{dd} for half and full duplex D2D protocols with different number of available users, where R_T = 1 bps/Hz, $\gamma_{d_1 b}$ = $\gamma_{d_2 b}$ = 10 dB and γ_{sd_1} = γ_{sd_2} = 10 dB.

This section studied the best cellular user selection scheme in a hybrid-duplex D2D cellular system. The integral form of the throughput of the hybrid-duplex D2D was derived. The result showed that hybrid-duplex D2D can select between half and full duplex according to different residual SI to enhance the throughput of D2D link. We are aware of the fact that practical systems may be more complicated than the system considered in this paper. Nonetheless, the analysis in this paper provides useful insights and a solid basis for further analysis.

4. MULTIPLE FULL-DUPLEX SMALL CELLS

4.1. Outdoor and indoor small cell system simulations

4.1.1. Introduction

This section provides system simulation results for full-duplex operation in multiple LTE small cells environment, assuming that there is only single full-duplex user equipment (UE) per cell. Therefore, the focus is on investigating the impact of inter-cell interference due to full-duplex transmission. As a result, we provide the SINR and throughput comparisons under indoor and outdoor environment with variable density of full-duplex small cell set-ups. Half-duplex TDD operation mode is used as the reference scheme in comparisons. User scheduling and power control is not considered in current simulations. Two types of multiple cell deployment scenarios are considered, namely indoor and outdoor scenarios.

4.1.2. Simulation parameters and assumptions

Full duplex is modeled so that each sub-frame of the frame is configured as a DL and UL sub-frame instead of DL or UL only, *i.e.*, transmission and reception simultaneously occur on the same bandwidth and transmission time interval. Self-interference is modeled as a fixed power level added as interference to the received signal. The path loss (*Pl*) between the transmitter (Tx) and receiver (Rx) antennas is assumed to be 0 dB. Self-interference cancellation is modeled as attenuation (similar to path loss) between the Tx and Rx antennas and is a configurable parameter, denoted as the self-interference cancellation (SI_C). Thus, the signal to interference plus noise ratio (SINR) at the receiver of interest equals to

$$SINR = \frac{P_{Tx} A_g P_g}{N + \sum_k ICI_k + SI \cdot SI_C}, \quad (5)$$

where P_{Tx} is the transmission power of the desired transmitter, A_g is the antenna gain including both Tx and Rx gains, P_g is the path gain including path loss and shadowing (as described next.), *N* is the noise, ICI_k is the inter-cell-interference component of the *k*th cell, and *SI* and SI_C are the self-interference and self-interference cancellation levels, respectively. Centralized network with 3GPP's LTE Layer 1 structure is assumed, as well as both DL and UL operate in OFDM mode.

4.1.2.1. Indoor scenario

In the indoor scenario, three dual strip blocks are placed within a macrocell area so that there is a single dual-strip block per each of the three sectors of the macrocell. Note, that the macro base station (BS) itself is disabled in these investigations.

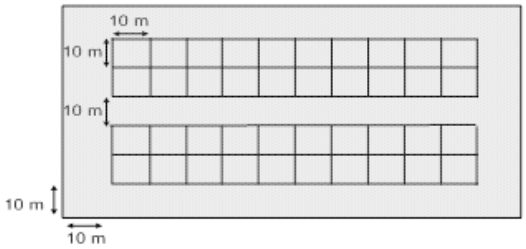

Figure 49. Single floor of the dual strip block.

Figure 49 illustrates a single floor of the dual strip block model. A dual strip block is randomly scattered within each macro cell area. The dual strip block consists of 2 6-floor buildings; there are 40 apartments of size 10 m by 10 m in each floor, and apartment strips are 10 m apart. Femto Base Stations (BSs) are uniformly dropped in random positions inside the apartments. In addition, a deployment ratio parameter *P* = 0.1 is used as the probability that there is an active BS in an apartment. Similarly, a UE is dropped within a room at a random position that is at least 3 m away from its serving BS. Notice that a UE can only connect to its collocated femto BS in the same room. The path loss attenuation between the UE and BS is given by $Pl\ [dB] = 38.46 + 20\log_{10} R + 0.7d2D$, where *R* and *d2D* are in meters, and *d2D* is the 2-dimensional distance taking into account the penetration loss due to the walls inside an apartment. The penetration loss of the walls separating apartments is *5* dB and the penetration loss of an outdoor wall equals 20 dB. The Shadowing standard deviation between outdoor picocells is 6 dB, while between pico and UE, it is 3 dB for LOS and 4 dB for NLOS. A shadowing correlation of 0.5 between picocells is also considered. Note that the 3GPP specifications in [7], [8] detail further these deployment scenarios.

Table 7. Indoor scenario femto BS and UE parameters.

UE antenna gain	0 dBi
UE noise figure	9 dB
UE power class	23 dBm
BS antenna gain	0 dBi
BS antenna pattern	Omni-directional
BS power class	20 dBm
BS noise figure	13 dB

The BS and UE parameters of the indoor scenario are summarized in Table 7**.**

4.1.2.2. Outdoor scenario

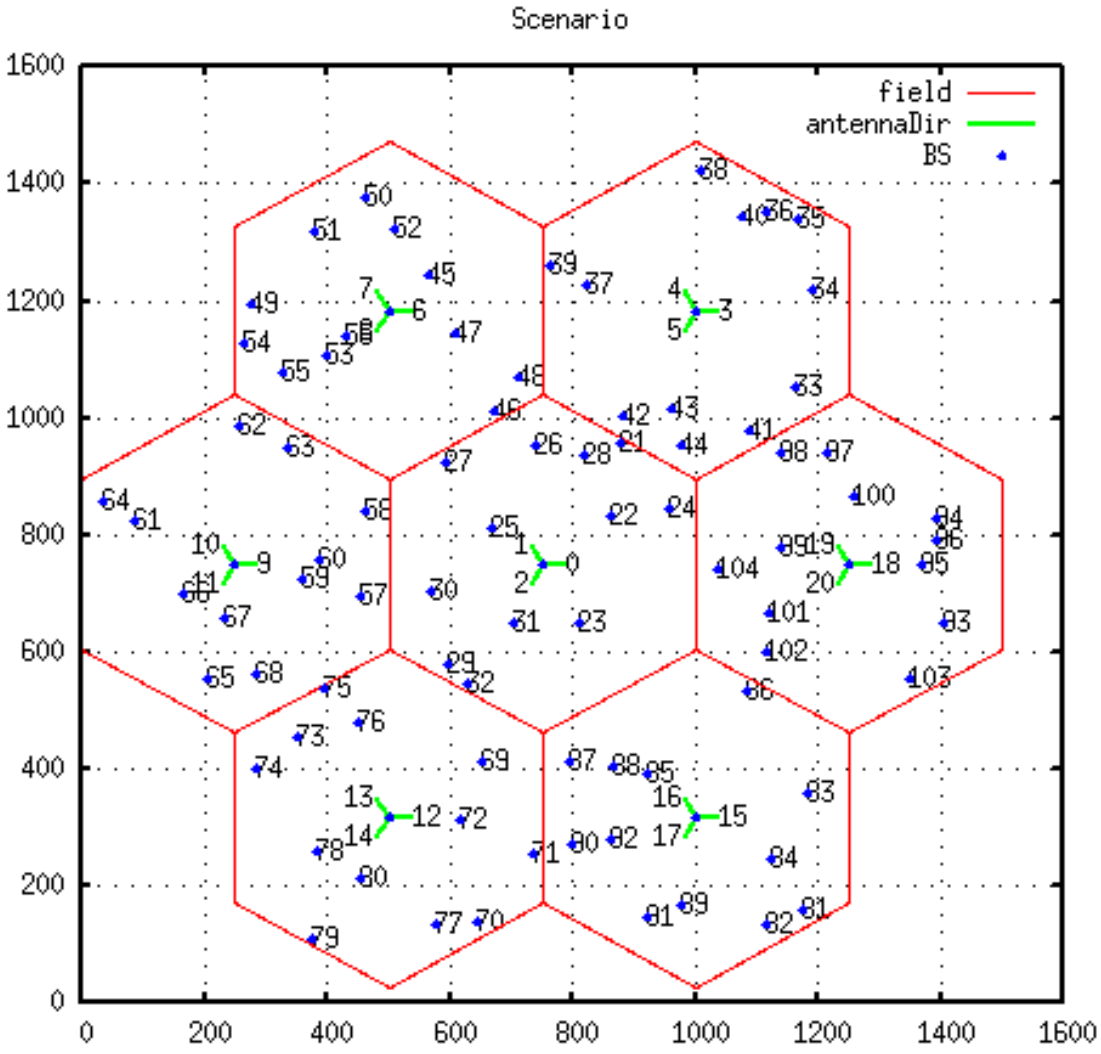

Figure 50: Outdoor scenario.

Figure 50 illustrates the outdoor scenario where 4 pico BSs are randomly deployed within each macro cell sector area. Note that Macro base stations are also disabled in this scenario. A UE is dropped at a random location within each picocell radius, which is *40* m. The path loss in the line-of-sight case is $Pl_{LOS}(R) = 103.8 + 20.9 \log_{10} R$, whereas the non-line-of-sight case is $Pl_{NLOS}(R) = 145.4 + 37.5 \log_{10} R$, where R is the distance in km. The line-of-sight probability at distance R equals $P_{LOS}(R) = 0.5 - \min\left(0.5, 5^{\left(-\frac{0.156}{R}\right)}\right) + \min\left(0.5, 5^{\left(-\frac{R}{0.03}\right)}\right)$. The details of this scenario can be found in [6] and Table 8 summarizes the BS and UE parameters specific to the outdoor scenario.

Table 8. Outdoor scenario pico BS and UE parameters.

Number of pico BSs	4 BSs/cell
BS Tx power (Ptotal)	24 dBm
BS antenna pattern	Omni-directional
BS antenna gain	5 dBi
BS cell radius	40 m
Minimum distance between BS and BS	40 m
Minimum distance between BS and Macro BS	75 m
BS deployment	random deployment
Penetration loss	0 dB
BS noise figure	13 dB
UE antenna gain	0 dBi
UE noise figure	9 dB
UE power class	23 dBm (200 mW)

4.1.3. Simulation parameters and assumptions

Table 9 summarizes the most relevant simulation parameters.

Table 9. Simulation parameters.

Link adaptation	Ideal with MCS selection with 10% BLER
Channel estimation	Ideal
UE UL Power control	Disabled
DL Power control (pico, femto)	Disabled
Small scaling fading channel	Not modeled
DL and UL modulation and coding schemes	Modulations {QPSK, 16QAM, 64QAM}
Antenna configuration	Single antenna
Bandwidth	10 MHz
Traffic model	Full buffer

In this investigation, the link adaptation is ideal, *i.e.*, the channel quality indicator (CQI) equals the received SINR. An actual value interface (AVI) table is used to map link to system level performance figures. Then, based on the estimated CQI, the highest modulation coding scheme (MCS) is select so that the packet error rate probability according to AVI tables is less than or equal to 10%. A weighted coin tossing approach (an idealized randomizing device with two states) is used to decide whether a packet was received correctly or not. The duplexing scheme does not change the link adaptation that is based on the received SINR alone. The MCS set follows the 3GPP's LTE specifications. Additionally, the frame format complies with the LTE TDD mode. The control signaling is not modelled: all symbols carry data. The power control algorithm is disabled for both DL and UL directions. No inter-cell-interference cancellation or mitigation schemes are considered at this stage.

4.1.3.1. Simulated cases

The following cases were simulated:

- Full duplex system with self-interference cancellation levels {70, 80, 90, 100, 110, 120} dB
- TDD system with equal share (50%) between DL and UL
- Flexible TDD system according to the 3GPP LTE release 12 with random DL/UL configuration.

In the full-duplex system under study, each link (a single link per BS) operates in full-duplex mode every time instant over the whole bandwidth. The full buffer traffic model is used to ensure that there is always data available to transmit. Herein, the TDD system is the reference scenario. In the TDD configuration, 50% of the time domain resources are used for DL and 50% for UL. As a result of assuming perfect time and frequency synchronization between BSs, there is no cross-link-interference in the TDD reference case. The Flexible TDD case is included to highlight the impact of cross-link-interference in TDD deployment scenarios. A random TDD configuration was enforced to guarantee that there always exists cross-link-interference in the flexible TDD case, even though such random selection is not the optimal from the traffic adaptation and performance point of view.

4.1.3.2. Numerical results

Numerical results are provided in terms of SINR and throughput figures: the former consists of the average UE SINR while the latter consists of the average UE throughput results. Investigations are carried out following simulation assumptions and configuration parameters in the 3GPP specifications [6]-[8].

4.1.3.3. Average UE SINR

In this section the CDFs of the average SINR per UE for DL and UL are presented for both the indoor and outdoor scenarios.

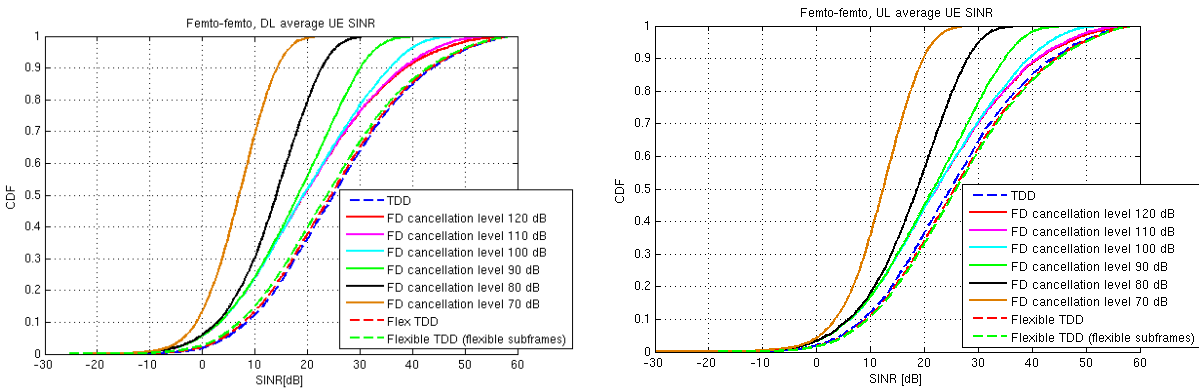

a) b)

Figure 51. Indoor a) DL and b) UL average UE SINR.

For the full duplex (with self-interference cancellation), TDD and flexible TDD configurations, Figure 51 a) and b) depict the average UE SINR in the DL and UL of indoor scenarios, respectively. In the legend of these figures, FD stands for full duplex. By setting a self-interference level of at least 100 dB, the full duplex performance in terms of the average UE SINR gets quite close to the one achieved in the half duplex scenarios. At the 10th percentile of the SINR plots, the TDD schemes outperform the full duplex configuration by nearly 5 dB in DL, while the difference is less than that in the UL. It is worth noticing that about the cancellation level of 100 dB the gain from self-interference cancellation saturates and the inter-cell-interference dominates the aggregate interference. The remaining SINR gap between FD and half duplexing schemes is caused by the additional cross interference caused by nodes transmitting simultaneously on both DL and UL directions. In fact, when compared to the FD deployment scheme, the perfect synchronization between nodes eliminates the cross-link-interference in the TDD scheme, while half duplexing allows fewer simultaneous transmissions per resource allocation (aggressor nodes) in the flexible TDD scheme. Note that the Flexible TDD (flexible sub-frames) identifies the SINR of the so-called flexible sub-frames: the SINR calculation excludes any sub-frame with fixed transmission direction due to possible sub-frame configurations.

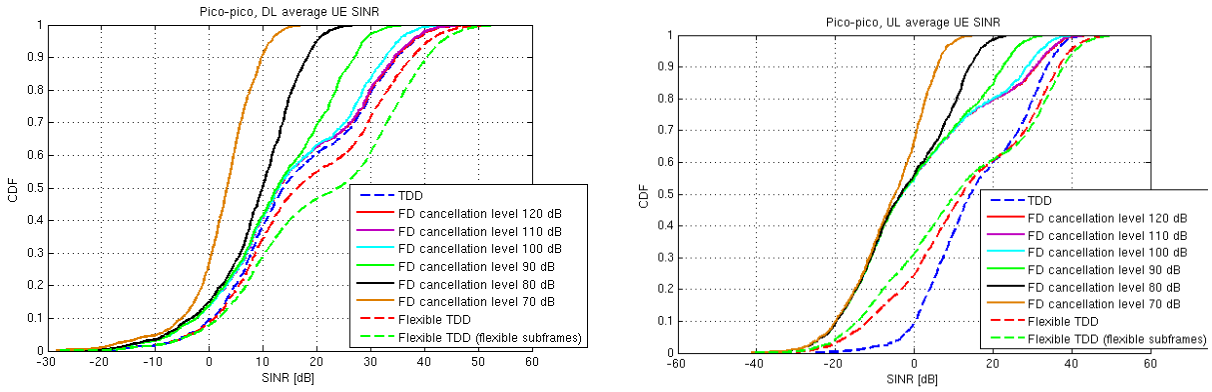

a) b)

Figure 52. Outdoor a) DL and b) UL average UE SINR.

Figure 52 a) and b) show the average UE SINR in the DL and UL of outdoor scenarios, respectively. As can be seen from the SINR results in Figure 52 a), the FD performance is on a par with the TDD schemes if the self-interference cancelation is more than 100 dB. It can also be seen that outdoor BSs lack wall isolation, as a result the cross-link-interference has a greater impact on the performance than was the case in indoor scenario. Therefore, it can be concluded, that because flexible TDD outperforms TDD in terms of DL SINR, UL to DL interference is less severe compared to DL to DL interference. From the average UE SINR results in Figure 52 b), we can confirm the previous conclusion about poor outdoor isolation by comparing the FD against TDD. Despite setting the self-interference cancelation level to 120 dB, the full-duplex scenario still suffers from very high DL to UL (BS to BS) cross interference due to the propagation characteristics of the outdoor scenarios (lack of isolation between outdoor BSs). In this configuration, the TDD scheme clearly outperforms the full-duplex mode in terms of the average UE UL SINR.

4.1.3.4. Average UE throughput

For both the indoor and outdoor scenarios, this section presents the average UE throughput results in the DL and UL directions.

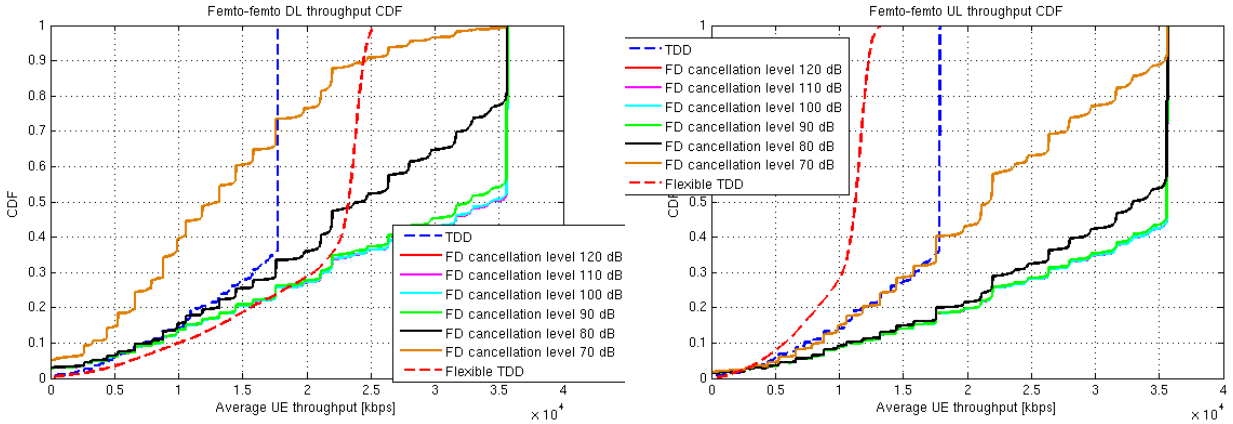

a) b)

Figure 53. Indoor a) DL and b) UL average UE throughput.

Figure 53 a) and b) present the CDF of the average UE throughput in the DL and UL of the indoor scenarios, respectively. From these figures, the maximum throughput in the FD deployment becomes twice as much the one achieved in TDD mode, as expected. It is worth noting that the FD scheme not only outperforms the TDD in the low SINR regime, but also guarantees the maximum

achievable throughput for about 50% of the FD UEs if the self-interference cancellation level is at least 80 dB. By comparing the FD and TDD coverage in this particular scenario, the former is only slightly worse than the latter in the DL, while both are equal in the UL. While the flexible TDD scheme outperforms the standard TDD in the DL, it performs poorer in the UL. The reason is the random selection of sub-frame sequences in the flexible TDD configuration. In other words, the flexible TDD configuration allows more DL than UL resources on the average as opposed to the standard TDD that splits resources between DL and UL equally (grants 50% of the available resources to each direction). In all cases, excluding FD with 70 dB self-interference cancellation, the used MCS limits the achievable maximum throughput.

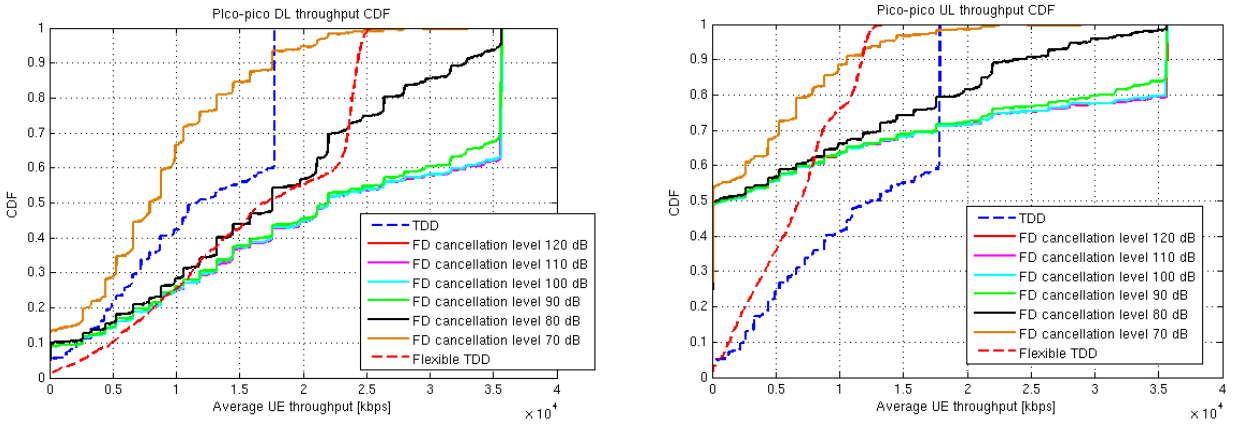

a) b)

Figure 54: Outdoor a) DL and b) UL average UE throughput.

Figure 54 a) and b) illustrate the average UE throughput in the DL and UL of the outdoor scenarios, respectively. In the DL of these scenarios, the FD scheme with self-interference cancelation of at least 80 dB achieves higher throughput than the standard TDD while providing almost similar coverage (low values of CDF). Moreover, about 40% of the FD UEs achieve the maximum throughput in the DL direction. In the UL, while nearly 30% of the FD UEs with self-interference cancelation of at least 90 dB achieve throughput higher than that of the TDD users, only about 20% of them perform as good when the cancelation level is 80 dB. The coverage is actually the main limitation of this scenario: only 5% of the TDD UEs are in outage in contrast with nearly 50% of FD ones. The reason is the additional inter-cell-interference in FD deployments, more specifically the DL to UL cross interference and poor isolation between outdoor BSs. When compared to reference TDD scheme, the flexible TDD improves the DL, but worsens the UL performance. Regarding the coverage, both cases perform fairly similar.

Based on the above results, it is evident that in indoor scenarios with good isolation between BSs, the full duplex configuration can outperform the TDD schemes in terms of average UE throughput

while providing similar coverage as long as the self-interference cancellation level is at least 80 dB. In addition, whenever the isolation between the BSs is poor, both the coverage and the achievable data rates of FD-enabled UEs decrease due to high DL to UL cross interference. However, these results are limited to scenarios with a single UE per cell site and further studies are needed to confirm if they still hold in multiuser deployments (more than one UE per cell). From these investigations, we also identified the need to devise interference mitigation techniques so as to reduce the DL to UL cross interference and, as a result, to enable full duplex communications in scenarios with poor isolation between nodes, especially BSs with high transmission power. For instance, power control and inter-cell-interference cancellation or coordination schemes are envisaged as promising for interference management solutions.

4.2. Multiple FD UEs per FD BS in multi cell deployment scenario

4.2.1. Introduction

Consider an interference-limited network where all nodes operate in FD fashion. The DL of a traditional HD network constitutes our benchmark scenario wherein the user of interest is interfered by surrounding small cells. BSs independently schedule a random user in every transmission interval. All communicating nodes are equipped with omni-directional antennas. BSs and UEs are also assumed to have full buffer and symmetric traffic patterns. We resort to an analytical framework which is introduced in [16], [17] and Section 4.1 of DUPLO deliverable D4.2 [5].

4.2.2. Simulation parameters and assumptions

Table 10 Simulation parameters

BSs Transmit Power	24 dBm
UEs Transmit Power	21 dBm
Path loss exponent	4
Minimum range Rm	50 m
Maximum range RM	250 m
Standard deviation	10 dB
Nakagami-m fading figure	2

Figure 55 depicts the Complementary Cumulative Distribution Function (CCDF) of the aggregate CCI at the tagged receiver for an increasing density interfering small cell BSs. Solid lines present the resulting aggregate CCI as a function of the increasing density of interfering BSs. Note the degradation effect of both the extra interference due to the co-channel UEs as well as to the self-interference. At a density of 10^{-4} BS/m^2, we first show the combined interference from co-channel ideal FD BSs and UEs with dashed lines, which represents the best case scenario. Then, from a more practical point of view, the total CCI at the FD user of interest for a SI attenuation of -80 dB and at the same density of interferers is represented by the dotted line curve. To illustrate our point, the tagged receiver only experiences aggregate CCI higher than -60 dBm for about 20% of the time when in HD mode, whereas the CCI is higher than that value for nearly 50% of the time in a practical FD setting.

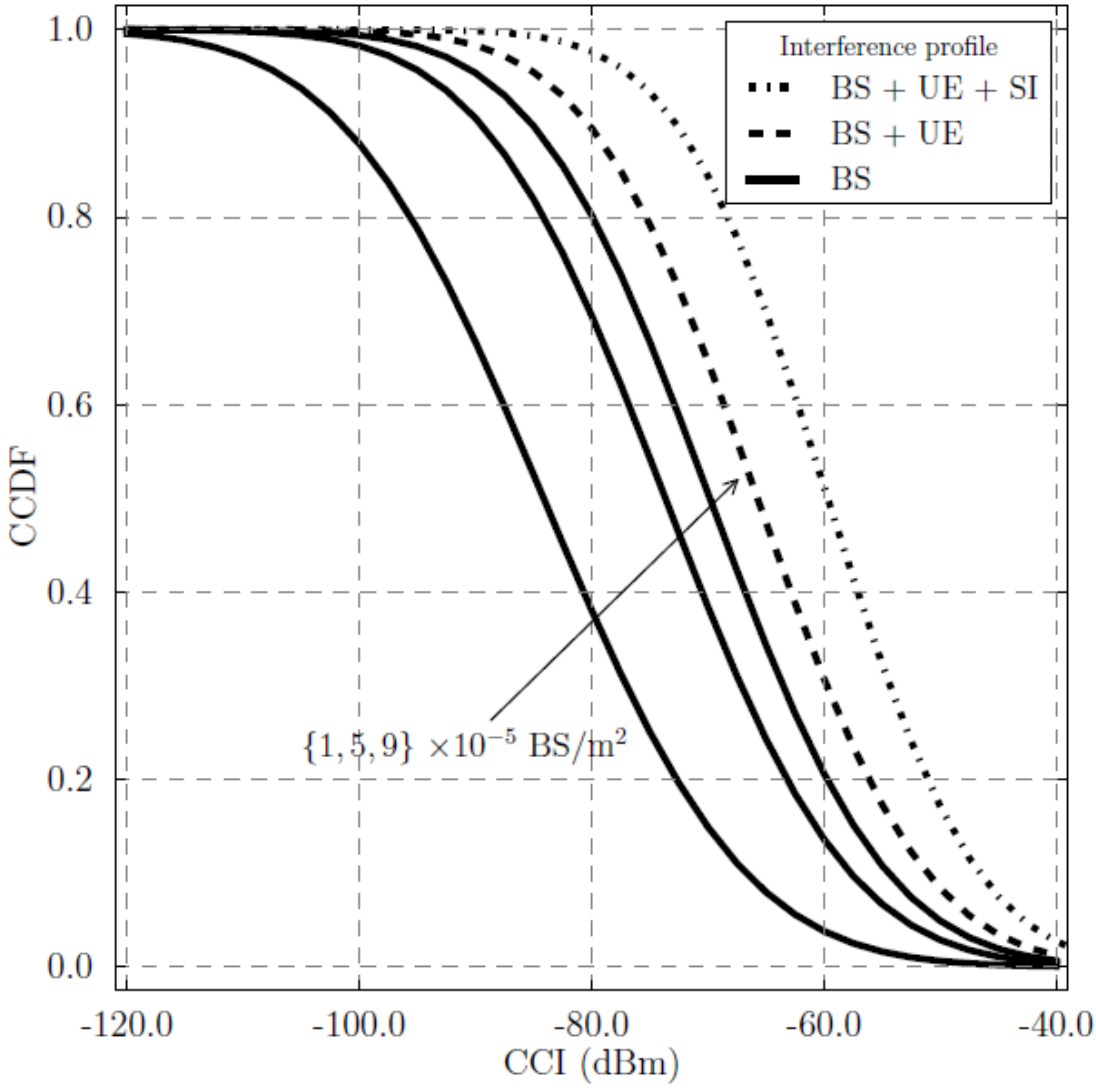

Figure 55 Shows, for increasing density of interferes, the CCDF of the aggregate CCI at the tagged receiver from an interfering tier of HD BSs (solid lines ideal FD BSs (no self-interference) and practical FD BSs.

Figure 56 depicts the average SIR as a function of the density of interferers for different values of SI cancellation coefficient. Notice that the quality of the SI cancellation scheme employed by the FD UEs considerable affects the perceived SIR. It is worth noticing that the HD scenario experiences higher SIR, while the performance of the FD scenario improves with higher SI mitigation values. We recall that different from the HD configuration, FD communications suffer additional interference from both adjacent BSs and extra self-interference.

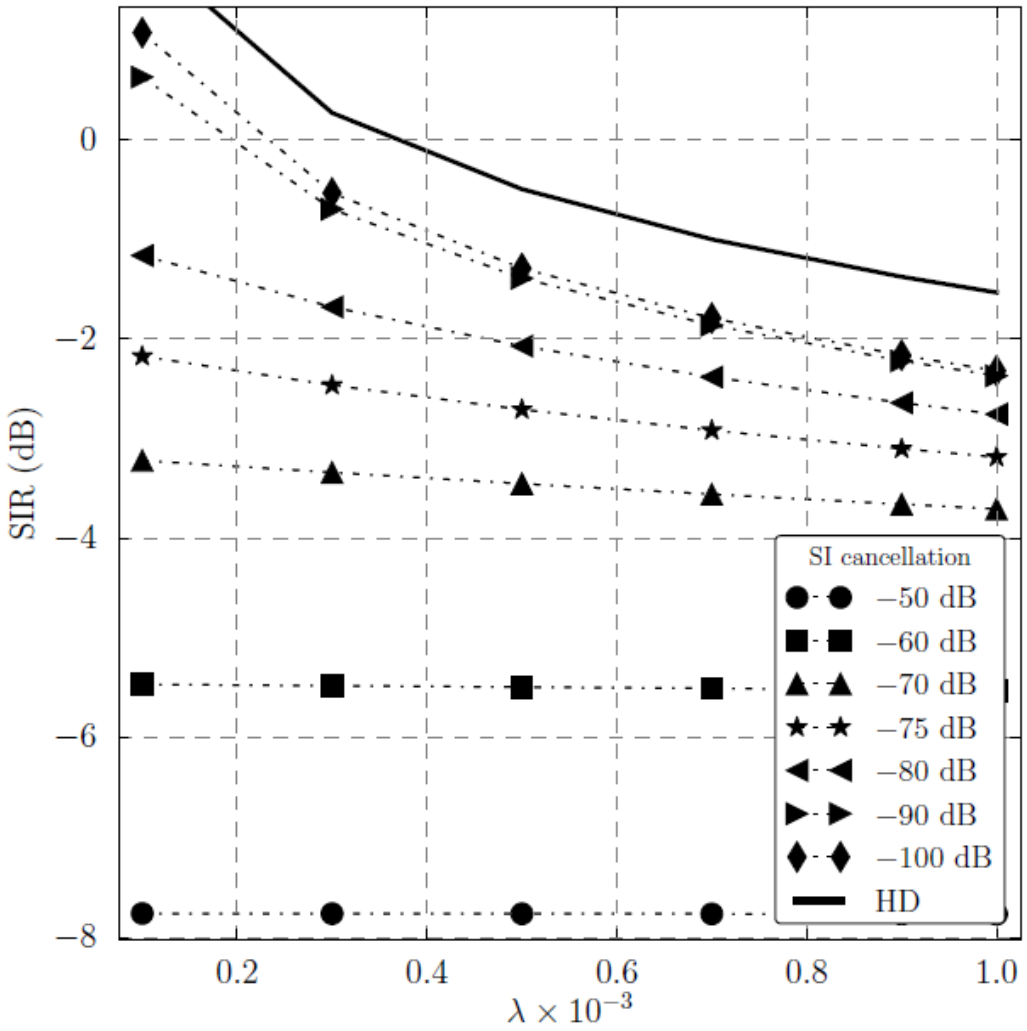

Figure 56 Shows, for increasing density of interferes, the average SIR values of self-interference cancellation, and the SIR of the HD case is shown as reference (solid line).

Next, Figure 57 shows the outage probability of the tagged receiver in FD mode as function of increasing density of interfering nodes and self-interference cancellation of δ=-100dB. In this configuration, the FD communications can effectively achieve much higher rates when compared to the traditional HD networks, even though suffering additional interference from neighboring UEs as well as self-interference. Actually, the FD network only becomes viable if the self-interference is cancelled by about -90 dB when the maximum rate nearly doubles the one achieved in HD mode.

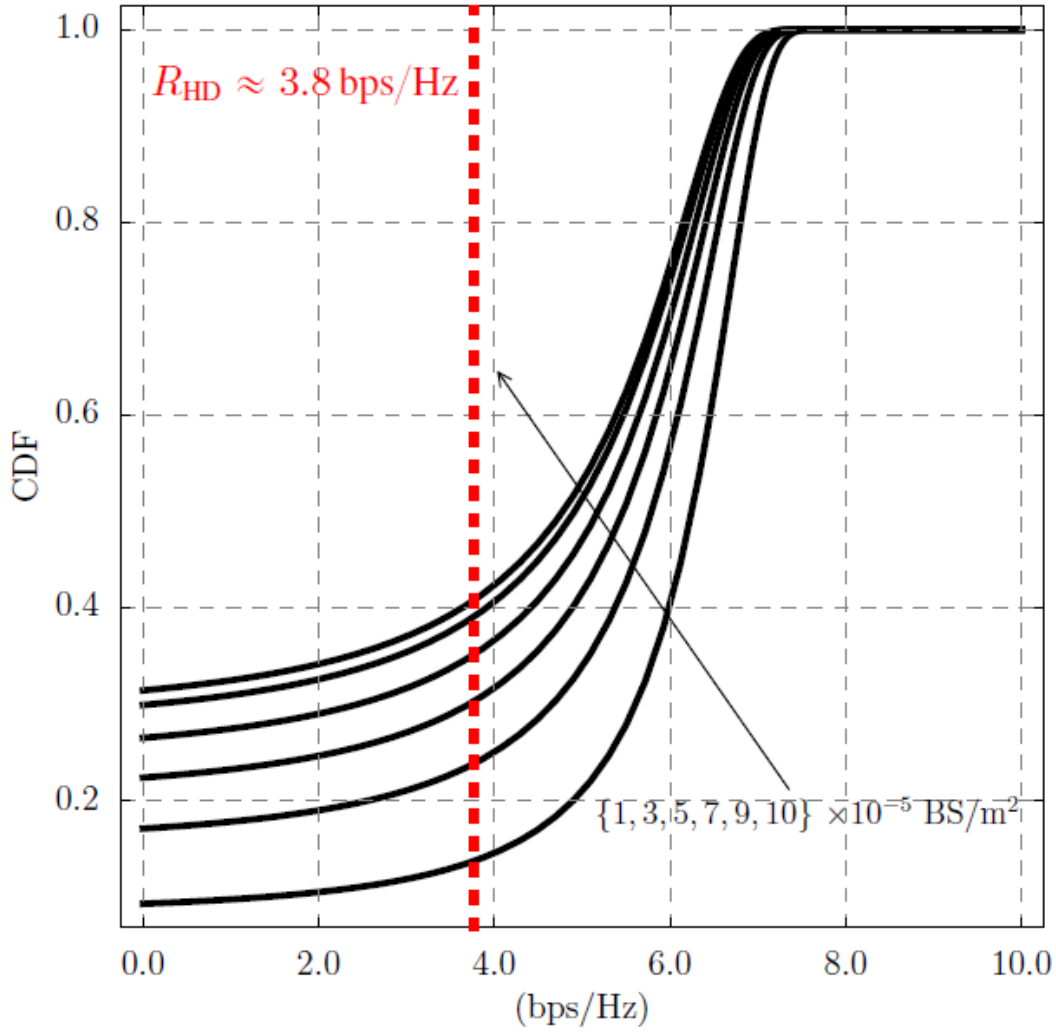

Figure 57 Shows the outage probability of the tagged receiver in FD mode as function of increasing density of interfering nodes and self-interference cancellation of δ = -100dB.

Figure 58 shows that spectral efficiency of FD schemes become more attractive and considerably outperforms the HD scheme even though suffering additional interference. For instance, for δ =-75dB and λ= 6 10^{-4}, FD scheme shows 50% higher spectral efficiency than the HD schemes, and even larger gains can be achieved if SI cancellation is improved further.

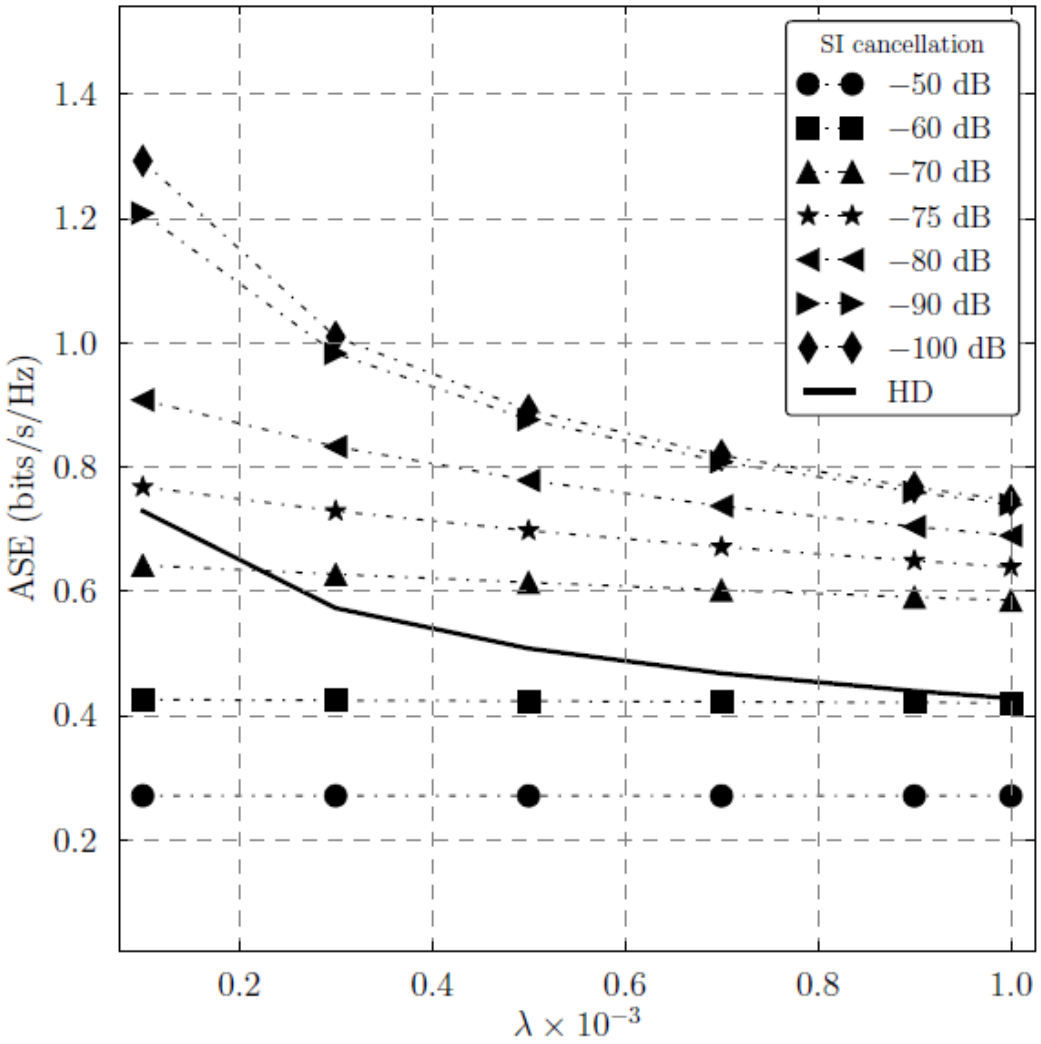

Figure 58 Depicts the SE of HD and FD cases as a function of density of interfering nodes for different SI cancellation coefficients

4.3. Multiple MIMO HD or FD UEs per MIMO FD BS in multi cell deployment scenario

4.3.1. Simulation parameters and assumptions

For the multi-user MIMO case, we consider an outdoor multi-cell scenario with eight Pico cells randomly dropped in an area of a hexagonal cell with radius of 500 meters. For brevity, we set the same number of transmit and receive antennas at each base-station and at each user. The base-stations are assumed to have 4 transmit and receive antennas, and randomly distributed 10 users in each cell are equipped with 2 transmit and receive antennas. Detailed simulation parameters are shown in the Table 11. Detailed algorithm is provided in Section 4.2 of DUPLO deliverable D4.2 [5].

Table 11: Simulation Parameters for Multi--Cell

Parameter	Settings
Cell Radius	40m
Minimum Distance between BSs	40m
Carrier Frequency	2GHz
Bandwidth	10MHz
Thermal Noise Density	-174dBm/Hz
Noise Figure	BS: 13dB, User: 9dB
Path Loss (dB) between BS and users (d in km)	LOS: $103.8 + 20.9 \log_{10} d$ NLOS: $145.4 + 37.5 \log_{10} d$
Path Loss (dB) between users (d in km)	$98.45 + 20 \log_{10} d,\ d \leq 50$m $175.78 + 40 \log_{10} d,\ d > 50$m
Path Loss (dB) between BSs (d in km)	LOS: $89.5 + 16.9 \log_{10} d,\ d < 2/3$km, LOS: $101.9 + 40 \log_{10} d,\ d \geq 2/3$km, NLOS: $169.36 + 40 \log_{10} d$
Shadowing Standard Deviation between BS and users	LOS: 3dB, NLOS: 4dB
Shadowing Standard Deviation between BSs	6dB

In Figure 59, the system behavior is observed in connection to the dynamic range, i.e., transmitter distortion k and receiver distortion b. While the full-duplex system performance drops rapidly as the dynamic range decreases, the half-duplex system shows much higher robustness. This is expected as the roles of transmitter distortion and receiver distortion are most effective in the self-interference channel where higher levels of error shall remain due to the higher signal intensity. For

very small values of dynamic range, where full-duplex and half-duplex system performance suffers simultaneously, as expected, only one communication direction is selected to achieve the optimal sum rate. It is interesting to observe that while for relatively higher dynamic range region, the system tends to assign higher rate to uplink, this role switches as the dynamic range decreases.

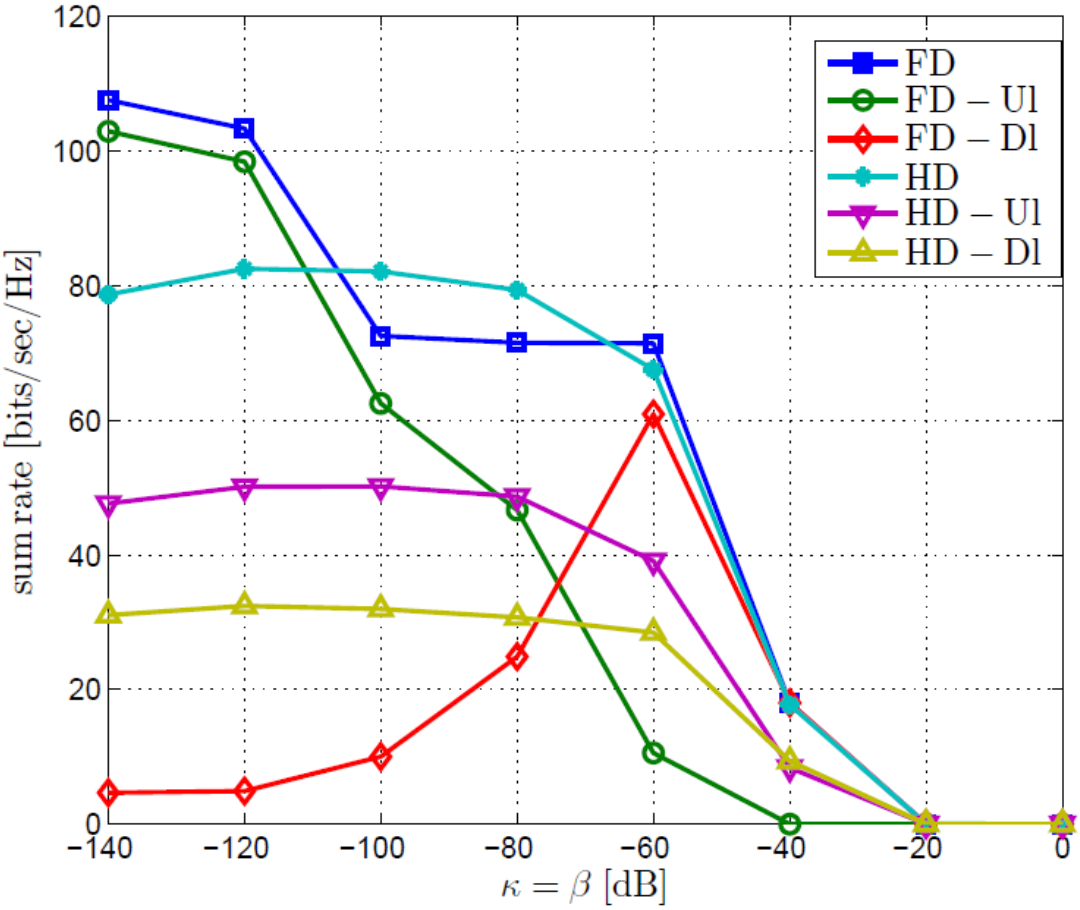

Figure 59 Network sum rate [bits/sec/Hz] vs. system dynamic range k, b .

It is important to note that while the channel matrices are assumed given for each user in our scenario, it is essential for a practical system to exploit a smart channel assignment algorithm prior to precoder/decoder design. This is particularly essential for a full-duplex setup as the CCI can be reduced by assigning the users with weaker interference paths into the same channel. In order to incorporate the effect of channel assignment into our simulation, we assume an attenuation coefficient, namely e on the CCI channels, which represent the degree of isolation among uplink and downlink users due to smart channel assignment. The effectiveness of the CCI isolation, based on a channel assignment stage is studied in Figure 60 which magnifies the importance of smart resource allocation schemes for full-duplex networking.

Note that our scenario, FD BS serving FD UEs, also covers the scenario FD BS serving HD UEs, because the additional interference paths introduced with the full-duplex operation of the users can be set to zero in FD user case, and thus the FD scenario comes down to HD scenario. In this regard, the algorithms proposed in D4.2 are readily applicable also to the HD case.

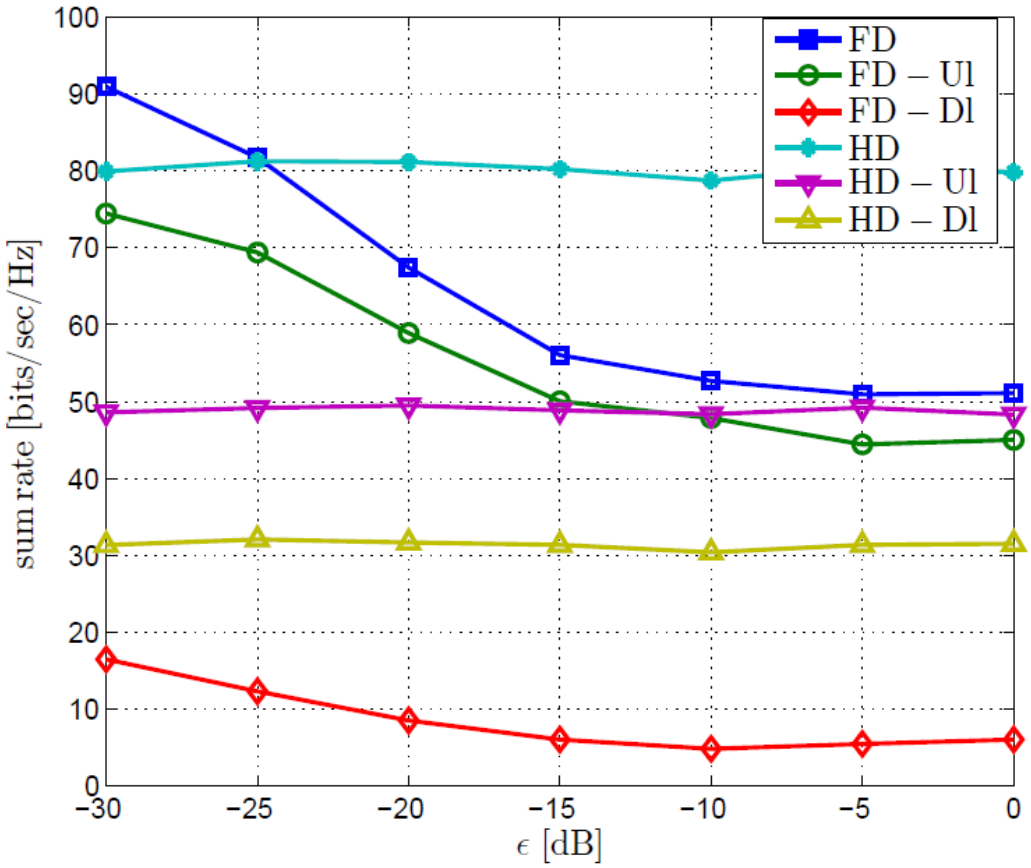

Figure 60 Network sum rate [bits/sec/Hz] vs. CCI isolation (ϵ).

5. FULL-DUPLEX RELAYING

5.1. Three node relaying case (multiple HD UEs per relay FD BS in single cell deployment scenario)

In this study we assume a Nakagami-m fading scenario for all channel links, including the self-interference. Based on this assumptions, the performance of dual-hop FD decode-and-forward relaying schemes subject to co-channel interference (CCI), self-interference at the relay (R), and noise at the relay and destination (D) is investigated. Please refer to Chapter 5 of DUPLO deliverable D4.2 [5] for a detailed system model description.

Some recent works examined the performance of dual-hop cooperative networks under CCI [18]-[20], but the analysis was performed in a HD relaying context. Herein, two main scenarios are considered. In the first scenario, the direct link between the source (S) and destination is seen as interference and a conventional FD dual-hop (FDDH) cooperative protocol is employed. On the other hand, in the second scenario the direct link is seen as useful information at the destination and a FD joint decoding (FDJD) cooperative scheme is adopted. In both schemes, the effect of self-interference at the relay (due to its full-duplex nature) is taken into account. Accurate, closed-form expressions for the outage probability are derived for the general case, in which CCI and noise are assumed at both the relay and destination. Based on these expressions, which are found in [21], we address special cases assuming CCI only at the relay and assuming CCI only at the destination. It is shown that CCI at the relay is more harmful for the system performance than CCI at the destination. The correctness of our formulations is verified by Monte Carlo simulations.

5.1.1. Analysis parameters and assumptions

Next, we introduce some representative numerical examples for the outage probability of the considered FD cooperative schemes. Unless otherwise stated, we assume a target transmission rate of $R = 2$ bits/s/Hz $\alpha = 4$ being the path-loss exponent. Moreover, we assume that R is at the middle of a normalized to unity straight line between S and D. Additionally, we assume that the self-interference is characterized by parameter $m = 1$ (equivalent to Rayleigh fading) and self-interference cancelation of $\delta = -40$ dB. We also assume that R and/or D suffers interference from $K = 5$ distinct nodes with parameters: fading figure $m = \{1.5, 2, 2.2, 2.6, 3.1\}$ and fading scale of $\Omega = \{1.3, 1.8, 2.5, 2.5, 3\}$. Without loss of generality we assume the same parameters for the interferers of R and D.

Notice that better R-D link brings performance improvements to FDDH, while the S-R link is impacted more on the FDJD scheme. The case in which both R and D suffer the effect from the co-channel interferers is seen in Figure 61 It is interesting to see that a better direct link does not bring

great performance gains, while the S-R link considerably affects the FDJD scheme and the R-D link has greater influence in the performance of the FDDH method. We recall that in FDDH the direct link is also seen as interference, thus such scheme has its performance considerably bounded by the interference level. Counter-intuitively, a better direct channel does not bring great advantage to the FDJD scheme; instead the performance is limited by the first hop.

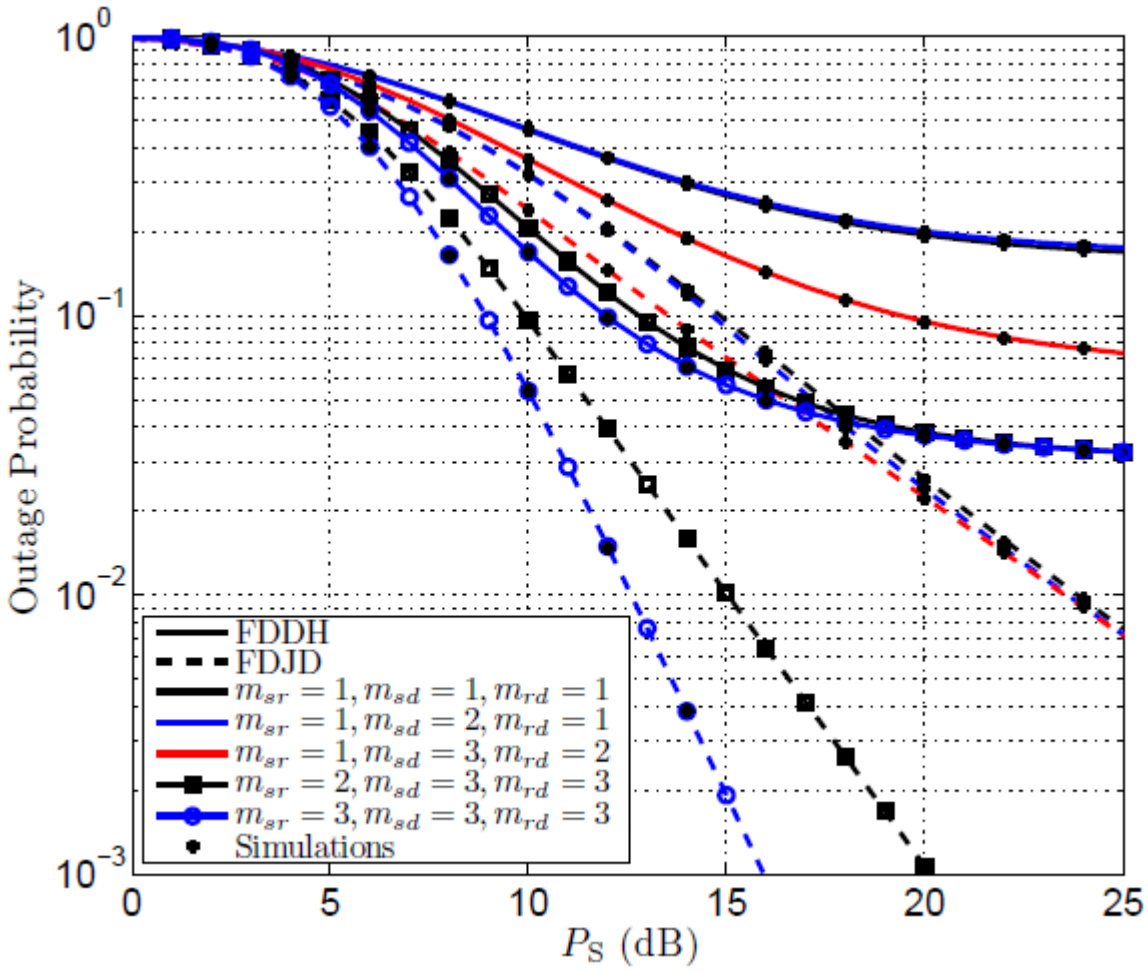

Figure 61 CCI at D and R. Outage probability as a function of PS for FDDH and FDJD for distinct m parameters.

Next, in Figure 62, we compare all three scenarios of FDJD with the case where R and D are only noisy. As we can see from Figure 62, CCI at R considerably damages performance, while only at D it is possible to achieve high diversity as well as low outage probability.

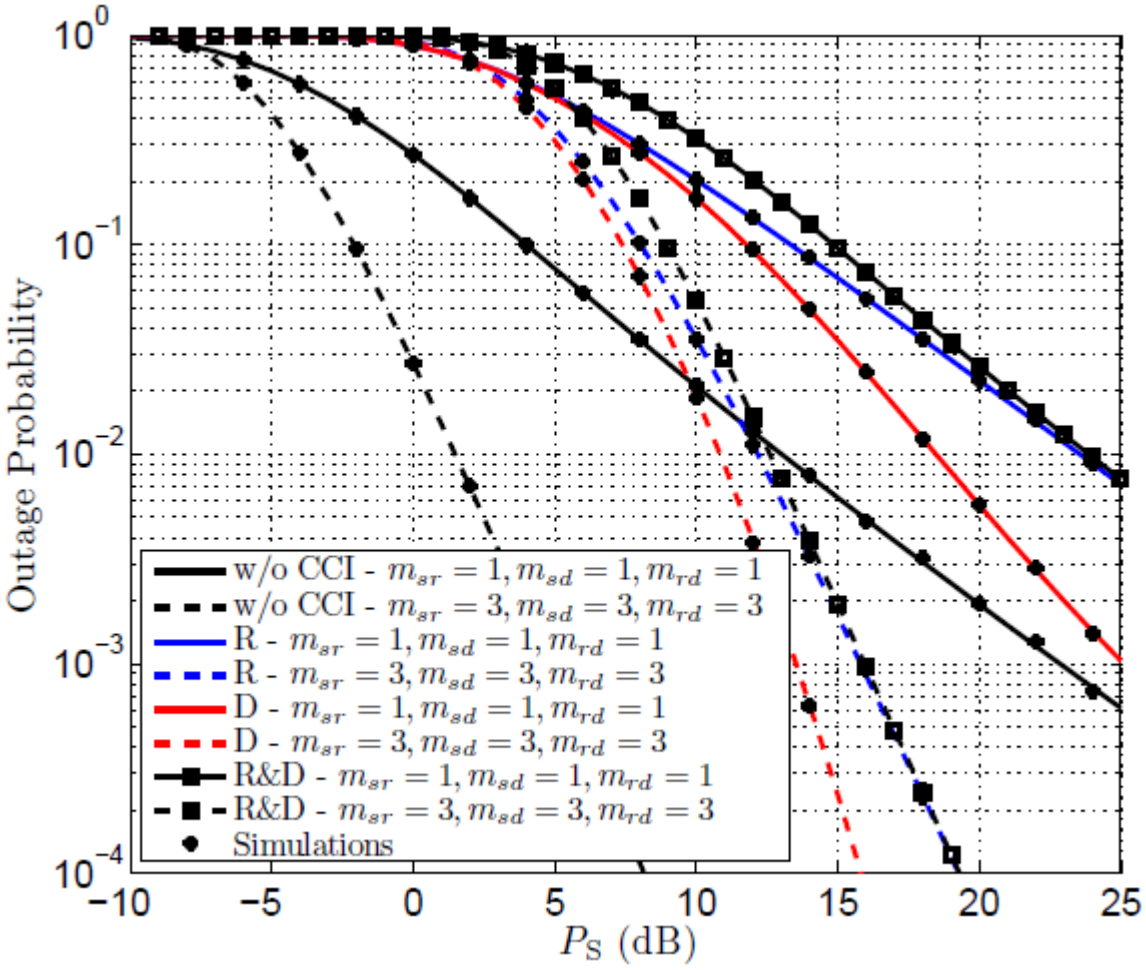

Figure 62 Outage probability as a function of PS for FDJD for distinct m parameters comparing all three scenarios.

5.2. FD relaying: network level analysis (multiple HD UEs per relay FD BS in multi cell deployment scenario)

Herein, a semi-Markov process is used to model relay selection procedure for cooperative diversity protocols in full-duplex networks. We investigate the impact of both the cost of selecting relays at hop basis and self-interference on the overall network performance. Thus, a dynamic relay selection procedure is considered where a suitable relay is selected at each hop and the cost of this selection procedure is incorporated into the achievable rate. Stochastic geometry is used to model network deployments, following the steps presented in [16], [17]. We study how fixed and reactive relay schemes perform in a FD configuration. In the reactive relay schemes, the standard binary tree algorithm is implemented – relay selection algorithms (RSA). In fact, a totally random approach based solely on the Standard Tree Algorithm (STA) is used to implement the RSA. We summarize its behavior as follows: the source sends a Request-to-Send (RTS) packet to initiate the relay selection procedure. Nodes that listen to this request reply with a Clear-To-Send (CTS) packet based on the probability of accessing the channel. If a collision occurs, nodes that have transmitted in previous slot retransmit or not through random process similar to a Q-sided coin. The source node should receive the replies from all the candidate relays so as to select the next relay greedily, for example the closest node to the destination whether there is one available.

5.2.1. Analysis parameters and assumptions

For the desired link and interferers, a composite fading channel model with Nakagami-m parameter of m=16 and shadowing standard deviation of 10 dB considered. Interferers are scattered over the network area with inner and outer radii given by R_m = 25 and R_M = 500 meters, respectively. A density of $\lambda = 5\,10^{-5}$ nodes/m2 is considered (which corresponds to a mean number of nearly 40 interferers) and the path loss attenuation is α=3. To compute the relay selection interval, we assume three contending relays within source's forwarding region.

Figure 63 shows the steady-state throughput efficiency $\bar{\eta}$ for increasing separation distance between source-destination pair. As evidenced by reactive relay curve (red dashed line), the steady-state throughput is severely compromised by the relay selection. On the other hand, when a fixed relay is considered within source's transmission range, becomes much less susceptible the degrading effect of longer separation distance between source and destination.

Figure 64 presents the steady-state throughput for increasing transmission power of source node, whereas interferers transmit at 30dBm. The separation distance between source and destination is kept at 50m and the relay is randomly located in the source's forwarding region. As expected the steady-state throughput improves with higher source's transmission power. The reactive relay benefits

most from high transmission power mainly because source can reach the destination more often without undergoing long relay selection intervals to select a suitable relay.

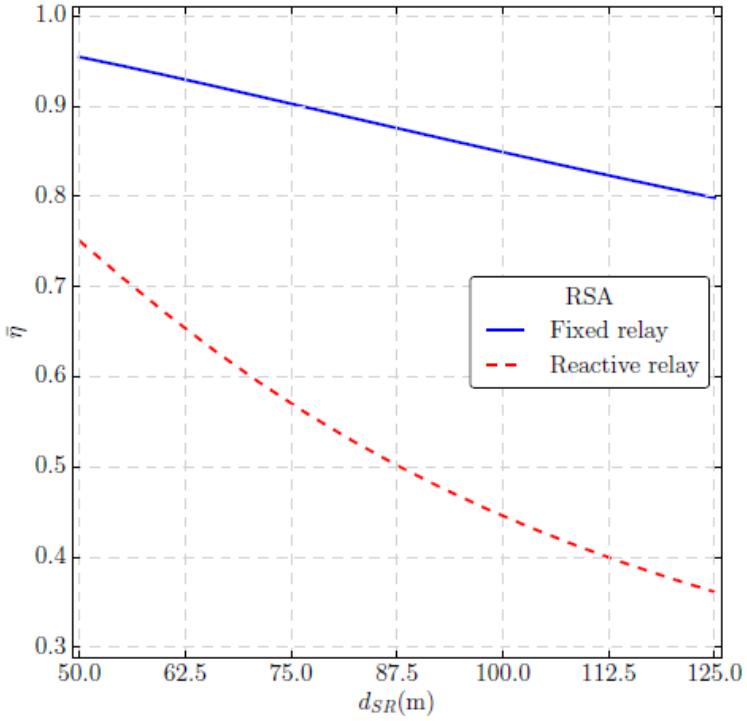

Figure 63 a) Steady-state throughput efficiency for increasing separation distance between source – destination pair in HD configuration.

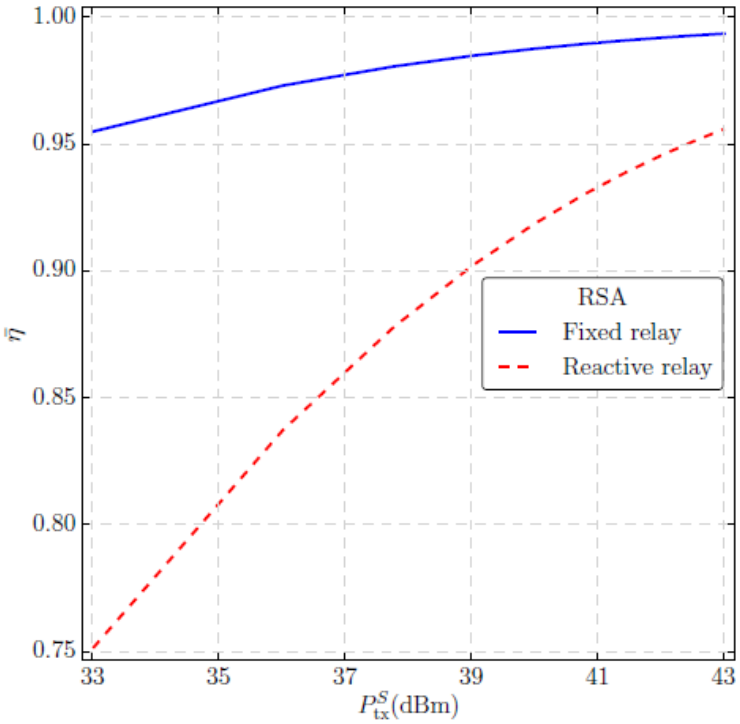

Figure 64 Steady-state throughput efficiency increasing source's transmission power in HD configuration.

Steady-state throughput efficiency for decreasing loop interference attenuation with FD configuration is shown in Figure 65. The separation distance between source-destination is set to 50m. As previously observed in the HD configuration, the steady-state throughput with reactive relay is severely degraded by the relay selection procedure and barely outperforms the HD scenario with 100dB loop interference attenuation. Regarding the fixed relay scheme, the FD configuration with loop interference attenuation ranging from -100 to nearly -70dB shows much better performance than HD mode, whereas the performance degrades faster with low attenuation values.

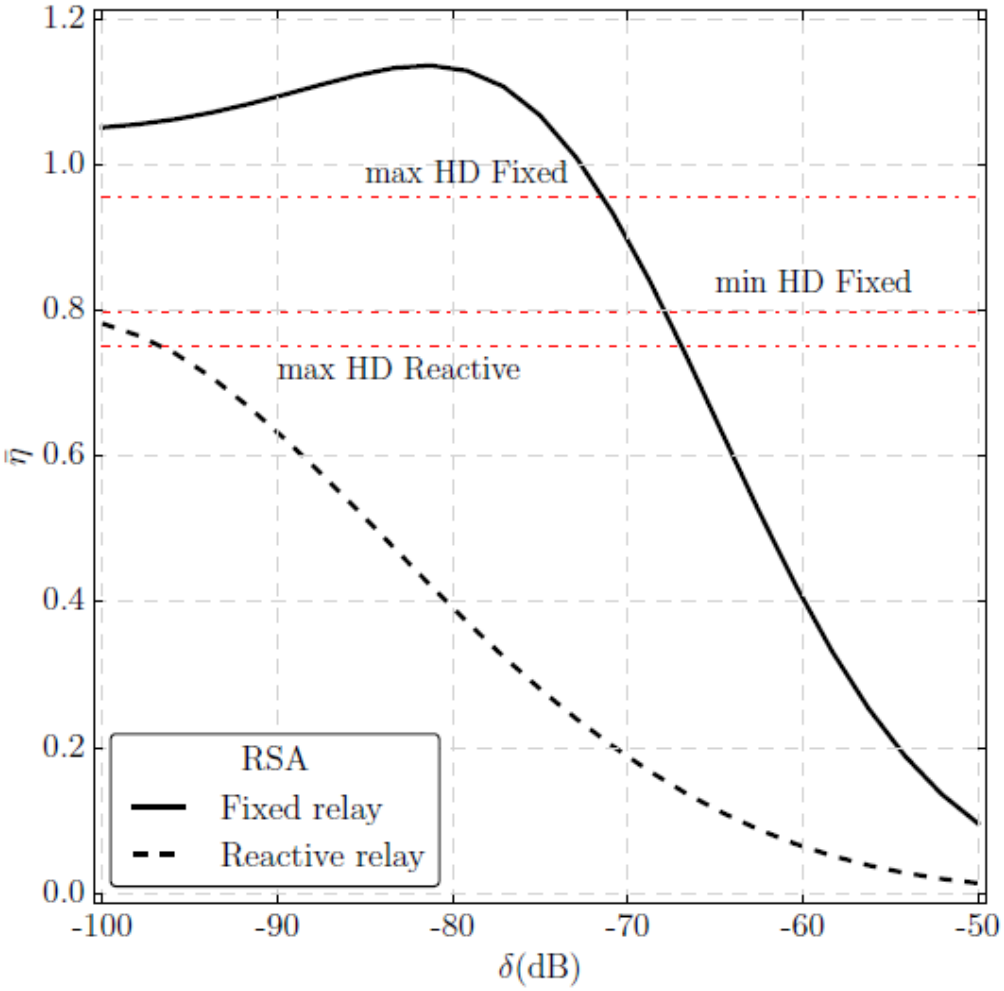

Figure 65 Steady-State Throughput as a function of the residual-self-interference cancellation at the FD relay

6. IEEE802.11 MANET WITH FD TRANSCEIVERS

6.1. Introduction

In this section, we provide scenarios and numerical results for the protocols devised in Chapter 6 of DUPLO deliverable D4.2 [5]. All the results given below were obtained through the OMNET++ simulator which served as our main development tool for the IEEE 802.11 MANET class of protocols.

6.2. Simulation scenarios

In order to assess the performance gains in full duplex in MANET environments, we have devised several scenarios in order to test the performance of the MAC protocol described in D4.2 section 6.1 as well as the performance improvements obtained through the use of full duplex aware routing mechanisms.

In the first set of scenarios, we study the performance improvements obtained through the use of the full duplex MAC on simple line topologies of 2 or 4 nodes shown in Figure 66 and Figure 67 respectively. In both cases, any node in the topology is in contact with its closest neighbors only. In order to measure the performance improvements, we use either UDP or TCP traffic.

In the case of UDP traffic, both extremities of the line are source and destination at the same time. By doing so, we enforce symmetry on the traffic. We generate Poisson distributed traffic with different arrival rates and measure the average throughput at both destinations.

In the case of TCP traffic, there is only one source and one destination which are the two extremities of the line. The traffic is no longer symmetric as data packets flow from source to destination while acknowledgement packets flow from destination to source.

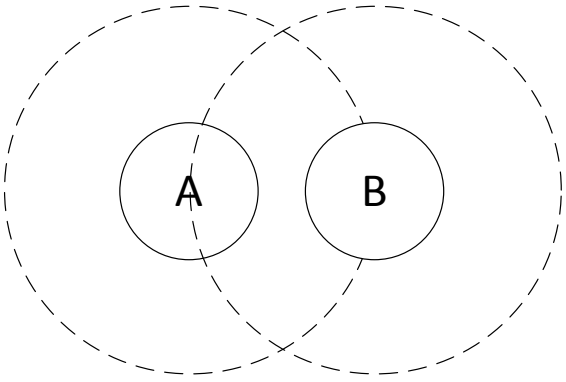

Figure 66 2 node topology

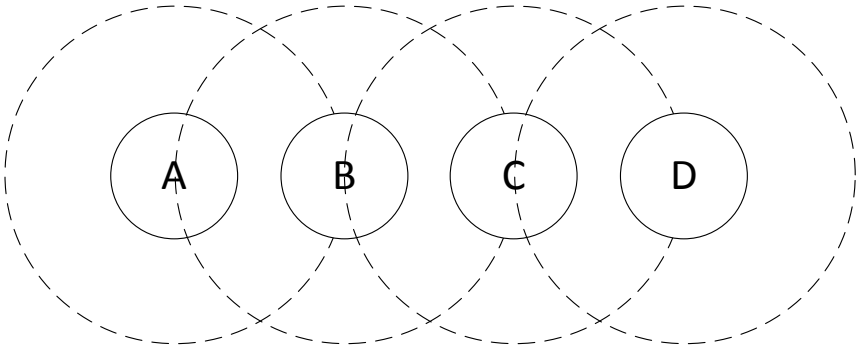

Figure 67 4 node topology

In the second set of scenarios, we study the impact of full duplex on ad-hoc routing. In order to do that, we start with a simple topology containing 6 nodes (see Figure 68). In this case, we consider 2 sources of traffic (nodes A and F) and 2 destinations (nodes F and A). Therefore, there are several possible routes to go from either sources to either destinations. We mainly focus on 2 paths:

- The path that goes through nodes B and C
- The path that goes through nodes D and E

We then generate Poisson distributed UDP traffic from both sources towards both destinations and measure the average throughput at the destinations. We do this for different routing schemes:

- Static routing
    - Same path routing
        - Both traffics go through the same nodes (e.g. ABCF and FCBA)
    - Different path routing
        - Traffics go through different paths (e.g. ABCF and FEDA)
- Ad-Hoc routing
    - AODV (reactive ad-hoc routing protocol)
    - Batman (pro-active ad-hoc routing protocol based on OLSR)

In order to study more thoroughly the impact of routing decisions on leveraging the full duplex bandwidth, we extend the tests on a bigger topology consisting of 30 nodes over a square surface of 0.5 km by 0.5 km. Nodes are randomly distributed according to a uniform law and several sources and destinations are randomly picked within those nodes. This is depicted in Figure 69

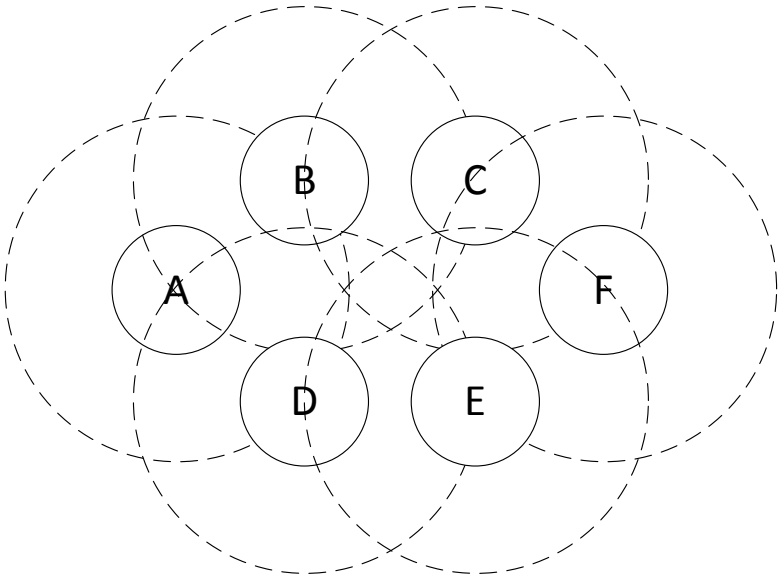

Figure 68 6 node topology

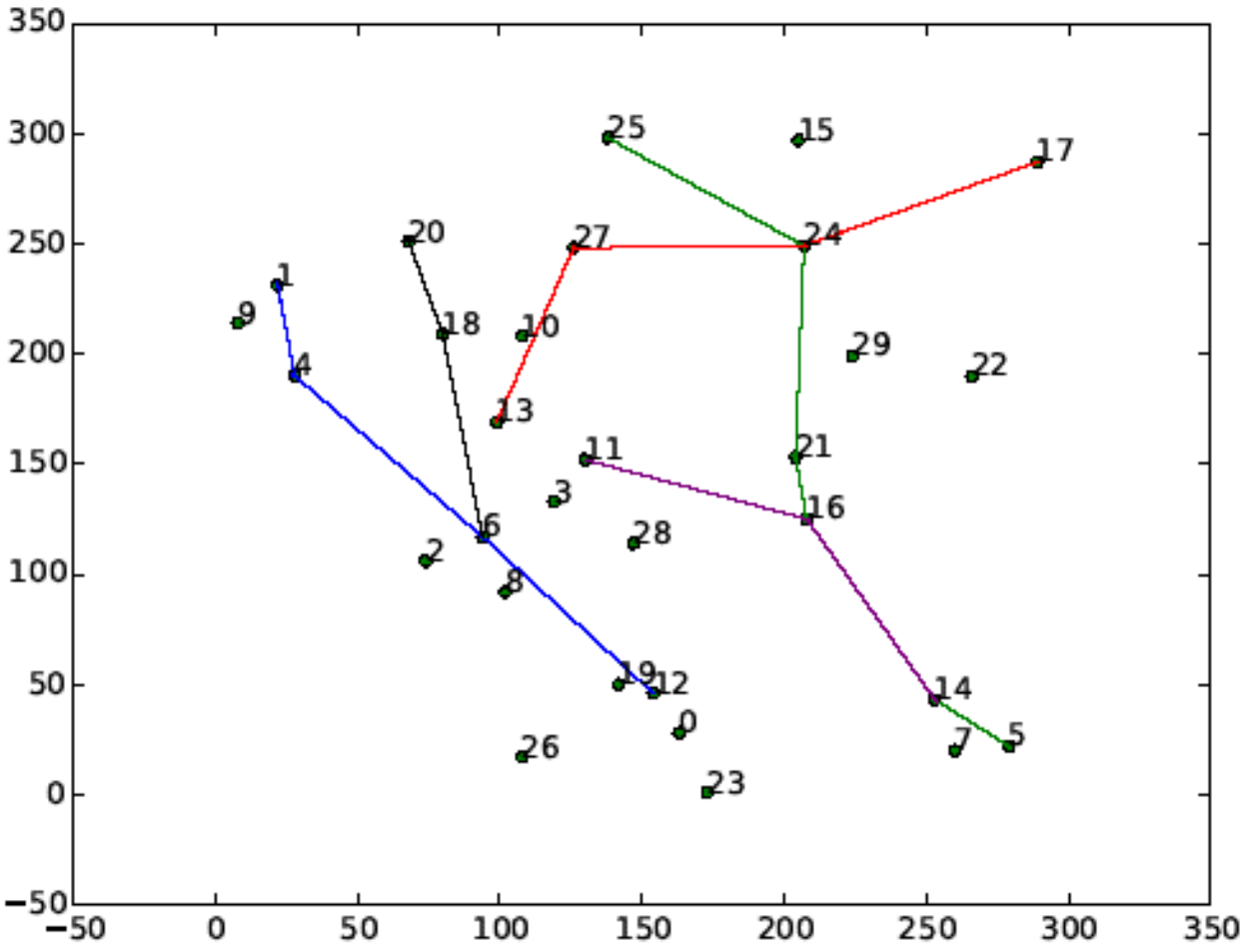

Figure 69 Large scale topology (dense network)

6.2.1. Simulation parameters and assumptions

All simulation parameters are given in Table 12:

Table 12 Simulation Parameters

Parameter	Value
Carrier Frequency	2.4 GHz
Transmission Power	1 dBm
Sensitivity	-85 dBm
Path Loss Model	Free Space
Path Loss Alpha	2
Simulation duration	1200s
Number of runs	12
Area	500 m x 500 m
Number of nodes	2 - 30

In all simulation scenarios, we assume that all nodes have enough SIC to compensate the SI over the whole range of transmission (defined in part by the sensitivity and transmission power of each node).

6.2.2. MAC Performance results

We first display the throughput measurements over the 2 node topology in Figure 70 and Figure 71. In the case of UDP - where two traffic flows occur at the same time (from A to B and from B to A) - we observe a 93% increase in average throughput in full duplex compared to half duplex for both flows. One may argue that typical traffic patterns do not display this kind of symmetry. This is the reason why we also ran a simulation using one TCP flow. In that case - where there is only one traffic flow (from A to B) - we still observe an 86% increase in average throughput using full duplex.

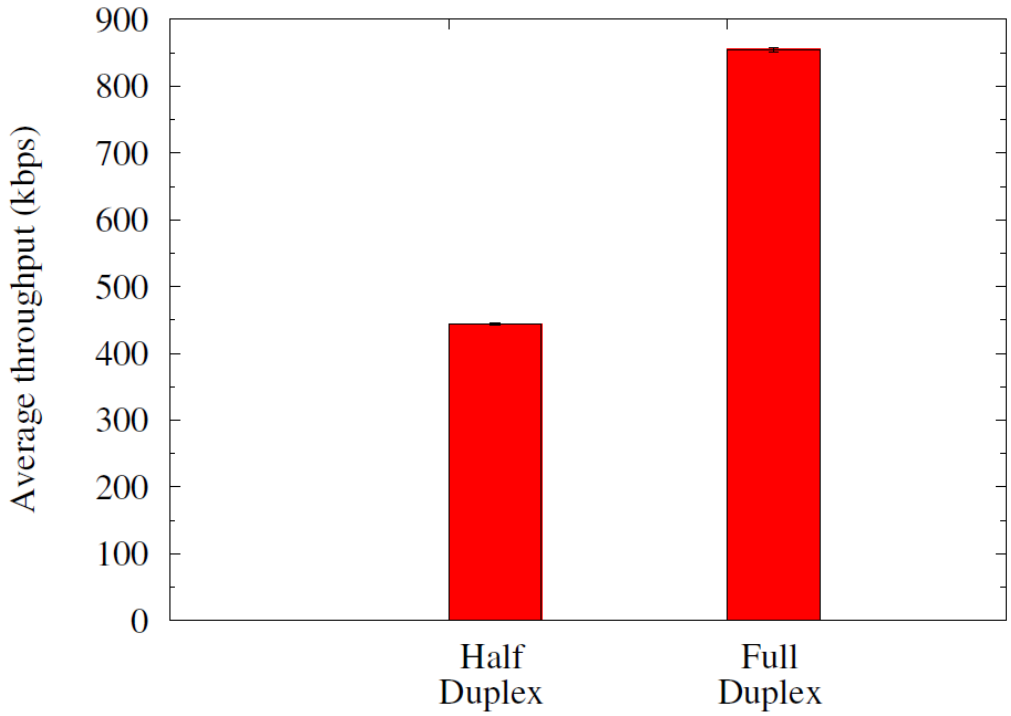

Figure 70 UDP throughput comparison

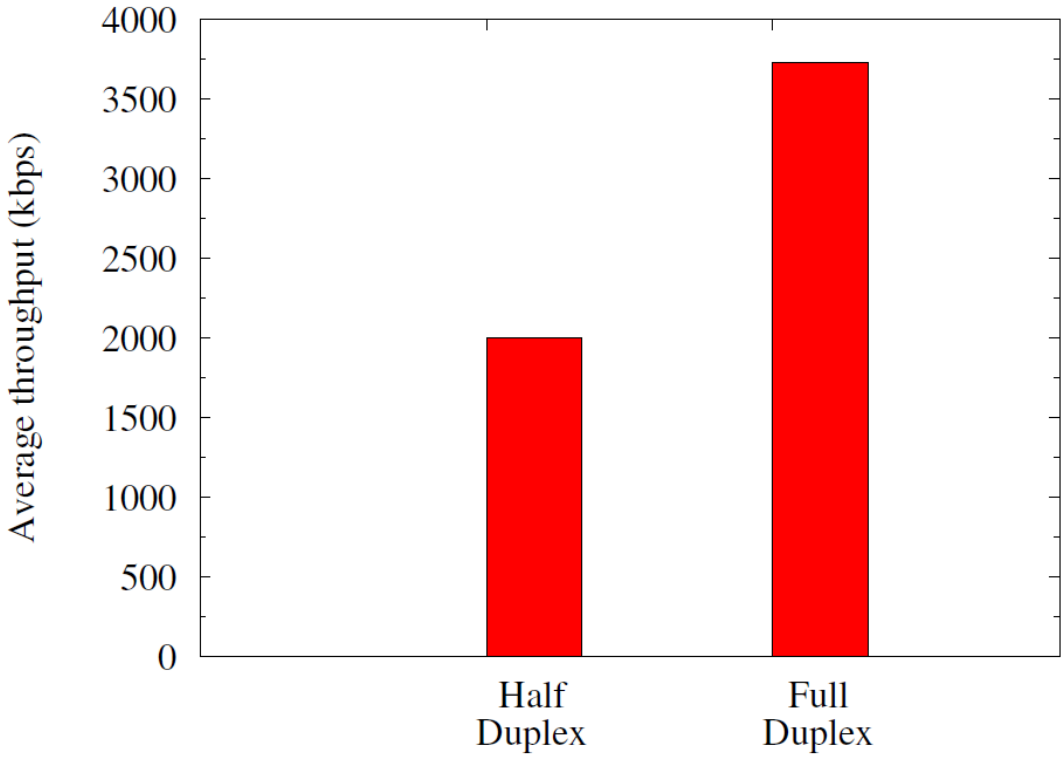

Figure 71 TCP throughput comparison

Running the same tests over the 4 node topology yields similar results, with full duplex yielding 237% increase in throughput in the UDP case and 54% increase in throughput in the TCP case.

All these results show the performance gains obtained through the use of a full duplex enabled MAC protocol. What we observe is that even in the case where we don't have symmetrical traffic; we still get important gains from the full duplex paradigm compared to half duplex.

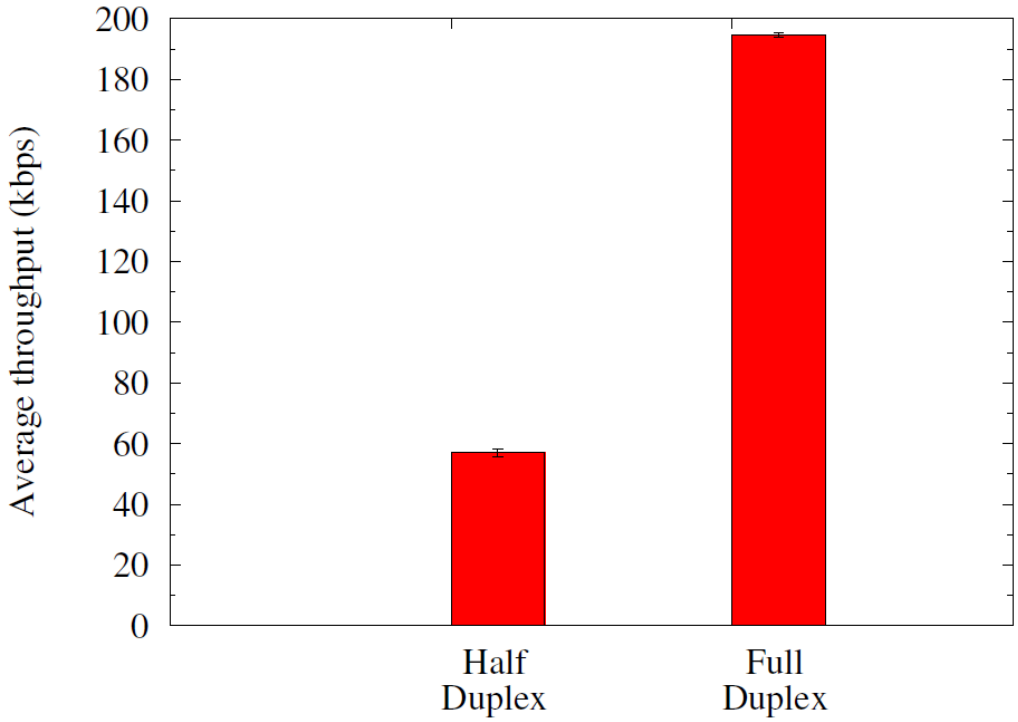

Figure 72 UDP throughput comparison

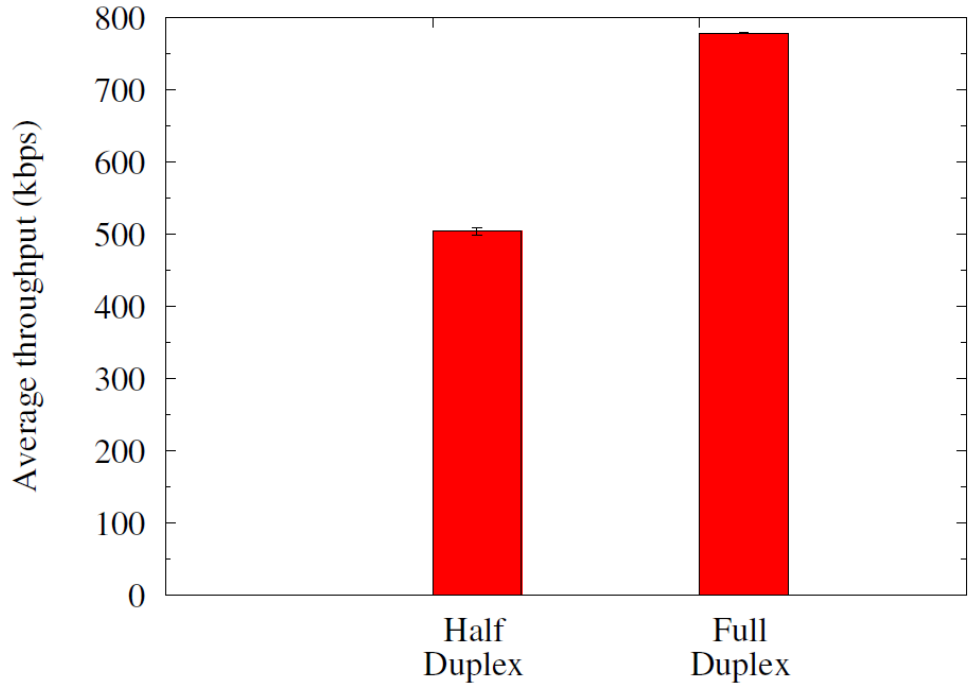

Figure 73 TCP throughput comparison

6.2.3. Routing results

In this section, we display the results relative to the second set of scenarios. We compare the different routing strategies described above and plot the CDF of the average throughput measured at both destinations for every case considered. The results in Figure 74 clearly show that using the “same route” routing scheme is beneficial on a full duplex network compared to all other routing approaches. This underlies the need for different routing approaches in wireless full duplex networks compared to wireless half duplex networks. Indeed, using the same path for both traffics presents the advantage mutualizing the radio resources every time packets need to be transferred between the relays. In those cases, full duplex exchanges occur while in the other schemes (like the “diff route” scheme) relays would have to exchange frames alternatively on every step in the path thus lowering the overall throughput.

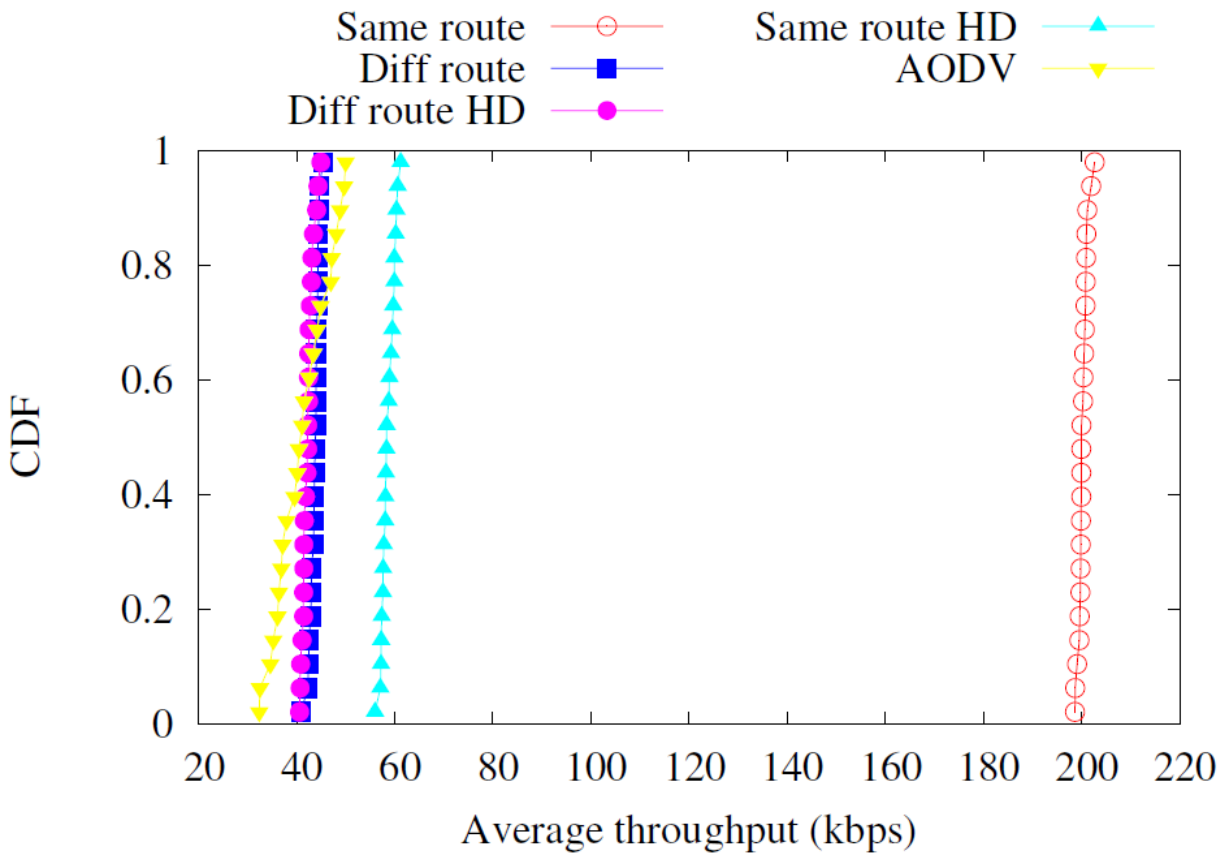

Figure 74 Routing comparison

We now focus on the large scale network results displayed in Figure 75. The results were obtained using UDP as a transport protocol and selecting 5 sources and 5 destinations over the 30 node network. Each simulation set is defined as a list of sources and destinations over a given

topology. When changing sets, the topology is randomly redefined and the sources and destinations are again randomly chosen. Once the parameters for a given set are chosen, we start multiple runs of simulations. The results obtained here show the average results over multiple simulation sets.

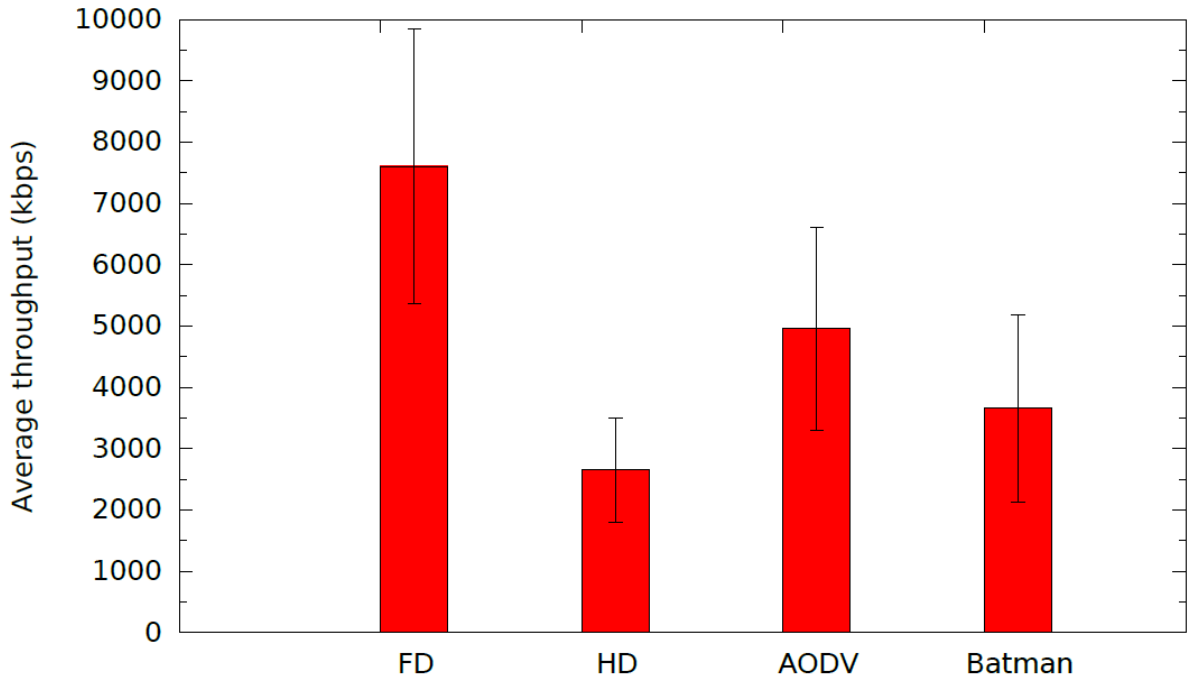

Figure 75 Large scale simulation results (with 95% confidence intervals)

The results in Figure 75 show the average throughput at both destinations and sources (bidirectional UDP traffic from source to destination and from destination to source).

What we observe at first glance is the net improvement of using full duplex when compared to half duplex in the static routing case. On average, we observe an increase of 187% in average throughput which is higher than the 100% increase expected from full duplex technology.

We also observe better performance by using static routing in FD mode than by using readily available ad-hoc routing protocols. Indeed, we observe that on average, static routing performs 53% better than AODV and 107% better than Batman. While these results can, in part, be accounted for by the overhead of signalling of both those ad-hoc routing protocols, they also show that having bidirectional routing paths in FD networks increases the overall throughput.

7. RECOMMENDATIONS AND FURTHER WORK

Herein, we provide (in a chapter by chapter basis) some recommendations and directions for further work in for the deployment of full-duplex small cells. There results introduced herein can be applied in the context of the upcoming next generation of wireless communication, known as 5G. Such networks will be highly dense and heterogeneous and will require high spectral efficiency, data rates, coverage and connectivity. Therefore, full-duplex systems, such as the ones studies in DUPLO, pave path for introducing full-duplex transmission as an air interface technology for future 5G systems.

Chapter 2 provided an analysis on full-duplex link rate region as well as power allocation policies for single full-duplex links. Although the numerical analysis has been done for typical LTE system carrier frequencies and signal bandwidths, the methodology can be applied and extended to account for mm-wave frequencies and much higher signal bandwidths (which of course require more sophisticated analog cancellation techniques). Typical use cases for this kind of single links are wireless fronthauling and backhauling in cellular networks.

Chapter 3 provides a comprehensive set of performance results for single full-duplex small cell deployment; while Chapter 4 assesses the performance of multiple full-duplex small cells. The study results in chapters 3 and 4 clearly demonstrate the importance of radio resource management (scheduling, power control) in optimizing the full-duplex system performance. DUPLO has mainly focused on single cell scenario as the first step in full-duplex system performance analysis in network level. Multiple cell scenarios have been covered in some specific cases. In the next years, there will be a significant increase on the number of small cells, thus *coordination*, *self-organization, flexible and efficient use of spectral resources, scheduling* and *radio resource management* in general are aspects that will be fundamental for the next generation of wireless communications. DUPLO have put some light into this matter, by providing benchmarks, guidelines and algorithms that deal with densification; however, those topics still need to further investigation. For example, the impact of signaling limitations and imperfect channel state information (e.g., in scheduling algorithms) on the system performance, solutions to combat with inter-cell interference, and co-existence with half-duplex systems require further studies to get more comprehensive view on how full-duplex could be best deployed to future 5G systems. Chapter 5 addresses full-duplex relaying. FD relaying overcomes the spectral inefficiency of its HD counterpart, and additionally enhances performance. In what regards to the design of cooperative networks with FD relays, DUPLO provides theoretical benchmark and guidelines. Therefore, practical protocols and implementation need to be assessed. When considering MANET as in Chapter 6, FD technology can help to provide enhanced throughput to all nodes in the network. This can be made possible when using a full duplex enabled MAC protocol. There are two types of full duplex MAC protocols proposed in the literature, i.e., bidirectional full duplex [16] and relay full duplex [17] [18]. While relay full duplex seems more adapted to MANETs, our studies show that the lack of

possible channel reservation in a three node setup leaves nodes open to interference from neighbors in a dense and/or busy network. Therefore, we have implemented our own bidirectional MAC protocol in order to test the performances of full duplex in MANETs. Our results show that, in the case of MANETs, full duplex can help provide throughput gains higher than 100% in certain topologies. Furthermore, we have observed that substantial throughput gains can be achieved even with non-symmetrical traffic, for instance when using TCP as a transport protocol. Thus, it is important to consider also higher layers aspects when evaluating the overall benefits of full-duplex transmission in different network topologies.

8. CONCLUSIONS

This deliverable outlines key findings and numerical results of the DUPLO WP4 work. The focus is on studying point-to-point full-duplex links, standalone single or multi-user small cells with single/multiple full- and/or half-duplex links, full-duplex relaying, mobile ad-hoc networks and their performance. Multiple cell scenarios, as well as device-to-device networks, have been covered in some specific cases.

Numerical results from link level performance studies show that self-interference cancellation of about 80-90 dB is needed to outperform HD links. It is also demonstrated that short distance links with low transmission power (such as 5G indoor small cells) are the most suitable use case for full-duplex communication. Energy efficiency of FD links proves also to be promising.

Numerical results from conducted performance studies in network level indicate that in small area systems full-duplex transmission can provide system level performance gains over half-duplex even with moderate self-interference cancellation levels (70 dB …90 dB). However, better self-interference cancellation capability in the full-duplex transceiver is beneficial in expanding the competitive operation range of full-duplex transmission. Maximum observed system level capacity gain of full-duplex transmission over half-duplex transmission in small cell networks varies from 40% to 80% depending on the study assumptions.

Conducted system studies with full-duplex MAC protocols in IEEE 802.11 MANET kind of network environment demonstrate that full-duplex transmission can provide substantial throughput gains even with non-symmetrical traffic, for instance when using TCP as a transport protocol.

All in all, the results are encouraging, and pave path for introducing full-duplex transmission as an air interface technology for future 5G systems.

9. REFERENCES

[1] A. Sabharwal, P. Schniter, D. Guo, D. Bliss, S. Rangarajan, and R. Wichman, "In-band Full-duplex Wireless: Challenges and Opportunities", IEEE Journal on Selected Areas in Communications (JSAC), vol. 32, no. 9, Sept. 2014.

[2] B.Debaillie, D.J. van den Broek, C. Lavin, B. van Liempd, E. A. M. Klumperink, C. Palacios, J. Craninckx, B. Nauta, and A. Parssinen, "Analog/RF solutions enabling compact full-duplex radios," IEEE Journal on Selected Areas in Communications, vol. 32, no. 9, pp. 1662-1673, Sept 2014.

[3] W. Li and J. Lilleberg, "Full-Duplex Link Performance Under Consideration of Error Vector Magnitude", In Proc. on IEEE Wireless Communications and Networking Conference WCNC 2014, pp. 654 – 659,Istanbul, Turkey, April 2014.

[4] W. Li, J. Lilleberg, and K. Rikkinen, " On Rate Region Analysis Of Half- and Full-Duplex OFDM Communication Links", IEEE Journal on Selected Areas in Communications (JSAC), Vol. 32, No. 9, pp.1688 - 1698, Sept. 2014.

[5] J. Seddar, "Radio resource management and protocol solutions for full-duplex systems", INFSO-ICT-316369 DUPLO - Report D4.2, May 2015.

[6] Visa Tapio, "System Scenarios and Technical Requirements for Full-Duplex Concept", INFSO-ICT- 316369 DUPLO - Report D1.1, April 2013.

[7] 3rd Generation Partnership Project, TS 36.104 V10.2.0, LTE; Evolved Universal Terrestrial Radio Access (E-UTRA); Base Station (BS) radio transmission and reception (Release 10).

[8] 3rd Generation Partnership Project, TR 36.828 V11.0.0, Technical Specification Group Radio Access Network; Evolved Universal Terrestrial Radio Access (E-UTRA); Further enhancements to LTE Time Division Duplex (TDD) for Downlink-Uplink (DL-UL) interference management and traffic adaptation (Release 11).

[9] 3GPP TR 25.996, "Spatial channel model for Multiple Input Multiple Output (MIMO) simulations", Release 11, Sept. 2012.

[10] J. Jang and K. B. Lee, "Transmit power adaptation for multiuser OFDM systems," IEEE Journal on Selected Areas in Communications, vol. 21, no. 2, pp. 171–178, Feb. 2003.

[11] W. Yu, W. Rhee, S. Boyd, and J. Cioffi, "Iterative water-filling for Gaussian vector multiple-access channels," IEEE Transactions on Information Theory, vol. 50, no. 1, pp. 145-152, Jan. 2004.

[12] D. Bharadia, E. Mcmilin, and S. Katti, "Full duplex radios," in ACM Special Interest Group on Data Communication, Aug. 2013, pp. 375-386.

[13] M. Duarte, C. Dick, and A. Sabharwal, "Experiment-driven characterization of full-duplex wireless systems," IEEE Trans. Wireless Commun., vol. 11, no. 12, pp. 4296–4307, 2012.

[14] T. Riihonen, S. Werner, and R. Wichman, "Mitigation of loopback self-interference in full-duplex mimo relays," IEEE Trans. Signal Process., vol. 59, no. 12, pp. 5983–5993, 2011.

[15] H. Alves, D. da Costa, R. Souza, and M. Latva-aho, "Performance of block-Markov full duplex relaying with self -interference in Nakagami-m fading," IEEE Wireless Commun. Letters, vol. 2, no. 3, pp. 311–314, 2013.

[16] C. H. M. de Lima, P. H. J. Nardelli, H. Alves, and M. Latva-aho, Full-duplex communications in interference networks under composite fading channel, in 2014 Eur. Conf. Networks Commun., 2014, pp. 1-5.

[17] H. Alves, C. H. M. De Lima, P. H. J. Nardelli, R. D. Souza, and M. Latva-aho, On the Average Spectral Efficiency of Interference-Limited Full-Duplex Networks, in 9th Int. Conf. Cogn. Radio Oriented Wirel. Networks, Oulu, 2014, pp. 1-5.

[18] D. B. da Costa, H. Ding, M. D. Yacoub, and J. Ge, "Two-way relaying in interference-limited AF cooperative networks over Nakagami-m fading," *IEEE Trans. Veh. Technol.*, vol. 61, no. 8, pp. 3766–3771, Oct. 2012.

[19] H. Yu, I.-H. Lee, and G. Stuber, "Outage probability of decode-and-forward cooperative relaying systems with co-channel interference,"*IEEE Trans. on Wireless Commun.*, vol. 11, no. 1, pp. 266–274, 2012.

[20] N. Wu and H. Li, "Performance analysis of SNR-based decode-and-forward opportunistic relaying in the presence of co-channel interference,"*IEEE Trans. Veh. Technol.*, available on Early Access 2013.

[21] H. Alves, R. D. Souza, and M. Latva-aho, Full-Duplex Relaying Systems Subject to Co-channel Interference and Noise in Nakagami-m, in VTC-2015 Work., 2015, pp. 1-5.

[22] S. Goyal, P. Liu, S. Panwar, R. DiFazio, R. Yang, J. Li, and E. Bala,"Improving small cell capacity with common-carrier full duplex radios," in *Proc. IEEE Int. Conf. Commun. (ICC 2014)*, pp. 4987-4993, June 2014.

[23] X. Shen, X. Cheng, L. Yang, M. Ma, and B. Jiao, "On the design of the scheduling algorithm for the full duplexing wireless cellular network," in *Proc. IEEE GLOBECOM*, pp. 4970-4975, Dec. 2013.

[24] A. C. Cirik, K. Rikkinen, Y. Rong, “A subcarrier and power allocation algorithm for OFDMA full-duplex systems”, accepted to EuCNC2015 conference, July 2015.
[25] A. C. Cirik, K. Rikkinen, M. Latva-aho, “Joint subcarrier and power allocation for sum-rate maximization in OFDMA full-duplex systems”, accepted to IEEE Vehicular Technology Conference (VTC2015-Spring), May 2015.
[26] A. C. Cirik, K. Rikkinen, R. Wang, and Y. Hua, “Resource allocation in full-duplex OFDMA systems with partial channel state information," accepted to IEEE China Summit and Int. Conf. Signal and Inf. Process. (ChinaSIP), July. 2015.
[27] 3GPP, TR 36.828 V11.0.0 (2012-06), “3rd Generation Partnership Project; Technical Specification Group Radio Access Network; Evolved Universal Terrestrial Radio Access (E-UTRA): Further enhancements to LTE time division duplex (TDD) for downlink-uplink (DL-UL) interference management and traffic adaptation (Release 11),” June 2012.
[28] A. C. Cirik, R. Wang, Y. Hua, and M. Latva-aho, “Weighted sum-rate maximization for full-duplex MIMO interference channels," *IEEE Trans. Commun.*, vol. 63, no. 3, pp. 801-815, March. 2015.
[29] A. C. Cirik, “Fairness considerations for full duplex multi-user MIMO systems," *IEEE Wireless Communications Letters*, in press, April. 2015.
[30] A. C. Cirik, R. Wang, Y. Rong and Y. Hua, “MSE based transceiver designs for full-duplex MIMO cognitive radios," *IEEE Trans. Commun.*, in press, May., 2015.
[31] D. Nguyen, L. Tran, P. Pirinen, and M. Latva-aho, “On the spectral efficiency of full-duplex small cell wireless systems,” IEEE Trans. Wireless Commun., vol. 13, no. 9, pp. 4896-4910, Sept. 2014.
[32] D. Nguyen, L.-N. Tran, P. Pirinen, and M. Latva-aho, “Precoding for full duplex multiuser MIMO systems: Spectral and energy efficiency maximization,” IEEE Trans. Signal Process., vol. 61, no. 16, pp. 4038-4050, 2013.
[33] S. Li, R. Murch, and V. Lau, “Linear transceiver design for full-duplex multi-user MIMO system,” IEEE Int. Conf. Commun. (ICC), pp. 4921-4926, June 2014.
[34] H. Malik, M. Ghoraishi, R. Tafazolli, “Cross-Layer Approach for Asymmetric Traffic Accommodation in Full-Duplex Wireless Network”, *European Conference on Networks and Communications (EUCNC) 2015*, Paris, France, July 2015.